UNIVERSITÀ
DEGLI STUDI
DI PADOVA

Sede Amministrativa: Università degli Studi di Padova

Dipartimento di MEDICINA MOLECOLARE

CORSO DI DOTTORATO DI RICERCA IN: BIOMEDICINA
CURRICOLO: MEDICINA MOLECOLARE
CICLO XXIX

YAP/TAZ TRANSCRIPTIONAL ACTIVITY IN TRIPLE NEGATIVE BREAST CANCER CELLS

Tesi redatta con il contributo finanziario della Fondazione Cariparo

Coordinatore: Ch.mo Prof. Stefano Piccolo
Supervisore: Ch.mo Prof. Stefano Piccolo
Co-Supervisore: Dr.ssa Francesca Zanconato

Dottorando Giusy Battilana

INDEX

ABSTRACT (English)

YAP and TAZ are two closely related transcriptional regulators involved in tissue growth, stem cell maintenance and cancer. YAP/TAZ are aberrantly activated in different tumors where they have causative roles in initiation, progression and metastasis. However, the transcriptional program they activate in cancer cells remains incompletely understood. Therefore, we tried to dissect YAP/TAZ direct target genes in a breast cancer cell line (MDA-MB-231 cells) by genome-wide analysis. In so doing, we discovered that YAP/TAZ mainly bind distal enhancers that contact target promoters through chromatin looping to activate a broad transcriptional program activating cell proliferation. We assessed that YAP/TAZ exploit TEAD proteins as DNA binding partners in breast cancer cells.

We then focused on the interaction of YAP/TAZ and TEAD with general transcriptional regulators, aiming at identifying indispensible co-factors for YAP/TAZ/TEAD transcriptional activity at enhancers. Our findings provide new details on YAP/TAZ behaviour, and open a new therapeutic perspective to achieve pharmacological inhibition of YAP/TAZ by impairing their nuclear function.

Part of this work has been published in Nature Cell Biology (Zanconato et al., 2015). Part is unpublished.

ABSTRACT (Italiano)

YAP e TAZ sono due regolatori trascrizionali strettamente correlati, coinvolti nella crescita dei tessuti, nella biologia delle cellule staminali e nel cancro. Un'espressione anomala di YAP e TAZ è riscontrata in diversi tipi di tumori; YAP/TAZ sono infatti coinvolti nella formazione, nella progressione e nella crescita metastatica di molti tumori umani. Tuttavia, il programma trascrizionale attivato da YAP/TAZ nelle cellule tumorali non è ancora ben definito. Pertanto, noi abbiamo ricercato, attraverso un'analisi ad ampio spettro, i geni trascrizionalmente regolati da YAP/TAZ utilizzando la tecnologia della ChIP-Seq in una linea cellulare di tumore alla mammella (cellule MDA-MB-231).

In questo modo, abbiamo scoperto che YAP/TAZ sono fattori che regolano la trascrizione genica prevalentemente legando siti enhancer che contattano i promotori dei geni regolati tramite il ripiegamento della cromatina. In particolare, YAP/TAZ attivano un programma di crescita cellulare, modulando l'espressione di centinaia di geni, come ad esempio MYC, nelle cellule MDA-MB-231.

YAP/TAZ non possono legare direttamente il DNA, ma solo tramite l'interazione con fattori di trascrizione; in particolare, nelle cellule di tumore alla mammella, sono risultati interagire con i fattori di trascrizione appartenenti alla famiglia TEAD.

In seguito, abbiamo ricercato possibili interazioni di YAP e TAZ con regolatori generali della trascrizione allo scopo di identificare co-fattori indispensabili per l'attività trascrizionale di YAP/TAZ/TEAD mediata da siti enhancer.

I nostri risultati hanno meglio elucidato l'attività trascrizionale di YAP/TAZ, aprendo una nuova prospettiva terapeutica; inibire farmacologicamente YAP/TAZ, agendo sulla loro funzione nucleare, potrebbe infatti essere una possibile strategia di cura per il cancro.

PUBBLICATIONS

Zanconato F, **Battilana G**, Cordenonsi M, Piccolo S (2016) YAP/TAZ as therapeutic targets in cancer. *Curr Opin Pharmacol*, Jun 2;29:26-33.

Zanconato F, Forcato M, **Battilana G**, Azzolin L, Quaranta E, Bodega B, Rosato A, Bicciato S, Cordenonsi M, Piccolo S (2015) Genome-wide association between YAP/TAZ/TEAD and AP-1 at enhancers drives oncogenic growth. *Nature Cell Biology*, Sep;17(9):1218-27

The work presented in this thesis was ideated and coordinated by Dr Francesca Zanconato, Prof. Michelangelo Cordenonsi and Prof. Stefano Piccolo. I performed experiments under their supervision, together with Dr Francesca Zanconato, Erika Quaranta and Letizia Filippi.

Important contributions to our work were given by our collaborators: Prof. Silvio Bicciato and Dr Mattia Forcato for bioinformatics, Prof. Michele Morgante and Dr Emanuela Aleo for ChIP-sequencing experiments, Prof. Giuseppe Basso and Dr Chiara Frasson for cytofluorimetry experiments.

INTRODUCTION

Yes-associated protein (YAP) and transcriptional coactivator with PDZ-binding motif (TAZ) are two closely related mammalian transcriptional regulators that shuttle between the cytoplasm and the nucleus to regulate transcription. YAP and TAZ are powerful regulators of cell proliferation, stem cell self-renewal, and fate decision and they have fundamental roles in organ growth, tissue homeostasis, and cancer.

Signals converging on YAP/TAZ

YAP/TAZ are mainly known as the key components of the Hippo pathway; nevertheless, in the past decade numerous publications identified YAP/TAZ as a signaling integrator of diverse upstream cues, such as cell polarity, mechanical cues and soluble signals (Piccolo, Dupont & Cordenonsi, 2014).

Hippo pathway

The Hippo pathway is an evolutionally conserved kinase cascade, firstly delineated in *Drosophila melanogaster*. Hippo signaling plays key roles in organ size control, tissue homeostasis and repair (Harvey, Zhang, & Thomas, 2013).

In mammals the core components of the Hippo cascade are the kinases MST1/2 and LATS1/2. When the Hippo kinases are active MST1/2, together with their adaptor protein SAV1 (Salvador homologue 1), form an active enzyme that phosphorylates and activates LATS1/2 and their regulatory subunits MOB1A/B. Activation of the LATS1/2-MOB1A/B complex results in YAP/TAZ phosphorylation at several serine residues (five in YAP, four in TAZ). YAP/TAZ phosphorylation leads to their sequestration in the cytoplasm, binding to 14-3-3 proteins, and proteasomal degradation mediated by the ubiquitin ligase β-TRCP (Hansen, Moroishi, & Guan, 2015). When the Hippo kinases are inactive, unphosphorylated YAP/TAZ accumulate in the nucleus where they regulate the transcription of target genes (Tremblay & Camargo, 2012).

No specific extracellular ligands or membrane receptors are known to activate the Hippo pathway; nevertheless multiple upstream branches of Hippo signaling control YAP/TAZ activity, such as NF2/Merlin and apical cell polarity proteins (Harvey et al., 2013).

YAP/TAZ phosphorylation by LATS is important, but not an absolute determinant of YAP/TAZ nuclear localization or stability. Therefore, YAP and TAZ integrate LATS-

dependent regulation and other independent cues.

Mechanical signals

Cell shape, plasticity of the extracellular matrix (ECM), and pulling forces exerted by neighbouring cells impact on the cell cytoskeleton and regulate YAP/TAZ localization and activity. Mechanical forces are intrinsic to the architecture and geometry of the tissues and can affect YAP/TAZ activity. Internal forces are always in perfect equilibrium with the external forces dictated by ECM rigidity or traction by neighbouring cells.

Increased cell tension (stiff extracellular environment, cell spreading, F-actin stabilization) induces nuclear YAP/TAZ localization, whereas loss of cellular tension (soft ECM environment, round cell shape, F-actin disruption) increases their cytoplasmic localization (Dupont et al., 2011).

Mechanical signals are independent from Hippo kinase; they are transduced to YAP/TAZ through Rho-GTPase and Rho-kinase and the actomyosin cytoskeleton. YAP/TAZ-mediated mechanical cues are biologically relevant, as they influence cell fate decisions and proliferation.

Cell adhesion and polarity signals

Tissue structures manifest a highly ordered spatial architecture that in normal condition is a potent suppressor of YAP/TAZ activity, in part due to the activation of Hippo pathway. Several reports point to cell polarity, cell-cell adhesion and cell density as regulators of YAP/TAZ localization.

Contact inhibition, a condition in which cells cease to proliferate when they come into physical contact with their neighbours, is known to strongly restrict YAP/TAZ in the cytoplasm (B. Zhao et al., 2007). In line, reduction of cell size leads to YAP/TAZ nuclear exclusion and inhibition of proliferation (Aragona et al., 2013).

Mammalian epithelial cells adhere to one another via junction protein complexes that may directly inhibit YAP and TAZ; for example, α-catenin and angiomotin, two components of adherent and tight junctions respectively, have been shown to interact with YAP/TAZ and to recruit them to the cell cortex, thus preventing YAP/TAZ nuclear activity.

Cell polarity is another potent suppressor of YAP/TAZ activity; a number of proteins that determine cell polarity were found to regulate YAP/TAZ, such as the Scribble-Dlg–Lgl basolateral complex, atypical protein kinase C and Crumbs (Varelas, 2014).For example, Scribble delocalization from the plasma membrane in mammary epithelial cells leads to TAZ

nuclear accumulation, a trait shared by a large number of malignant breast cancers (Cordenonsi et al., 2011). Instead, other polarity proteins contribute to YAP/TAZ repression by sequestering them at cell junctions, as the apical Crumbs complex (CRB) (Varelas et al., 2010).

GPRC signaling

An important class of YAP/TAZ regulators is the G-protein coupled receptors (GPCRs). GPCRs detect extracellular molecules and relay signals through associated G proteins. According to the G protein involved and the stimulating molecules (as hormones), the activity of YAP/TAZ can be either down-regulated or up-regulated by GPRCs. Thus, GPCRs provide a large number of potential mechanisms for YAP/TAZ control, that can be either Hippo-dependent or independent (Hansen et al., 2015).

Wnt

Recent evidences indicate that Wnt/β-catenin signaling and YAP/TAZ signaling are closely related (Azzolin et al., 2014). YAP/TAZ are target of the same destruction complex (the APC/GSK3/Axin complex) that regulates β -catenin. Without Wnt ligands YAP and TAZ are retained in cytoplasm in the destruction complex and mediate β-catenin degradation through the recruitment of β-TrCP. Instead Wnt ligands release not only β-catenin, but also YAP and TAZ from the destruction complex, and allow YAP/TAZ nuclear accumulation.

YAP/TAZ in the nucleus

All the upstream cues listed above converge to regulate YAP/TAZ subcellular localization. YAP/TAZ are found both in the cytoplasm and in the nucleus, where they regulate gene transcription; as such, YAP/TAZ nuclear availability is a key determinant of their function.

The broad spectrum of YAP/TAZ regulation greatly implies a large number of genes whose expression can be specifically regulated by YAP/TAZ. To date, only few YAP/TAZ target genes, with uncertain functional significance and general relevance, have been described (Piccolo et al., 2014). Indeed, the number of YAP/TAZ established effectors is growing larger (*CTGF*, *CYR61*, *ANKRD1*, *BIRC5*, *AXL*, *InhA*, *Col8a1* and others), but none can explain the biological effects of YAP/TAZ; as such, the transcriptional program that YAP/TAZ activate to achieve their biological effects remains poorly understood (Hong & Guan, 2012).

YAP and TAZ possess a strong transcriptional activation domain, but they do not carry a DNA-binding domain; so they can contact DNA only indirectly, through DNA-binding partners. In the nucleus, YAP/TAZ interact with DNA-binding transcription factors to form functional transcription complexes that recognize *cis*-regulatory elements and activate the expression of target genes.

Several YAP/TAZ transcriptional partners have been proposed, such as Runx1/2, ErbB4, PPAR-g, Pax3 and T-box transcription factor 5 (TBX-5) (Pan, 2010). YAP and TAZ were also found to bind Smads; cytoplasmic YAP/TAZ participate in Smad2/3 cytoplasmic retention, even overruling the effects of high levels of TGF-B ligands (Piccolo et al., 2014). Moreover, p73 (a p53 family member) is potentially interesting as the p73-YAP complex is formed after DNA damage, leading to activation of a cell death program (Mo, Park, & Guan, 2014). However, TEAD/TEF family of DNA-binding proteins has been established as the main YAP/TAZ interacting transcription factors in mammals and their homolog Scalloped in *Drosophila* (S. Wu, Liu, Zheng, Dong, & Pan, 2008; Heng Zhang et al., 2009; B. Zhao et al., 2008). The four TEAD family members (TEAD 1-4) are widely expressed in most mammalian tissues and organs (Pan, 2010). A series of studies suggested that TEAD proteins mediate a number of YAP/TAZ functions in mammalian cells, including contact inhibition, epithelial-mesenchymal transition and trophectoderm development (Piccolo et al., 2014; B. Zhao et al., 2008). However, it is still unknown to what extent the transcriptional activity of YAP/TAZ overlaps with TEAD activity, and whether the YAP/TAZ and TEAD complex operates on specific genes, rather than on entire gene-expression programs.

Another under-investigated issue is what takes place between the recognition of a specific locus by YAP/TAZ and downstream transcriptional events. It has been recently reported that YAP and TAZ can interact with components of the SWI/SNF chromatin remodelling complex and recruit NCOA6 histone methyltransferase complex to increase H3K4 methylation and transcription of target genes (Oh et al., 2013; Qing et al., 2014; Skibinski et al., 2014). YAP/TAZ-TEAD complex can also operate as transcriptional corepressors by recruiting the NuRD histone deacetylase complex (Kim, Kim, Johnson, & Lim, 2015). Very recently, Camargo and colleagues reported that YAP modulates transcription by regulating promoter-proximal polymerase II (Pol II) pause release by interacting and recruiting the Mediator complex to enhancers, allowing the recruitment of the CDK9 elongating kinase (Galli et al., 2015).

YAP/TAZ biological functions

Early embryonic development

Accurate control of the levels and localization of YAP/TAZ is essential for early developmental events. This is demonstrated by the severe phenotypes associated with ablation of YAP and/or TAZ genes: in mouse embryos, YAP/TAZ double null mutants die before implantation (Nishioka et al., 2009); $YAP^{-/-}$ embryos die after gastrulation, around stage E8.5 (Morin-kensicki et al., 2006); $TAZ^{-/-}$ embryos display high rates of embryonic lethality, but a fraction of mutants develop to term and die of polycystic kidney disease and pulmonary emphysema (Makita et al., 2008).

The nuclear/cytosolic distribution of YAP/TAZ defines the first cell choice in the mouse embryo, where embryonic cells decide to become either trophectoderm (TE) or Inner Cell Mass (ICM). At the blastocyst stage, YAP/TAZ accumulate in the nuclei of outer TE cells, while they are distributed throughout the cytoplasm in cells of the ICM. Nuclear YAP/TAZ control the expression of multiple genes including the induction of Cdx2, the master gene associated with TE fate, important to establish strong apicobasal polarity and tight junctions (Nishioka et al., 2009; Piccolo et al., 2014).

Stem cells

YAP/TAZ have been extensively portrayed as "stemness factors": transgenic mice overexpressing nuclear YAP - or carrying mutations in Hippo pathway components - display dramatic embryonic organ overgrowth, potentially by expanding the number of somatic stem cells in those trangenic organs (Piccolo et al., 2014; Ramos & Camargo, 2012). Perhaps consistently, in adult tissues, YAP/TAZ are enriched in anatomical compartment containing stem and progenitor cells, for example in stem cell compartment of the intestinal epithelium (Camargo et al., 2007). Tissues such as skin and skeletal muscle show graded YAP levels based on differentiation status: YAP is nuclear (and thus active) in stem/progenitor cells, and cytoplasmic (inactive) in mature cells. Cytoplasmic restriction of YAP/TAZ is a prerequisite for tissue homeostasis, whereas nuclear YAP/TAZ promotes progenitor renewal and proliferation, essential in conditions in which stem cells need to be amplified such as tissue regeneration. Indeed, YAP/TAZ are essential for physiological tissue repair upon injury (Cai et al., 2010).

This spatial organization indicates that the transcriptional activity of YAP/TAZ could be important in the maintenance of stem cell traits in normal tissues (Ramos & Camargo, 2012).

Our group recently published that transient expression of exogenous YAP or TAZ in primary differentiated mouse cells could induce conversion to tissue-specific stem/progenitor cell state ex vivo (Panciera et al., 2014), highlighting an unprecedented connection between YAP/TAZ and cell plasticity and between YAP/TAZ and the somatic SC state.

Cancer

A number of studies suggest that YAP/ TAZ play causative roles in tumor initiation, progression and metastasis in various human organs, including breast, colon, lung and liver. Characterization of human tumor samples highlighted that YAP/TAZ are frequently overexpressed and activated during tumorigenesis. Moreover, aberrant YAP and/or TAZ nuclear localization, or high expression of YAP/TAZ target genes, are associated with poor outcome in large datasets of breast and colon cancer patients (Piccolo et al., 2014).

YAP/TAZ oncogenic potential lies in their capacity to direct cell proliferation, cell survival and cancer stem cell fate (Mo et al., 2014). Sustained activation of YAP/TAZ promotes aberrant cell proliferation (Camargo et al., 2007) and an increased resistance to cell death (B. Zhao et al., 2012). Moreover, YAP/TAZ are active in the cancer stem cell (CSC) fraction, and they are functionally instrumental and required for CSC expansion (Piccolo et al., 2014). It has been reported that YAP/TAZ can reprogram non-stem tumor cells into cells with full CSC attributes (Bartucci et al., 2015; Cordenonsi et al., 2011).

An additional cancer-associated trait regulated by YAP/TAZ includes the ability to induce chemoresistance; tumor cells with activated YAP/TAZ display indeed resistance to chemotherapeutic drugs. In a breast cancer contest, TAZ sustains survival of cancer stem cells treated with conventional chemotherapeutics, such as paclitaxel and doxorubicin, both in vitro and in mouse models (Bartucci et al., 2015; Cordenonsi et al., 2011).

Furthermore, YAP/TAZ influence the chemical, physical, and cellular composition of the tumor microenvironment; in some context, they induce the secretion of growth factors, matricellular proteins and interleukins to orchestrate crosstalk from cancer cells and normal cells (Piccolo et al., 2014).

Even though YAP/TAZ are frequently deregulated in human tumors, no germline or somatic mutations have been identified in YAP or TAZ, nor in most of the components of the Hippo pathway. Indeed, with the exception of inherited disorders associated with *NF2*, somatic mutations in the core Hippo members are extremely rare in human tumors (Harvey et al., 2013). Considering that YAP/TAZ activation cannot be explained by mutations in Hippo pathway components, other YAP/TAZ modulations should be crucial for their activity in

human cancers. Mechanical cues have an important role in YAP/TAZ regulation during tumorigenesis, where integrity of tissues is disturbed. YAP/TAZ can be re-activated by cell shape distortions or attachment to an increasingly abnormal and rigid ECM (Zanconato, Cordenonsi, Piccolo, 2016). That said, the transcriptional programs induced by YAP/TAZ that lead to cancer development is unknown (Moroishi et al., 2015).

Anti-YAP/TAZ therapeutic interventions

YAP/TAZ are broadly activated in different human cancers, where they are involved in many aspects of cancer biology. Further, YAP/TAZ are largely dispensable for normal homeostasis in the healthy tissue whereas they are essential for tumor development. These evidences make them appealing therapeutic targets for cancer (Piccolo et al., 2014). Genetic evidences in mouse models, collectively indicating that inactivation of YAP/TAZ in several adult organs - including breast, liver, pancreas, skin and intestine- renders those tissues immune to cancer emergence or progression (Azzolin et al., 2014; Chen et al., 2014; Zhang et al., 2014).

To identify candidate drugs able to modulate YAP/TAZ activity, most efforts have been dedicated to YAP/TAZ upstream inducers and signaling pathways. Considering that they integrate several signaling cascades, many therapeutic options are emerged, targeting mechanotransduction, the energy metabolism (statins), GPCR signaling (Gα inhibitors) and turning off Wnt signaling (Tankyrase inhibitors**)** (Zanconato, Battilana, Cordenonsi, & Piccolo, 2016). However, the complexity of YAP/TAZ regulation makes this approach poorly efficient, since cancer cells may use different combinations of upstream inputs in a tumor-specific way, and even between different areas of the same lesion (Zanconato, Cordenonsi, Piccolo, 2016). Since all upstream regulators ultimately impact on YAP/TAZ nuclear availability and transcriptional responses, designing compounds able to interfere at these levels may represent a "universal" anti-YAP/TAZ inhibition. This approach may also display an added advantage of reduced toxicity compared to drugging upstream signaling molecules that might lead to pleiotropic effects.

Verteporfin (VP) is an example of YAP/TAZ targeting molecule that affects transcriptional activity. This compound belongs to the porphyrin family, and it is able to inhibit the physical association between YAP and TEAD proteins. From the literature is known that VP can reduce liver overgrowth in mice upon YAP overexpression or NF2 knockout (Liu-chittenden et al., 2012). Moreover, VP has been successfully used to restrain the growth of uveal

melanoma cells in an orthotopic mouse model (Yu, Zhang, & Guan, 2014) and of pre-established xenografts of prostate cancer cells bearing activated YAP (Nguyen et al., 2015). However, a recent study reported that VP suppresses the proliferation of cancer cells by inducing toxicity, acting independently of YAP (H. Zhang et al., 2015).

Irrespectively, targeting YAP/TAZ transcriptional mechanisms is a potentially promising area to design new therapeutic interventions. For this, the mechanisms by which nuclear YAP/TAZ control gene expression needs to be further investigated.

AIM OF THE PROJECT

Recently YAP/TAZ activity has been the main object of investigation in our laboratory, in particular in breast cancers (BC). It has been reported that YAP/TAZ have several roles in breast cancer development; yet, the transcriptional program they activate to promote cell transformation is still poorly understood. The aim of our project is to collect genome-wide data about YAP/TAZ transcriptional activity in cancer cells, use it to dissect the mechanisms by which YAP/TAZ exert their oncogenic functions and derive from this analysis new strategies of intervention.

RESULTS

Identification of YAP/TAZ DNA binding sites at genomic level in a breast cancer cell line.

We chose MDA-MB-231 cells, as the main model for the investigation of YAP/TAZ transcriptional program. This represent a model of Triple Negative Breast Cancer that is considered one of the most aggressive and heterogeneous forms of mammary tumors. Inportantly, these cells bear genetic inactivation of the Hippo pathway (*NF2* null) causing constitutive activation of YAP/TAZ (Aragona et al., 2013); furthermore, these cells are almost mesenchymal and do not express the classic cell-cell adhesion molecules that are responsible of Hippo activation in normal epithelial cells. Finally, they easily adopt a well-spread morphology, translating in increased YAP mechanotransduction. In sum, MDA-MB-231 cells concentrates a number of features that potently sustain YAP/TAZ activity. To elucidate how YAP/TAZ regulate gene expression in these cells, we decided to identify the genomic loci bound by YAP/TAZ through chromatin immunoprecipitation assays followed by next-generation sequencing (ChIP-seq).

ChIP-seq: method overview

Chromatin immunoprecipitation is a method to detect interactions between proteins and genomic DNA (Figure 1A) (Kharchenko, Tolstorukov, & Park, 2008; Schmidt et al., 2009). Living cells are reversibly crosslinked by formaldehyde, locking transcription factors to their DNA binding sites in the genome. Cells are chemically lysed to isolate cell nuclei and these nuclei are then sonicated, in order to obtain chromatin fragments sized 200-600 base pairs through high-frequency sound waves (Figure 1B). Specific antibodies are used to immunoprecipitate transcription factors of interest together with their bound DNA fragments. These protein-DNA complexes are then isolated by protein A-functionalized magnetic beads. DNA is eluted from the magnetic beads and the covalent DNA–protein crosslinks are reversed by heating. Enriched DNA fragments are purified for downstream analysis to identify the sequences bound by the protein. Usually, ChIP is coupled with quantitative real-time PCR (ChIP-qPCR), genomic microarray (ChIP-chip) or deep sequencing (ChIP-seq).

ChIP-seq allows the unbiased identification of transcription factor binding sites in the genome. Common “adapter sequences” are ligated to the ends of ChIPed DNA. DNA fragments of the appropriate size range (150-300 base pairs) are selected by running the DNA

in an agarose gel to set the binding site resolution. Then, the library is amplified by bridge PCR, where adaptors provide a target sequence for the primers to generate the template for sequencing. In our case, the amplicons were sequenced by Illumina platform. For ChIP-seq experiments, short reads (40 base pairs) from one end of the fragments provide sufficient information (Figure 1C). The recommended sequencing depth is ~20 mln uniquely mapping reads/sample; an increased depth of coverage allows the detection of more sites that have lower levels of enrichment over the genomic background.

Uniquely mapping sequences are aligned to the genome and the alignment of sequenced tags to the genome results in two peaks (one for the positive and one for the negative DNA strand) that flank the binding region of the protein of interest. These two strand-specific peaks of tags are combined to generate an approximate profile of fragment distribution. Then, a "peak caller" algorithm scans the genome to identify regions that are significantly enriched in the ChIP sample relative to the experimental control. The final output consists in genome locations that represent likely binding sites of the protein of interest.

Chromatin immunoprecipitation of endogenous YAP/TAZ

The reliability of a ChIP experiment depends on the specificity and efficiency of the antibodies in recognizing and immunoprecipitating the target protein. Thus we performed trial experiments to assess the capacity of antibodies to immunoprecipitate endogenous YAP/TAZ from cross-linked chromatin. We used a monoclonal antibody targeting YAP (abcam, ab52771) and polyclonal antibodies targeting TAZ (sigma aldrich, HPA007415), both raised in rabbit. As negative control, we performed the immunoprecipitation with pre-immune immunoglobulins produced in rabbit. We isolated chromatin from MDA-MB-231 cells and we performed an immunoprecipitation experiment with the selected antibodies. After the recovery and elution of the immunoprecipitated protein-DNA complexes, we checked the result of the immunoprecipitation step by western blot (Figure 2A). The YAP monoclonal antibody specifically recognized and immunoprecipitated YAP, whereas TAZ polyclonal antibodies bound both YAP and TAZ, probably due to the high homology between the two proteins. In a second experiment, we performed ChIP with the same antibodies from chromatin obtained from MDA-MB-231 cells transfected with control or YAP/TAZ siRNAs. As read-out of the specificity of these experiments, we carried out quantitative real-time PCR on the promotorial sequences of known YAP/TAZ target genes (CTGF and CYR61) (ChIP-PCR). As shown in Figure 2B, specific pull-down of YAP/TAZ bound-DNA could be detected from unmanipulated cells, but not from YAP/TAZ-depleted cells. In no case,

negative control ChIPs with pre-immune rabbit IgGs gave any signal (Figure 2B). As further control, a genomic fragment belonging to the β-globin locus (which is not expressed in MDA-MB-231 cells, and is thus expected to be devoid of functional YAP/TAZ binding sites) is poorly amplified in all samples. Overall, we were confident that the antibodies could be used to reliably identify YAP/ TAZ binding sites genome-wide.

YAP/TAZ ChIP-seq

Having established that the two antibodies for YAP and TAZ are specific and efficient, we proceeded with ChIP-seq experiment. We performed chromatin immunoprecipitation from MDA-MB-231 cells with both YAP/TAZ polyclonal antibodies and with pre-immune rabbit IgGs as a negative control. We carried out two independent experiments, so that we could define as YAP/TAZ binding sites only those sequences that were bound by YAP/TAZ in both replicas (but not in the two negative control samples). We verified the enrichment of known YAP/TAZ-bound sequences in ChIPed DNA by qPCR to make sure of the experiments' quality as already detailed in Figure 2.

ChIPed DNA samples were processed for deep sequencing in the laboratories of IGA (Istituto di Genomica Applicata, Udine). About 60 x 10^6 reads were obtained from each sample (Figure 3A). Bioinformatic analysis was performed by our collaborators at the University of Modena (Mattia Forcato and Silvio Bicciato). Non-redundant sequences that could be mapped to a single site of the human genome were used to identify YAP/TAZ binding sites. After aligning to the human genome ChIP-seq reads from two replicate experiments, we identified a total of 7710 and 9798 regions bound by the monoclonal YAP antibody and the polyclonal TAZ antibodies, respectively. 7107 peaks were identified with both antibodies (Figure 3B). Given the high similarity between YAP and TAZ and their functional redundancy, we decided to focus on the common set of binding sites, that we renamed "YAP/TAZ" peaks. As to the antibody-specific peaks, we do not exclude that they might well represent YAP-specific or TAZ-specific binding sites but, for this work, we decided to sidestep them in favor of the genomic regions providing the highest confidence.

We scanned the ChIP-seq profiles and found that YAP/TAZ peaks were present on the promoters of previously established YAP/TAZ direct targets, thus validating our ChIP-seq procedure (Figure 3C). The plot of the negative control sample, instead, displayed few tags aligned with the same regions, without any appreciable difference with background noise. By ChIP-qPCR, we validated that YAP/TAZ antibodies were truly able to bind some of the

newly discovered *cis*-regulatory regions from control cells, but not from YAP/TAZ-depleted cells (Figure 3D).

Distribution of YAP/TAZ binding sites in the genome

One important step to understand how YAP/TAZ regulates transcription is to characterize their DNA-binding sites. In particular, defining genome-wide distribution of YAP/TAZ binding sites could be useful to make inferences about their activity. Therefore, we analyzed the position of YAP/TAZ binding sites referred to genes annotated in the human genome, to investigate in which genomic regulatory regions they are preferentially located. In detail, we evaluated the distance of each peak from the closest transcription start site (TSS) using annotatePeakInBatch function of ChIPpeakanno R package and GENCODE annotation version 16; only genes classified as protein coding were considered (done in collaboration with Mattia Forcato). We found that YAP/TAZ are preferentially bound far from TSS. Indeed, only a small fraction of peaks (3.3%) mapped close (±1 kb) to TSS, whereas the vast majority of peaks (~85%) were located farther than 10kb from the closest TSS (Figure 4A, B).

Due to their remote location, we asked whether most YAP/TAZ peaks are located in enhancers. Enhancers are short DNA fragment that are able to increase transcription of a target gene. They can exert their function over long distances, either from upstream, downstream, or within a transcriptional unit. Enhancers can be distinguished from promoters by their epigenetic features (Calo & Wysocka, 2013); enhancers are marked by monomethylation of histone 3 at lysine 4 (H3K4me1), whereas trimethylation at the same residue of histone 3 (H3K4me3) identifies promoters. In their active state, enhancers also show acetylation on H3K27 (H3K27ac). The distribution of histone post-translational modifications in the genome can be assessed by ChIP-seq with antibodies that specifically recognize the modified epitopes. We used published ChIP-seq datasets for H3K4me1, H3K4me3, H3K27ac in MDA-MB-231 cells to obtain a map of promoters and enhancers (Rhie et al., 2014): H3K4me3 peaks close to a TSS (±5 kb) were defined as promoters, whereas H3K4me1 peaks were defined as enhancers; regions with the co-presence of H3K4me1 and H3K4me3 peaks were defined as promoters or enhancers after the evaluation of the proximity to a TSS and the comparison of the enrichment signals. Promoters or enhancers were defined as active if overlapping with H3K27ac peaks. Peaks without any of the previous characteristics were defined as "not-assigned".

We used bioinformatic tools to compare this published map of epigenetic marks with our YAP/TAZ ChIP-seq data (Figure 4C). We found that only a very small fraction (3.6%) of YAP/TAZ peaks are located on promoters (H3K4me3). Instead, about 91% of peaks are located in enhancer regions (H3K4me1); most of these regions (96.5%) are in an active transcriptional state (H3K27ac) (Figure 4D).

DNA regions that actively regulate transcription are predominantly found in sites of accessible chromatin, characterized by eviction of nucleosomes. Therefore we also compared the YAP/TAZ bound regions with the nucleosome-free regions of MDA-MB-231 cells. These data were already available from previously published FAIRE-Assays (Rhie et al., 2014). Formaldehyde-assisted identification of regulatory elements followed by deep sequencing (FAIRE–seq) is a method used for determining genomic open regions, unoccupied by nucleosomes, whereby cells are chemically crosslinked with formaldehyde, chromatin is sheared by sonication and nucleosome depleted DNA molecules are separated from DNA regions crosslinked to nucleosomes by phenol-chloroform extraction (the latter are trapped in the organic phase) and then sequenced. We found that that >80% of the YAP/TAZ bound active enhancers display reduced nucleosome occupancy at the peak center (Figure 4E).

Association of YAP/TAZ peaks to enhancer elements

As our goal is – ultimately – to identify YAP/TAZ target genes, we next sought to link YAP/TAZ peaks to the promoters they regulate. All the peaks located in promoter regions, that corresponded to YAP/TAZ peaks close to a TSS (± 5kb), and whose summit was overlapping with H3K4me3 peaks, were assigned to the nearest gene (Figure 5A).

However, we reasoned that this proximity criterion was questionable for the vast majority of YAP/TAZ peaks located in enhancers. Enhancer elements can be very far away from their target promoters; enhancers regulate target promoter by physically associating to them and doing so typically by "skipping" neighbouring genes. The logic of enhancer-promoter interaction is independent of the linear proximity and relies on long-distance chromatin looping that defines the 3D organization of the genome. Therefore, we committed to identify the promoters that are in physical contact with YAP/TAZ-occupied enhancers.

Interactions between distant chromatin regions such as promoters and enhancers can be detected with chromatin conformation capture (3C) technologies. These methods aim to generate a 3D map of chromosomes on the basis of the frequency at which genomic loci are

in close proximity inside the nucleus. The initial step includes fixation of cells with formaldehyde to crosslink chromatin regions that are in close spatial proximity. The chromatin is then fragmented by restriction enzyme digestion to generate small complexes of protein and DNA. A ligation reaction is then performed: in this step interacting DNA fragments are turned into a single hybrid DNA molecule; chromatin is highly diluted before digestion, so that only DNA fragments that are covalently linked together form ligation products. The hybrid DNA molecules are purified and analysed to identify the distant genomic regions that were close to each other in the nucleus.

Depending on the method used to reveal the identity of the interacting DNA sequences, 3C based method can reach different levels of resolution. At the highest resolution (Hi-C), all ligation products are identified by next-generation sequencing, thus allowing to map virtually all the interaction in the genome in an unbiased manner.

High-resolution map of chromatin interactions (Hi-C) has been recently produced from human cells (Jin et al., 2013). In detail, Jin and colleagues performed Hi-C in human primary fibroblasts (IMR90 cells) to detect genome-wide 3D interactions. By bioinformatic algorithms, they filtered for functional interactions -not random- determining over one-million long-range chromatin interactions at 5-10 kb resolution. Also, they uncovered general principles of chromatin organization at different types of genomic features. Secondly, they used their map to predict enhancers-promoter pairs with great accuracy. Therefore, considering that the large majority of these long-range chromatin interactions are conserved across cell types (Rao et al., 2014), we decided to use above published map of enhancer-promoter pairs to identify the target promoters of YAP/TAZ-bound enhancers (Figure 5B). We assigned enhancer peaks to promoters that can physically interact with them according to high-resolution chromatin conformation capture data. Therefore, we obtained a list of candidate YAP/TAZ direct targets (TABLE 1). But which one is indeed functionally induced in MDA-MB-231 cells?

Identification of YAP/TAZ direct target genes

To define what fraction of the putative YAP/TAZ target genes identified above is regulated by YAP/TAZ, we focused on gene expression profiles of MDA-MB-231 cells were previously generated in our laboratory with Affymetrix Microarrays. Cells were transfected with control siRNA or two different pairs of YAP/TAZ siRNAs to identify genes whose

expression depends on YAP/TAZ activity. We found that YAP/TAZ knockdown downregulates the expression of about 1500 transcripts in MDA-MB-231 (out of more than 18000 detected transcripts) (Figure 6A). A similar number of transcripts were upregulated, indicating the potential of YAP/TAZ to either directly or indirectly negatively regulate gene-expression. In any case, we focused only on genes that are activated by YAP/TAZ, to conform in this first exploration to the more established role of YAP/TAZ as transcriptional co-activators.

We compared the list of genes with YAP/TAZ binding sites on their cis-regulatory regions obtained above with the gene expression data. Of YAP/TAZ positive target genes (1534), 435 (28%) are associated to YAP/TAZ peaks. These are bona-fide YAP/TAZ direct target genes. The vast majority of these (86%) are regulated by YAP/TAZ from distant enhancers. Notably, most (58%) of YAP/TAZ-occupied enhancers are located farther than 100,000 bp from the corresponding TSS (Figure 6B).

A YAP/TAZ-regulated transcriptional program driving cell proliferation

YAP/TAZ direct target genes are regulators and effectors of cell growth

We performed gene ontology (GO) annotation of YAP/TAZ direct targets to identify the main biological processes regulated by YAP/TAZ through the functions of the genes they regulate. The Gene Ontology (GO) project has described genes in biological databases with "terms" that provide functional information about the gene product. Each gene in a list can be annotated with GO terms; then, the GO annotations can be used to determine which biological processes, molecular functions, and/or subcellular locations are significantly over-represented in a group of genes. A GO term - and the function it describes - is "enriched" in a set of genes (for example, positive YAP/TAZ targets) when a higher proportion of genes with that annotation are present among the differentially expressed genes compared to a “background” set of genes (for example, all the genes expressed by the cells being examined).

We used DAVID (Database for Annotation, Visualization and Integrated Discovery) to identify enriched GO terms associated with direct YAP/TAZ positive target genes. A large fraction (154 genes, 36%) resulted to be linked with cell cycle progression. Other positive targets (14% of the total) are connected to RNA metabolism and RNA transport. No other biological processes were significantly regulated by YAP/TAZ (Figure 7A).

Overall, GO annotation indicated that YAP/TAZ activate a growth program in breast cancer cells, in line with their well-established roles in organ growth and cell proliferation. Genes in the YAP/TAZ growth program encode for proteins directly involved in specific steps of the cell cycle. We could identify genes playing roles in the assembly of the licensing complex, DNA synthesis and DNA repair (e.g. *CDC6*, *GINS1*, *MCM3*, *MCM7*, *POLA2*, *POLE3*, *TOP2A*, *RAD18*), transcriptional regulators of the cell cycle (e.g. *ETS1*, *MYC*, *MYBL1*), cyclins and their activators (*CCNA2* and *CDC25A*), and completion of mitosis (e.g. *CENPF*, *CDCA5*, *KIF23*).

First of all, we validated a subset of these new YAP/TAZ target genes by qRT-PCR using TaqMan Low Density Arrays. We quantified the expression of 46 new target genes (expression levels are normalized to GAPDH) in MDA-MB-231 cells transfected with YAP/TAZ siRNAs. Both YAP/TAZ siRNA mixes efficiently downregulated new targets in two biological replicates (Figure 7B). For a subset of genes, the downregulation of the corresponding proteins was also verified by Western blot (Figure 7C).

All the genes in the YAP/TAZ growth program were associated with at least one YAP/TAZ peak located on enhancers. We experimentally re-confirmed by ChIP-qPCR the presence of YAP/TAZ on a selection of these enhancers (Figure 7D).

MYC and TOP2A promoters are in contact with YAP/TAZ-occupied enhancers via chromatin looping

The procedure we used to "connect" YAP/TAZ-occupied enhancers with their target promoters was based on chromatin conformation data obtained from human lung fibroblasts. The loop structure was reported to be conserved across histotypes (Rao et al., 2014); yet, as proof of concept, we decided to verify the interaction between some enhancer-associated YAP/TAZ binding sites and their predicted in our cellular system.

We selected two representative targets belonging to the YAP/TAZ growth program, TOP2A and MYC. As shown in figure 8A no YAP/TAZ peaks are present close to the TSS of MYC gene. However, several enhancers that are predicted to interact with MYC or TOP2A promoters were occupied by YAP/TAZ in our ChIP-seq experiment.

We performed chromatin conformation capture (3C) analysis in MDA-MB-231 cells (Bodega et al., 2009). We digested crosslinked chromatin with HindIII, ligated DNA regions that were in close proximity and purified hybrid DNA molecules. We then detected the ligation products by PCR. We designed PCR primers to measure the frequency of interaction of TOP2A and MYC TSS with a wide region surrounding the relative candidate enhancers. A

common reverse primer (called "anchor") was designed to anneal in the proximity of a HindIII restriction site near promoter; several forward primers (called "preys") were designed to flank HindIII sites in the chromosomal regions containing YAP/TAZ-occupied enhancers. As amplification efficiency may not be the same for all primer pairs, a reference template was generated by mixing and ligating bacterial artificial chromosomes spanning the genomic regions of interest, and the amount of PCR products obtained from the 3C template was normalized to the reference template. As shown in figure 8B HindIII fragments close to YAP/TAZ peaks on two MYC candidate enhancers display a higher ligation frequency with MYC promoter, compared with more distal sequences, showing that these YAP/TAZ-bound enhancers actually interact with MYC promoter in MDA-MB-231 cells. We obtained similar results with TOP2A TSS and two of its predicted enhancers (Figure 8C).

We then asked whether YAP/TAZ actually regulate the activity of these enhancers. Transcriptionally active chromatin is marked by acetylation on K27 residue of histone 3. Thus, we performed ChIP-qPCR experiments to compare the levels of H3K27ac (normalized to total H3 levels) in MDA-MB-231 cells transfected with control or combined YAP/TAZ siRNAs. In YAP/TAZ-depleted cells, the level of H3K27ac decreased on MYC and TOP2A enhancers (Figure 8D). Overall, data suggest that YAP/TAZ recruitment to enhancers is functional for their activation, and thus for the transcription of downstream target genes.

MYC is a mediator of YAP/TAZ proliferative activity

As proof of concept of the biological validity of our findings, we studied in more depth the role of MYC as YAP/TAZ-regulated gene. A large body of evidence shows that MYC is one of the best-established factors that promote cell cycle progression and Myc deregulation is a major driving force of human tumorigenesis (Dominguez-Sola & Gautier, 2014). In line with this notion, we verified that MYC depletion with two independent siRNAs reduced the growth rate of MDA-MB-231 cells (monitored by crystal violet staining), with a larger fraction of cells blocked in the G1 phase of the cell cycle (as determined by cytofluorimetric analysis of DNA content) (Figure 9A-C).

To better define the role of MYC as a mediator of cell proliferation downstream of YAP/TAZ, we performed a rescue experiment in which we overexpressed MYC cDNA in YAP/TAZ-depleted cells. MDA-MB-231 cells were transduced with lentiviral vectors carrying MYC or EGFP coding sequences under the control of a tetracycline response element (TRE), together with a vector encoding the doxycycline responsive transactivator rtTA, so that MYC (or EGFP) expression was induced only upon doxycycline administration

(Figure 9D). We transfected these cells with a control siRNA or anti-YAP/TAZ siRNA, and we monitored cell growth and cell cycle progression in the presence or absence of doxycycline. As shown in figure 9E, YAP/TAZ depletion leads to an almost complete growth arrest; MYC re-expression triggered a partial rescue of cell proliferation and allowed progression to the S-phase of the cell cycle in YAP/TAZ-depleted cells; EGFP induction had no effect. As a comparison, reintroduction of YAP or TAZ in YAP/TAZ-depleted cells completely rescued cell growth (Figure 10 N,0). This indicated that although MYC represents an important functional effector of YAP/TAZ in MDA-MB-231 breast cancer cells, YAP/TAZ orchestrate cell growth by controlling a number of other direct targets.

Genome-wide recruitment of YAP/TAZ to chromatin through TEAD factors

YAP/TAZ cannot interact with DNA by themselves because they do not possess a DNA binding domain. They rely on DNA binding factors to exert their transcriptional functions. Several TFs have been proposed to mediate YAP/TAZ interaction with chromatin (p73, Runx2, Smad, TEAD/TEF transcription factors) (Piccolo et al., 2014). In particular, TEAD proteins are known to be functional for YAP/TAZ-induced oncogenic transformation; however, we had no cues about the real extent of YAP/TAZ-TEAD interaction or the relevance of other DNA-binding partners when all the genome is taken into account, rather than specific loci or functions.

DNA binding proteins recognize specific DNA sequences, called motifs. Therefore, the identity of YAP/TAZ partners can be inferred from the nucleotide sequence of YAP/TAZ peaks, found by ChIPseq. We used bioinformatic tools to search for recurrent motifs in the sequences bound by YAP/TAZ. Algorithms for *de novo* motif finding scan a pool of input DNA sequences (we used 500 bp sequences centred at the summit of YAP/TAZ binding sites) and annotate enriched "words" that recur with a higher frequency compared with a pool of background (random) 500bp DNA fragments. Then, enriched "words" are compared with a database of motifs to identify their cognate TF. This analysis revealed that the most enriched motif in YAP/TAZ peaks matched the consensus sequence for TEAD binding sites (62%) (Figure 10A). This percentage further increased (~75%) if we extended the search to known TEAD-responsive elements (i.e. if we scanned YAP/TAZ peaks looking for known TEAD motifs) (Figure 10B). Furthermore, TEAD motif frequently occupied the summit of YAP/TAZ peaks (the point where the signal is highest, where the protein is assumed to sit),

suggesting that TEADs might be the platform through which YAP/TAZ bind DNA in a large majority of peaks in MDA-MB-231 cells (Figure 10C).

The presence of the motif indicates that a chromatin segment can be bound by a TF, but it is not predictive of real binding. Thus, to support above bioinformatics results and verify if TEAD factors really co-occupy DNA sites with YAP/TAZ, we performed ChIP-seq for endogenous TEAD4 in MDA-MB-231 cells. We chose TEAD4 because it is highly expressed in MDA-MB-231 cells; furthermore a good ChIP-grade TEAD4 antibody was available, allowing us to immunoprecipitate the endogenous protein. Indeed, we performed a preliminary validation experiment, and we verified that TEAD4 antibody specifically enriched ANKRD1 and CTGF promotorial sequences in ChIP'd DNA from control MDA-MB-231 cells, but not from TEAD4 depleted cells (Figure 10D).

We prepared sequencing libraries from two independent chromatin immunoprecipitations with TEAD4 antibody. We obtained 8406 TEAD4 peaks. Similarly to YAP/TAZ, TEAD4 resulted to be located far from TSS, most likely on enhancer elements.

We then compared YAP/TAZ and TEAD4 ChIP-seq data. 5522 YAP/TAZ binding sites (78%) overlapped with TEAD4 peaks, and the summits of TEAD4 peaks are located at the summits of the corresponding YAP/TAZ peaks (Figure 10E-G). By measuring peak signals, we also noticed a strong linear correlation between the strengths of TEAD4 and YAP/TAZ binding, suggesting that the more TEAD4 binds to DNA the more YAP/TAZ are associated to the same element (Figure 10H).

To verify if TEAD is instrumental for YAP/TAZ binding to chromatin, we performed a ChIP-qPCR experiment for YAP in TEAD-depleted cells. YAP recruitment to DNA was strongly decreased in all tested loci in the absence of TEAD proteins, reinforcing the notion that TEADs mediate YAP/TAZ recruitment to chromatin (Figure 10I).

The large majority (85%) of direct YAP/TAZ targets, including those controlling cell cycle progression, are associated with TEAD4 peaks. To investigate if large part of the YAP/TAZ transcriptional and biological effects depended on TEAD factors, we monitored the effects of TEAD 1/2/3/4 knockdown in MDA-MB-231 cells (validated by gene expression, Figure 11A). We analysed gene expression levels YAP/TAZ targets by custom TaqMan Low Density Arrays (expression levels are normalized to GAPDH) (Figure 11B). TEAD depletion with two siRNAs mixes efficiently downregulated YAP/TAZ targets involved in cell cycle control. Functionally, TEAD downregulation caused cells to slow down proliferation and rest in the G1 phase of the cell cycle (Figure 11 C, D). In line, overexpression of a mutant YAP

(or TAZ) that is defective for TEAD-binding cannot rescue proliferation in YAP/TAZ-depleted MDA-MB-231 cells, whereas overexpressed wildtype YAP or TAZ can fully substitute the endogenous proteins (Figure 11 E, F).
Summing up, YAP/TAZ biological effects in MDA-MB-231 cells are mediated by TEAD transcription factors, which were detected in the vast majority of YAP/TAZ binding sites and are required for YAP/TAZ binding to DNA.

YAP/TAZ as enhancer-associated transcription factors: focusing on Brd4

Summing up, our genome-wide analysis has revealed some general features of YAP/TAZ transcriptional activity. ChIP-seq data for YAP/TAZ and TEAD4 revealed that YAP/TAZ interaction with TEAD (previously demonstrated for a few, well characterized target genes, such as CTGF) extends to the vast majority (~80%) of YAP/TAZ binding sites. Second, YAP/TAZ and TEAD bind enhancers, which are usually actively engaged in transcriptional regulation (H3K27ac positive).
While we were carrying out this study in breast cancer cells, other groups obtained similar results in different cellular contexts. Stein et al. performed YAP and TEAD1 ChIP-seq in glioblastoma cells; they reported that 90% of YAP peaks are co-occupied by TEAD, and that only 4% of YAP/TEAD binding sites are located within 2kb of a TSS, whereas most of them are located on distal H3K27ac-positive regions; these results are strikingly similar to our own. Galli et al. profiled YAP, TEAD1 and TEAD4 chromatin occupancy in cholangiocarcinoma cells. The authors retrieved a small number of YAP binding sites compared to TEAD peaks (847 vs 11827); anyway, all YAP peaks had an overlapping TEAD peak and were located >20kb away from the closest TSS. In the same study, the authors observed that YAP-positive enhancers displayed a significantly higher density of H3K27 acetylation and H3K4 monomethylation compared to the average signal at active enhancers not occupied by YAP, that are features of the so-called super-enhancers (Galli et al., 2015). Super-enhancers are exceptionally large enhancer domains, containing clusters of “concatenated” enhancers; they display an unusually strong enrichment for the binding of transcriptional co-activators, such as Mediator (Med1), the histone acetyltransferases p300 and CBP or chromatin factors such as cohesion. Super-enhancers are occupied by master transcription factors and associated with key cell type-specific genes, implicating super-enhancers in the control of mammalian cell identity. Super-enhancers are enriched for disease-associated SNPs, particularly when the

super-enhancers were defined in disease-relevant cell types. In cancer cells, super-enhancers are enriched at genes with known oncogenic function.

Some associations between YAP/TAZ and proteins of the so-called "enhanceosome", a nucleoprotein complex that assembles at enhancers and connects transcriptional activators with the transcriptional machinery, have been recently reported. For example, YAP/TAZ interact with Med1, and they are functionally linked to p300 and CDK9. However, the nuclear mechanism of YAP/TAZ activity at enhancers remains poorly understood.

Super-enhancers in tumour cells are strongly enriched for binding of BRD4. BRD4 is a chromatin reader that positively regulates transcription by binding acetylated histones and core components of the transcriptional apparatus. BRD4 interacts directly with the Mediator complex, linking transcription factors with RNA PolII complex, and it facilitates of recruitment of the positive transcription elongation factor (PTEFb) to paused RNA PolII, allowing transcriptional elongation (Chiang, 2009). Given the important roles of both BRD4 and YAP/TAZ on the enhancers of cancer cells, we decided to investigate whether a functional interaction could exist between YAP/TAZ/TEAD and BRD4. We decided to focus on BRD4 also in light of the the availability of drugs targeting BET-proteins, which might be used to inhibit YAP/TAZ nuclear activity in cancer cells.

YAP/TAZ/TEAD interact with BRD4

We speculated that, if BRD4 has a role in activating the transcription of YAP/TAZ target genes, this must entail a contact between BRD4 itself and YAP/TAZ or TEAD.

To verify our hypothesis, we performed co-immunoprecipitation (IP) assays in nuclear extracts of MDA-MB-231 cells with anti-BRD4 antibody (we used pre-immune IgGs as negative control). We found that endogenous BRD4 associated with endogenous YAP and TEAD1. In a reciprocal experiment, we performed IP with anti-YAP antibody and we could detect BRD4 (along with TEAD1) in YAP immunocomplexes (Figure 12A).

To confirm *in vivo* the previously detected biochemical interactions, we performed Proximity Ligation Assay (PLA) in MDA-MB-231 cells. This immunofluorescence-based technique allows the visualization of endogenous protein complexes in individual fixed cells, as fluorescent dots appear only when proteins are very close to each other (40nm) (Koos et al., 2014). Furthermore, this assay allows to appreciate the subcellular localization of protein complexes.

MDA-MB-231 cells were seeded on fibronectin-coated glass chamber slides and fixed in 4% PFA before performing the proximity ligation assays with anti-BRD4 and anti-TEAD antibodies. As shown in figure 12B, we could detect BRD4-TEAD complexes (red dots) in the nuclei of MDA-MB-231 cells. As control, no dots could be detected in the nuclei when we performed the PLA omitting either of the primary antibodies. We couldn't find a good BRD4 primary antibody raised in mouse to be combined with our best performing YAP and TAZ antibodies produced in rabbit.

To better characterize the relationship between YAP/TAZ/TEAD and BRD4 proteins, we studied protein-protein interactions via biochemical analysis with purified, isolated proteins. First, we overexpressed HA-BRD4 in HEK293T cells and we used anti-HA antibodies to immobilize it on protein A-agarose beads. Then, we incubated this HA-BRD4-loaded resin with FLAG-tagged YAP, TAZ, or TEAD1 isolated from HEK293T protein extracts. After extensive washing, we checked by immunoblot which proteins had been capture by HA-BRD4. As shown in Figure 12C, FLAG-TEAD1 was efficiently captured by the HA-BRD4-loaded resin. FLAG-YAP interacted with HA-BRD4 only in the presence of FLAG-TEAD1, whereas FLAG-TAZ showed a tiny interaction with BRD4 and a stronger binding in the presence of FLAG-TEAD1. These data suggest that TEAD have a prominent role in stabilizing (if not mediating) the interaction between YAP/TAZ and BRD4.

Next, we immobilized HA-YAP on agarose beads and we incubated the HA-YAP-loaded resin with isolated FLAG-TEAD and FLAG-BRD4. BRD4 could be captured by HA-YAP only in the presence of FLAG-TEAD1, reinforcing the conclusion of the previous experiment (Figure 12D).

Overall, these data indicate that the transcriptional coactivator BRD4 can physically interact with YAP/TAZ/TEAD in the nucleus of MDA-MB-231 cells; within the complex, there is a direct interaction between BRD4 and TEAD, which serves to stabilize the YAP/TAZ-BRD4 interaction.

BRD4 binds the cis-regulatory elements of YAP/TAZ/TEAD target genes

We then wanted to assess if BRD4 occupies the cis-regulatory regions of YAP/TAZ target genes.

First of all, we performed chromatin immunoprecipitation with anti-BRD4 antibody followed by qPCR (ChIP-qPCR) in control and BRD4-depleted MDA-MB-231 cells, to verify the

specificity of the antibody. As a negative control, we performed the immunoprecipitation with pre-immune immunoglobulins to measure background signal. As shown in figure 13A, DNA regions enriched by BRD4 ChIP in control cells are not enriched in cells transfected with BRD4 siRNA, confirming the reliability of BRD4 antibody for ChIP.

We next verified that BRD4 could co-occupy chromatin with YAP/TAZ. Indeed, the sequences of a sample of YAP/TAZ-occupied enhancers were enriched in BRD4 ChIP, as well as their target promoters (even if the TSSs did not display YAP/TAZ binding sites) (Figure 13B).

At the time of writing this thesis, we just performed ChIP-seq experiments for BRD4, to assess the overlap between YAP/TAZ/TEAD and BRD4 binding sites genome-wide. Data analysis is currently in progress. However, preliminary visual inspection of some loci confirmed the results of ChIP-pPCR experiments described above.

Inhibition of BRD4 impairs the expression of YAP/TAZ/TEAD target genes.

Data presented so far prove that YAP/TAZ/TEAD can interact with BRD4 on chromatin in MDA-MB-231 cells. What are the functional implications of this interaction? To answer this question, we decided to investigate the effect of BRD inhibition at the genome wide level by RNA-sequencing in MDA-MB-231 cells, and to compare it with the effect of YAP/TAZ silencing.

We used two strategies to inhibit BRD. First, we knocked down BRD4 and its cognate proteins BRD2 and BRD3 with siRNAs; we chose to knockdown all the BRD transcripts because depletion of the sole BRD4 might induces compensatory effects by other BET-proteins, thus being not effective. Second, we pharmacologically inhibited BRD4 with a small molecule. As previously anticipated, BRD4 is an attractive therapeutic target. To date, a large number of compounds that target BET family proteins have been developed, and many are currently under clinical evaluation for the treatment of cancer. These small-molecules, such as JQ1, PFI-1 and I-BET762, directly target BRD4 and other BET proteins by occupying the amino-terminal bromodomains and impeding their binding to acetylated lysines of histones and transcription factors, thus restraining BRD activity (Filippakopoulos & Knapp, 2014). Early clinical trials have shown promising effects on treatments with BET-inhibitors in a variety of malignancies (Shi & Vakoc, 2014). We selected as paradigm JQ1 (thieno-triazolo-1, 4-diazepine), a potent and specific inhibitor of BET bromodomains.

We prepared duplicate samples for each of the following experimental conditions:

a) MDA-MB-231 cells transfected with control siRNA, or treated with DMSO (vehicle);
b) MDA-MB-231 cells transfected with two independent combinations of YAP/TAZ siRNAs for 48h;
c) MDA-MB-231 cells transfected with two independent combinations of siRNAs targeting BRD2-3-4 for 72h;
d) MDA-MB-231 cells treated with 1mM JQ1 for 24h.

Total RNA was extracted, depleted of rRNAs and analysed by sequencing. To get a general picture of the results, we performed unsupervised hierarchical clustering of samples, based on the transcripts displaying the highest variations between the various experimental conditions: we found that samples treated with JQ1 clustered with BRD-depleted cells, and with YAP/TAZ depleted cells, suggesting that YAP/TAZ depletion and BRD inhibition must have some overlapping effects (Figure 13C). More in detail, YAP/TAZ/TEAD-dependent transcription in MDA-MB-231 cells was in large part sensible to BRDs depletion or JQ1 treatment. In particular, YAP/TAZ are required for the activation of ~2100 genes; 68% of these genes were downregulated after JQ1 treatment (Figure 13D), and most of these genes (~930) were also downregulated by BRD depletion with both combinations of siRNAs. Although JQ1 has, as expected, a wider effect compared to YAP/TAZ depletion (inducing the downregulation of ~3000 genes), our data suggest that it can inhibit the expression of a large fraction of the YAP/TAZ transcriptional targets in MDA–MB-231, and that YAP/TAZ target genes are more likely to be sensitive to JQ1 treatment compared with non YAP/TAZ targets (Chi-square test with Yates correction, $p < 0.0001$). We plan to complement this analysis which ChIP-seq results, to assess to which extent this positive correlation between YAP/TAZ activity and sensitivity to JQ1 can be attributed to the joint control of the promoter by BRD4 and YAP/TAZ.

BRD4 is instrumental for YAP/TAZ biological activity

We then wanted to assess whether BRD inhibition could block YAP/TAZ biological activity. As readout, we evaluated transforming capacity, as measured by colony formation in soft agar, a clonal assay in anchorage-independent growth conditions, used to test cell transformation and aberrant growth.

First, we examined colony formation after knockdown of BRD4 in MDA-MB-231 cells, whose ability to form colonies in soft agar depends on YAP/TAZ. For this, we transduced MDA-MB-231 cells with lentiviruses carrying doxycycline inducible shRNAs (shCO, shBRD4#1 or shBRD4#2). By immunoblotting, we validated the efficiency of shRNAs for BRD4 in MDA-MB-231 cells. Both BRD4 shRNAs were able to reduce BRD4 protein levels upon shRNAs expression by doxycycline treatment for 5 days (Figure 14A). Cells were seeded into soft agar in the absence or presence of doxycycline and allowed to grow for 3 weeks; subsequently, cells were fixed and the number of colonies was recorded. BRD4 knockdown reduced the number of colonies formed by MDA-MB-231 cells (Figure 14B).

Next, we tested if BRD4 is instrumental for YAP/TAZ activity during transformation in another system. For this, we transduced immortalized non-tumorigenic mammary epithelial cells (MCF10A) with vectors encoding for an activated version of YAP (YAP5SA, lacking all LATS phosphorylation sites causing increased YAP nuclear localization). Control cells (empty-vector-transduced) were not able to form colonies in soft agar, whereas YAP overexpression conferred MCF10A cells the capacity to seed colonies with high efficiency. YAP5SA-overexpressing cells were transduced with lentiviral vectors carrying inducible shRNAs (shCO, shBRD4#1 or shBRD4#2; see figure 14C for knockdown efficiency); combined expression of YAP5SA and BRD4 shRNAs strongly reduced colony formation compared to cells expressing both YAP5SA and shCO (Figure 14D). Summing up, BRD4 is required for YAP-dependent transformation of mammary epithelial cells.

Prompted by these results, we next asked whether we could achieve inhibition of YAP oncogenic function by pharmacological inhibition of BRD4 with JQ1. Consistently with the results obtained with BRD4 shRNAs, treatment with JQ1 blunted or even abolished the growth of colonies in soft-agar from both MDA-MB-231 cells and YAP-overexpressing MCF10A cells in a dose-dependent manner (Figure 14E,F).

Next, we asked if JQ1 affected colony progression, beyond colony initiation. For this, we performed soft agar assays with MCF10A-YAP cells and started JQ1 treatment at different time points (at the moment of seeding, or 7 or 15 days later). Starting the treatment 7 or 15 days after seeding, fewer cells grew enough to form sizable colonies, thus confirming that JQ1 impaired the growth of already established colonies (Figure 14G). In conclusion, YAP/TAZ require BRD4 to mediate oncogenic cell growth in vitro, and treatment with JQ1 led to significant inhibition of YAP/TAZ-dependent proliferation, phenocopying BRD4 knockdown.

JQ1 does not affect BRD4-TEAD interaction or YAP/TAZ recruitment on enhancers

Results described so far delineate a model whereby a physical interaction between YAP/TAZ/TEAD and BRD4 on chromatin mediates the activation of YAP/TAZ target genes and YAP/TAZ biological activity in breast cancer cells; inhibition of BRD4 with JQ1 blocks these events.

We have performed some experiments to investigate how JQ1 impairs the activity of the YAP/TAZ/TEAD/BRD4 complex.

As shown in figure 12, BRD4 could directly interact with TEAD1 and this interaction stabilized BRD4 association with YAP and TAZ, too. We found that JQ1 does not interfere with these interactions. HA-BRD4 immobilized on agarose beads was able to capture FLAG-TEAD1 also in the presence of JQ1 in the reaction buffer (Figure 15A).

In cell extracts of MDA-MB-231 cells treated with 1 mM JQ1 for 6h (a time sufficient to detach BRD4 from chromatin, see below), TEAD1 and YAP co-precipitated with BRD4 also in the presence of JQ1. A different compound targeting the bromodomain (PFI-1) had the same inconsequential effect as JQ1 (Figure 15B). These results exclude that JQ1 directly changes the affinity between BRD4 and TEAD1 (and YAP).

JQ1 competes with acetylated histone tails to bind the bromodomain of BET-proteins, resulting in BRD4 release from chromatin. We reasoned that JQ1 (while not affecting the capacity of BRD4 to interact with TEAD and YAP/TAZ per se), might lead to the detachment of the whole complex from chromatin.

Thus, we performed ChIP-qPCR experiments with anti-YAP/TAZ antibodies in MDA-MB-231 cells treated with 1 mM JQ1 for 6h. Contrary to our hypothesis, YAP/TAZ bound their cis-regulatory regions with the same strength both in DMSO and in JQ1-treated cells (Figure 15C). Instead, BRD4 binding to the same loci was reduced in the presence of JQ1 (Figure 15D). These results suggest that JQ1 does not affect YAP/TAZ capacity to remain bound on chromatin.

Loss of BRD4 impairs Pol II recruitment on YAP/TAZ/TEAD-regulated genes

Our evidence indicates that BRD4 has an essential role in mediating YAP/TAZ/TEAD transcriptional and biological activities in breast cancer cells and that BRD4 acts after YAP/TAZ recruitment to chromatin.

BRD4 interacts with Mediator complex, linking transcription factors with RNA-polymerase II (Pol II). In particular, BRD4 recruits PTEF-b (positive transcriptional elongation factor b), which contains a kinase (CDK9) that phosphorylates Pol II on its carboxy terminal domain (CTD), activating transcriptional elongation by releasing Pol II promoter pausing.

Thus, we compared the phosphorylation state of Pol II in MDA-MB-231 cells by immunoblotting upon depletion of BRDs or YAP/TAZ by siRNAs, or JQ1 treatment. The level of Pol II protein was the same in all the different conditions, but the phosphorylation of Pol II on Ser2 (the target of CDK9) was reduced (Figure 16A). Thus, active elongation is impaired in YAP/TAZ depleted cells, as well as after BRD inhibition.

We reasoned that defective elongation might be explained either by the specific inhibition of elongation, or by a reduced recruitment of Pol II on transcription start sites (TSS). To discriminate between these two possibilities, we performed ChIP-qPCR experiments with anti-Pol II antibody (and with pre-immune immunoglobulins as negative control) in MDA-MB-231 cells, upon transfection with siBRDs, siYAP/TAZ or treatment with JQ1. We investigated the recruitment of Pol II on the TSS of genes regulated by YAP/TAZ from enhancers, that we know to be regulated by YAP/TAZ and BRD from our RNA-seq analysis. We found that Pol II loading on the promoters of YAP/TAZ target genes is specifically reduced upon depletion of YAP/TAZ or BRDs or JQ1 treatment, compared to control cells (Figure 16B). Instead, Pol II recruitment to GAPDH promoter (representing a non-YAP/TAZ target) was either not affected or even increased in the case of JQ1, suggesting a specific effect on YAP/TAZ target genes, rather than a general/aspecific reduction of Pol II recruitment to TSSs.

In conclusion, our results pointed to recruitment of Pol II as the crucial step downstream YAP/TAZ/TEAD and BRD4 interaction.

DISCUSSION

YAP/TAZ bind distal enhancers to activate a cell-growth transcriptional program

The work here presented focuses on YAP/TAZ nuclear function as regulators of gene expression. YAP/TAZ have fundamental roles in important biological processes and much effort has been dedicated to the study of their function in embryonic development, normal tissue homeostasis and cancer, and to the investigation of the mechanisms that regulate YAP/TAZ nuclear availability. Instead, how YAP/TAZ work in DNA the nucleus (the genetic program they activate, the way they interact with chromatin, their co-factors) have received less attention. Most of our knowledge was based on few paradigmatic target genes (such as the regulation of CTGF), but systematic studies were missing.

In this thesis, we performed an unbiased study of YAP/TAZ transcriptional activity, by carrying out genome-wide analyses of YAP/TAZ binding sites in breast cancer cells through ChIP-seq, coupled to transcriptomic profiling. Our analysis revealed that the vast majority (91%) of YAP/TAZ-bound cis-regulatory regions coincides with enhancer elements, located distant from transcription start sites (TSS). The only previous genome-wide analysis of YAP binding sites used DNA microarrays to identify ChIP'd DNA (ChIP on chip), and the array only contained promoter sequences; thus, it actually could detect only a fraction of YAP binding sites (B. Zhao et al., 2008). Our discovery that YAP/TAZ binding to enhancers was confirmed by other groups in different tumour types (Galli et al., 2015; Stein et al., 2015), strongly suggesting that binding to distal regulatory regions is the preferred modality of gene regulation by YAP/TAZ, at least in cancer cells.

Recent studies reported that enhancer usage is altered in cancer cells in comparison with their normal counterparts (Pott & Lieb, 2015). We speculate that YAP/TAZ aberrant activation in cancer might have a role in the reshuffling of enhancer usage in tumor cells.

As we aimed at defining YAP/TAZ transcriptional program in MDA-MB-231 cells, we had to deal with the task of matching YAP/TAZ-occupied enhancers with the genes they regulate. Most strategies to assign a TF binding site to its target gene are based on proximity, that is, it is assumed that the target promoter is the closest one in the linear DNA sequence. However, genomes are known to be organized in 3D structures, whereby distant enhancers are in physical contact with regulated promoters by chromatin looping. Recently, Jin et al. defined a map of enhancer-promoter contacts in human fibroblasts by Hi-C. We used this map to

associate distal YAP/TAZ-binding sites with regulated promoters, discovering a wide list of new YAP/TAZ direct target genes. By gene ontology analysis, we identified the regulation of cell proliferation as the main biological process in which are involved YAP/TAZ direct target genes. In fact, most YAP/TAZ effectors are proteins directly involved in specific steps of the cell cycle, such as assembly of the licensing complex, DNA replication and repair, chromosome segregation and cytokinesis. These are critical and common elements in most YAP/TAZ-dependent biological events, such as organ growth and tissue regeneration, that can hardly be explained by sporadic set of YAP/TAZ downstream targets discovered so far in mammalian cells. Instead, we show that the growth-controlling transcriptional program of YAP/TAZ is vast and redundant and includes other transcription factors, that might propagate YAP/TAZ message. MYC is one example. We exploited MYC as a paradigm to verify that transcription is directly controlled in breast cancer cells by YAP/TAZ-bound enhancers through chromatin looping. Functionally, MYC is a relevant, albeit only partial YAP/TAZ effector.

YAP/TAZ associate with TEAD transcription factors genome-wide

YAP/TAZ indirectly bind DNA through other transcription factors. A number of DNA-binding platforms have been reported for YAP/TAZ, including TEAD1-4, RUNX, p73, TBX5, and others. Most of these studies have been based on few targets or reporters, but a genome-wide view of the determinants that recruit YAP/TAZ to the chromatin was lacking. Our genome-wide data revealed that TEAD proteins are the major platform through which YAP/TAZ bind DNA in breast cancer cells. 75% of YAP/TAZ ChIP-seq peaks contain a TEAD motif that often occupies the summit of YAP/TAZ peak, i.e. the point where the immunoprecipitated protein sit. By carrying out a TEAD4 ChIP-seq, we confirmed that 78% of YAP/TAZ binding sites are indeed shared by TEAD. TEADs are required to recruit YAP/TAZ to chromatin and they are essential for YAP/TAZ transcriptional functions, supporting the view that TEADs determine where YAP/TAZ bind DNA to regulate transcription. Thus, even though a plethora of potential partners exist, our data indicate that YAP/TAZ mainly cooperate with TEAD proteins in MDA-MB-231 cells. In fact, by comparison, of the various transcription factors proposed to work as YAP/TAZ DNA-binding platforms, only RUNX1/2 motif is observed in YAP/TAZ peaks on MDA-MB-231 cells. However, RUNX1/2 is not preferentially enriched close to the summit of the YAP/TAZ peaks and thus it is unlikely that YAP/TAZ bind RUNX1/2 to attach to DNA.

YAP/TAZ interact with the transcriptional regulator BRD4

How do YAP/TAZ activate transcription? What connects them with the RNA polymerase complex?

The finding that YAP/TAZ occupy enhancers suggested us to focus on BRD4. BRD4 was found to regulate the expression of oncogenic drivers through occupying super-enhancers in multiple myeloma cells and other tumors (Lovén et al., 2013), nicely paralleling YAP/TAZ oncogenic transcriptional activity (Galli et al., 2015).

BRD4 was originally identified as a mitotic chromosome binding protein that remains associated with acetylated chromatin throughout the entire cell cycle providing an epigenetic memory (mitotic bookmark) (Zhao, Nakamura, Fu, et al., 2011). BRD4 also participates in transcription: first, it acts as a scaffold, recognizing active DNA sites and recruiting transcriptional apparatus through Mediator complex and PTEFb elongation factor; second, BRD4 shows a kinase activity, which phosphorylates C-terminal domain (CTD) of the Pol II. Recently, it was demonstrated that BRD4 is also a histone acetyltransferase (HAT) that evicts nucleosome from chromatin (Devaiah et al., 2016).

BRD4 is essential for mouse embryonic development: *Brd4* full knockout results in early embryonic lethality, and heterozygosity for *Brd4* leads to pre- and postnatal growth defects that are associated with reduced proliferation in vitro and in vivo (Houzelstein et al., 2002). These data support the essential role of BRD4 in normal cells.

In cancer, BRD4 represents a non-oncogenic addiction: it is not an oncogene (unless when fused with NUT in the very rare and aggressive midline carcinoma), but its function is required for cancer cell survival. Indeed, BRD4 is an attractive therapeutic target and several drugs targeting BET-proteins are available (Filippakopoulos & Knapp, 2014). Some of the chemical compounds targeting BRD4 are currently under pre-clinical or clinical evaluations for the treatment of cancer and show promising effects in a variety of malignancies (Shi & Vakoc, 2014). That said, not all tumor cells are equally sensitive to BET-inhibitors, and it is still unclear what determines therapy efficacy or failure.

Prompted by the prominent role of both YAP/TAZ and BRD4 on enhancers in cancer cells, we postulated that they might indeed work together. Actually, we demonstrated that BRD4 could form a complex with YAP/TAZ through direct binding with TEAD proteins in the nucleus of breast cancer cells, connecting YAP/TAZ with the basal transcriptional machinery. By ChIP experiments, we observed that BRD4 could occupy enhancers and promoter regions of YAP/TAZ target genes. Thus, we speculated that BRD4 is necessary to relay YAP/TAZ transactivating signal to target genes.

BET inhibitors block YAP/TAZ transcriptional and biological activity

In the first part of our project, we discovered that YAP/TAZ regulate a complex transcriptional program mediating their biological functions. Notably, both BRD4 depletion and JQ1 treatment led to significant inhibition of YAP/TAZ-dependent cell transformation and aberrant growth in vitro. Overall, YAP/TAZ/TEAD and BRD4 interactions resulted essential for YAP/TAZ biological activity in vitro. Transcriptome analysis by RNA-seq suggested that YAP/TAZ/TEAD-dependent transcription in breast cancer cells was in large part sensible to BRD proteins depletion or JQ1 treatment. BRD4 is a general regulator of transcription, thus we reasoned that the above transcriptional effects on MDA-MB-231 cells of BRDs knockdown, as well as the pharmacological inhibition that we observed, might be the result of a global inhibition of transcription. We observed that JQ1 treatment inhibited and activated the expression of similar number of transcripts, suggesting that it does not act as an aspecific inhibitor of transcription; instead, it seems to induce specific changes in the cellular transcriptional program mediated by YAP/TAZ.

How does JQ1 impair the activity of the YAP/TAZ/TEAD/BRD4 complex? We excluded that JQ1 inhibitor directly changes the affinity between BRD4 and TEAD1 (and YAP), nor it affects YAP/TAZ capacity to remain bound on chromatin. More studies will be required to decipher the molecular mechanism of the interaction between YAP/TAZ/TEAD and BRD4, and how it's affected by JQ1. At the end of this cascade, BRD proteins mediate the recruitment of Pol II to the TSSs of YAP/TAZ target genes, as demonstrated by Pol II ChIP-qPCR experiments.

In conclusion, we have identified BRD4 (a general transcriptional regulator) as a functional partner of YAP/TAZ/TEAD, revealing a new aspect of YAP/TAZ activity as transcriptional co-activators on enhancers. Conversely, we wish that the follow-up of this study will shed new light on BRD4 activity in cancer cells.

The underlying molecular mechanism of BRD4 activity in cancer is poorly understood. In agreement with our transcriptomic data, studies with BET inhibitors indicate that not all genes are equally affected by JQ1, but instead transcription is disproportionately suppressed at specific sites. Little is known about how the gene-specific activity of BRD4 is determined (Wu et al., 2013). BRD4 lacks specific DNA binding motif. Our data rise the possibility that BRD4 and its associated transcriptional complex are recruited to gene-specific promoters/enhancers by YAP/TAZ in cancer.

In the long run, we wish to establish a functional link between the addiction to YAP/TAZ that some cancer cells display, and responsiveness to drugs targeting BET proteins. If this link

indeed exists, it might provide the rationale to use YAP/TAZ activation (which can be diagnosed in tumor biopsy by IHC for YAP/TAZ themselves, or by gene expression profiling) as a predictive marker for response to BET-inhibitors.

MATERIALS AND METHODS

The methods here listed are part of the Piccolo's Lab protocol book and thus presented with minor modifications, if any, in respect to published material or other thesis works published by our Lab.

Reagents and Plasmids

pCS2-FLAG-mTAZ, pCDNA-HA-YAP, pCDNA-FLAG-YAP and pBABE-hygro-FLAG-mTAZ wild-type were previously described (Zanconato et al., 2015). FLAG-mTAZ S51A was generated by PCR from pCS2 FLAG mTAZ wild-type (Dupont et al., 2011) and subcloned in pBABE-hygro. pBABE-puro-hYAP wild-type was obtained subcloning FLAG-hYAP1 wild-type siRNA insensitive (pCDNA3-FLAG-hYAP1 wild-type siRNA insensitive) in the retroviral vector. FLAG-hYAPS94A was generated by PCR from pCDNA3-FLAG-hYAP wild-type (Aragona et al., 2013) and subcloned in pBABE retroviral plasmid (pBABE-puro) to establish stable cell-lines. pBABE-hygro (#1765) and pBABE-puro (#1764) empty retroviral vectors were purchased from Addgene. pCMV6-FLAG-MYC-TEAD1 was from Origene.

FU-tet-o-hc-myc (#19775, Maherali et al., 2008) and FUdeltaGW-rtTA (#19780, Maherali et al., 2008) were purchased from Addgene. FU-tet-o-EGFP-ires-PURO was described in Cordenonsi et al., 2011. pCMV2-FLAG-BRD4 was from Addgene (#22304). pCS2 HA-BRD4 was generated by PCR from pCMV2-FLAG-BRD4 and subcloned in pCS2+ plasmid.

Annealed oligos for shRNAs (shCO –mNF2-, shBRD4#1, shBRD4 #2, listed in TABLE 3) were cloned into TetON pLKO.puro from Addgene (#21915).

All constructs were confirmed by sequencing.

Doxycycline and PFI-1 were from Sigma Aldrich; JQ1 was from BPS Bioscience (#27402).

Cell culture conditions

MDA-MB-231 cells were from ICLC. MDA-MB-231 cells were authenticated by DNA profiling of highly polymorphic STR loci. MDA-MB-231 cells were cultured in DMEM/F12 (Life Technologies) supplemented with 10% FBS (foetal bovine serum), 1% (2mM) glutamine and 1% antibiotics. After infection with doxycycline-inducible vectors, MDA-MB-231 cells were maintained in media supplemented with Tet-approved FBS (Clontech), to reduce background expression of the transgene in the absence of doxycycline.

MCF10A cells were from ATCC. MCF10A cells were cultured in DMEM/F12 (Life Technologies) with 5% HS (horse serum), 1% glutamine and 1% antibiotics, freshly supplemented with insulin, EGF, hydrocortisone, and cholera toxin. HEK293T and 293GP cells (packaging cell lines for viral particles production) were cultured in DMEM (Life Technologies) supplemented with 10% FBS, 1% glutamine and 1% antibiotics.

siRNA transfection

siRNA transfection was performed using Lipofectamine® RNAiMAX (Life technologies) in antibiotics-free medium (Opti-MEM® Medium). Cells were seeded in a 6-well plate to be 30-40% confluent at transfection. For each transfection, 100 pmol of siRNA were diluted in 250 µl of Opti-MEM® medium and subsequently added to 5 µl of Lipofectamine® RNAiMAX Reagent diluted in 250 µl of Opti-MEM® medium. This mix was incubated for 15 minutes at room temperature and added to the cells. siRNA sequences are in TABLE 3. Cells were harvested 48h after transfection, unless differently specified.

DNA transfection

DNA transfections were performed with TransitLT1 (Mirus Bio). LT1 reagent and serum free medium (Opti-MEM® Medium) were mixed and incubated 5 minutes; then we added plasmid

DNA to previous mix, incubating other 15 minutes. Finally, the transfection mix is homogeneously distributed on cells.

Total RNA extraction and cDNA synthesis

RNA was purified using RNeasy mini kit (Qiagen; 74106). Cells were harvested in Buffer RLT supplemented with 40mM dithiothreitol. Lysates were mixed with one volume of 70% ethanol, transferred to RNeasy Mini spin columns and centrifuged for 30 seconds. The column was washed with RW1 Buffer, and then incubated for 15 minutes at room temperature with DNaseI in RDD Buffer to minimize contamination of the extracts with cellular DNA. A wash with RW1 Buffer and other two washes with RPE Buffer were necessary to improve RNA yield and purity. RNA was eluted in 30-50µL of RNase-free water by centrifuging columns for 1 minute. Total RNA was quantified using the NanoDrop ND-1000 Spectrophotometer (NanoDrop Technologies Inc.).

1ug of total RNA was heated for 5 minutes at 70°C and left on ice for 1 minute to denature possible secondary structures that could interfere with the retrotranscription process. Then, retrotranscription reaction mix was added; the mix contains FS buffer, 0,01M DTT, 2 mM dNTPs mix, 25 ng of oligo-dT , 100U Mo-MLV Reverse Transcriptase (Life Technologies; 28025-013), 40U RNaseOUT (Life Technologies; 10777-019) and RNase-free water (Ambion) up to 11 µL. Retrotranscription was carried out for 1hour and half at 37°C. The reaction was then inactivated at 70°C for 10 minutes and samples were prepared for qRT-PCR

Quantitative Real-Time PCR (qRT-PCR)

Quantitative real-time PCR (qPCR) analyses were carried out on retrotranscribed cDNAs with Rotor-Gene Q (Quiagen) thermal cycler. Every amplification reaction contained: 5 µL of diluted cDNA, 0.75 µL of forward and reverse primers (0.5 µM each), and FastStart SYBR Green Master (Roche) in 15 µL. Amplification was carried out as follows: 10 seconds at 95 °C, 15 seconds at 60 °C, 20 seconds at 72 °C for 40 cycles. Each sample was run in triplicate; expression values of test genes were normalized to GAPDH expression.

Primer sequences are listed in (TABLE 4).

For gene expression analysis with TaqMan Arrays cDNA was synthesized with High Capacity RNA-to-cDNA Kit (Invitrogen). Target genes were then quantified with custom TaqMan Low Density Arrays on a 7900HT Fast Real-Time PCR System (Applied Biosystems), using TaqMan Universal PCR Master Mix (Applied Biosystems). TaqMan assays included in the array are listed in TABLE 6. Expression levels are normalized to GAPDH.

RNA sequencing

For total RNA extraction RNeasy Mini Kit (QIAGEN) was used, and contaminant DNA was removed with RNase-Free DNase (QIAGEN). Libraries for deep-sequencing were prepared with the Illumina TruSeq Standard Total RNA with Ribo-Zero GOLD kit, and sequencing was performed with Illumina HiSeq2500. About 20M reads/sample were obtained. Reads were aligned to the human genome (GRCh37/hg19) with TopHat2; expression levels and differentially expressed genes were determined with HTseq and edgeR.

ImmunoBlot analysis

Whole cell lysates were obtained by sonication in lysis buffer (20 mM HEPES [pH 7.8], 100 mM NaCl, 5% glycerol, 5 mM EDTA, 0.5% Np40, and protease and phosphatase inhibitors) with a water bath cell disruptor (Diagenode Bioruptor). The lysate was centrifuged 10 minutes at 4 °C to eliminate the insoluble fraction. Total protein concentration of lysates was measured by Bradford quantitation, staining proteins with Coomassie Blue G250 and measuring the absorbance of the solution at 595 nm (a calibration curve was prepared with

increasing BSA amounts). Protein extracts were boiled 3 minutes at 95 °C in 1X FSB (50mM Tris-HCl, pH 6.8; 2% SDS; 0.1% bromophenol blue; 10% glycerol; 2% 2-mercaptoethanol).
Equal amounts of protein were separated by SDS-PAGE in commercial 4-12% or 10% Nupage MOPS acrylamide gels (Invitrogen) and transferred onto PVDF membranes (ImmobilonP) by wet electrophoretic transfer (50 mM Tris; 40 mM Glycine; 20% methanol; 0.04% SDS). In general, blots were blocked one hour at RT with 0,5% non-fat dry milk (BioRad) in TBSt (0,05% Tween) and incubated o.n. at 4°C with primary antibodies (listed in TABLE 2). Horseradish peroxidase-conjugated secondary antibodies were incubated 1 hour at RT. Blots were developed with Pico or Dura SuperSignal West chemiluminescent reagents (Pierce). Chemiluminescence was digitally acquired with ImageQuant LAS 4000.

Immunoprecipitation
For immunoprecipitation experiments from whole cell lysates, cells were lysed by sonication lysis buffer (20 mM HEPES pH 7.8, 400 mM KCl, 10% Glycerol, 5 mM EDTA, 0.4% NP40), freshly supplemented with 1 mM DTT, and protease and phosphatase inhibitor cocktails and cleared by centrifugation. Before immunoprecipitation, extracts were diluted to 20 mM HEPES (pH 7.8), 100 mM NaCl, 5% Glycerol, 2.5 mM MgCl2, 1% TritonX100 and 0.5% NP40 and incubated O/N at 4°C with specific primary antibody or IgG (listed in TABLE 2). Protein A or G-magnetic beads (from Invitrogen) were incubated O/N at 4°C in PBS with 2% BSA and 0.05% CHAPS. Next, immunoprecipitation preps were incubated with magnetic beads at 4 °C for 2 hours. Immunocomplexes were then washed with cold binding buffer four times, resuspended in SDS sample buffer, and subjected to SDS-PAGE and Immuno blot analysis. For overexpressed proteins, HEK293T cells were firstly transfected with 80 ng/cm^2 of relative plasmid; DNA amount was adjusted to 160 ng/cm^2 with pBluescript.
For immunoprecipitation of endogenous nuclear proteins, we performed nuclear protein extraction. MDA-MB-231 cytoplasmic membranes were first lysed by hypotonic buffer (20mM HEPES, 20% Glycerol, 10mM NaCl, 1.5mM $MgCl_2$, 0.2mM EDTA, 0.1% NP40). Nuclei were then obtained by centrifugation and lysed with hypertonic buffer (hypotonic buffer, 500mM NaCl). Extracts were diluted to 140mM NaCl. Next, samples are processed as above.
For immuniprecipitation from purified proteins, HA-tagged protein (BRD4 or YAP) was overexpressed in HEK293T cells; anti-HA antibody was used to immobilize HA-tagged protein on protein A-agarose beads. HA-resin was incubated with FLAG-tagged proteins, isolated from HEK293T protein extracts, at 4C O/N. Immunocomplexes were then washed with binding buffer.
Where indicated, cells were treated for 24h with chemical compounds, contained also in buffers for immunoprecipitation.

In situ proximity ligation assay (PLA)
In situ PLA was performed with DuoLink In Situ Reagents from Olink Bioscience (Sigma). MDA-MB-231 cells seeded in fibronectin-coated glass chamber and fixed slides 24h later in 4% PFA for 10 min at RT. Proximity ligation assays were performed as indicated by the provider's protocol, after an overnight incubation with primary antibodies (listed in TABLE 2) following the immunofluorescence protocol: slides were permeabilized 10 min at RT with PBS 0.3% Triton X-100, and blocking in 10% Goat Serum (GS) in PBST for 1 hr followed by incubation with primary antibody (diluted in 2% GS in PBST) for 16 hr at 4 C. Images were acquired with Leica SP5 confocal microscope equipped with a CDD camera; for each field, a Z-stack was acquired; images were processed using Volocity software (PerkinElmer).

Growth Assay

For growth assays, cells were seeded in 96-well plates (4000 cells/well) and fixed daily (or at the time points indicated in figures), starting 18h after seeding, to verify that a similar number of cells was present in all experimental conditions at the beginning of the time course. siRNA transfection was performed in cell culture dishes for 6h before seeding cells in 96-well plates. Doxycycline was added at the time of transfection, if required. For fixation and staining, wells were washed once with PBS and cells were incubated with a crystal violet solution (0.05% w/v Crystal violet, 1% formaldehyde, 1% methanol in PBS) for 20 min at room temperature; stained cells were washed with water until a clear background was visible, and air-dried. Crystal violet was extracted with 1% SDS (w/v in ddH_2O, 100 mL/well) and absorbance at l=595 nm was measured with an Infinite F200PRO plate reader (TECAN). 8 replicates were analysed for each sample; data are presented as mean + SD.

Cell cycle analysis

To determine the fraction of cells in each phase of the cell cycle, subconfluent cells were trypsinized 48 hours after siRNA transfection, washed with PBS and fixed in cold 70% ethanol at -20 °C for at least one hour. Doxycycline was added at the time of transfection, if required. Fixed cells were washed in PBS and incubated in PBS containing Triton 0.1%, 20 μg/ml Propidium Iodide and 0.2 mg/ml RNaseA for 20 minutes at room temperature. Stained cells were analyzed on a FC500 cytofluorimeter (Beckman Coulter).

Soft agar assay

For soft agar assay, 10^4 MCF10A cells/well and $3*10^4$ MDA-MB-231 cells/well in complete growth medium with 0.35% agar were layered onto 0.5% agar beds in six-well plates. Complete medium was added on top of cells and was replaced with fresh medium twice a week for 15-21 days. Complete medium contained also treatments as indicated. Colonies larger than threshold of diameter were counted as positive for growth. Thresholds were arbitrary set to classify colonies according to their size.

Generation of Retroviral and Lentiviral particles and infection

To generate retroviral particles we used 293 GP cells, a packaging cell line that constitutively express retroviral proteins: Gag and Pol, whereas are supplied by transient transfection of an expression vector. These proteins are required for the correct formation of our retroviral particles. Our retroviral vector and the plasmid expressing Env (pmd2-Env) were all transfected with TransIT-LT1 (MirusBio) in 293 GP packaging cell line, previously seeded on a 10 cm diameter dish. Colture medium containing viral particle was collected 24-48 hours after transfection and filtered to discard an cellular debris. Viral surnatant was diluted with complete colture medium of cells to infect. Infection was performed by colturing cells with virus-containing medium for 24 hours. Our retroviral vectors contain an antibiotic resistance gene that allows us to select infected cells, by maintaining them in medium with antibiotic (1μg/mL of Puromycin, Higromycin). Together with infected cells transduced cells were cultured in the presence of antibiotic to verify the effective disappearance of not-resistant cells. Usually in a week all un-transduced cells should die, meaning the correct functioning of the selection agent and infection procedeure.

Similar procedure has been followed for the production of lentiviral particles: lentiviral vectors were transfected in 293T cells in combination with Gag-Pol (psPAX2) and Env (pmd2-VSVG) coding plasmids. In contrast to retroviral constructs, lentiviral vectors do not contain any resistance gene. Recombinant lentiviral particles were harvested from the supernatant and used to transduce cells.

Chromatin immunoprecipitation (ChIP)

Cells were seeded in 175 cm^2 cell culture dishes, and transfected with siRNA if required. After 48 hours, 1/10 volume of fresh 11% Formaldehyde Solution (50 mM Hepes-KOH pH 7.5, 100 mM NaCl, 1 mM EDTA, 0.5 mM EGTA, 11% Formaldehyde) was added to plates and they were swirled at room temperature for 10 minutes. Formaldehyde was quenched by adding 1/20 volume of 2.5 M glycine to plates for 5 minutes. Cells were washed twice with ice-cold PBS and harvested in PBS supplemented with protease inhibitors. Collected cells were centrifuged and pellets were resuspended in Lysis Buffer 1 (50 mM Hepes-KOH pH 7.5, 10 mM NaCl, 1 mM EDTA, 10% glycerol, 0.5% NP-40, 0.25% Triton X-100) and incubated at 4°C for 20 minutes. Cells were centrifuged and pellets were washed in Lysis Buffer 2 (10 mM Tris-HCl pH 8.0, 200 mM NaCl, 1 mM EDTA, 0.5 mM EGTA) by gently rocking at room temperature for 10 minutes. After centrifugation, pellets were resuspended in Lysis Buffer 3 (10 mM Tris-HCl pH 8.0, 100 mM NaCl, 1 mM EDTA, 0.5 mM EGTA, 0.1% Na-Deoxycholate, 0.5% N-lauroylsarcosine). Chromatin was sheared to 200-600bp fragments using a Branson Sonifier 4500D for 4 minutes (30% output, 0.4s duty cycle). Lysates were cleared by centrifugation. The size of fragment was checked by agarose gel electrophoresis. 1% Triton X-100 was added to chromatin before immunoprecipitation.

For ChIP-qPCR, ~100 µg of sheared chromatin and 3-5µg of antibody were used. For ChIPs of modified histones, at least 50 µg of chromatin were incubated with 2 µg of antibody. These mix were left rotating overnight at 4°C. Immunocomplexes were recovered with magnetic beads functionalized with Protein A (Dynabeads protein A from Invitrogen), blocked overnight in PBS + 0.5% BSA. Chromatin preps were incubated with magneti beads at 4°C for 2 hours. Using a magnetic stand, the beads were collected and washed twice with Wash Buffer Low Salt (0.1% SDS, 2 mM EDTA, 1% Triton X-100, 20 mM Tris pH 8.0, 150 mM NaCl) and Wash Buffer High Salt (0.1% SDS, 2 mM EDTA, 1% Triton X-100, 20 mM Tris pH 8.0, 500 mM NaCl). Beads were finally washed with Tris-EDTA containing 50 mM NaCl. The elution was performed by incubating the beads in elution buffer (Tris-EDTA + 1% SDS) at 65°C for 20 minutes. Beads were removed and the supernatants were incubated at 65°C overnight to reverse crosslink. RNA and proteins were digested by adding RNaseA (0.2 µg/ml final concentration) and proteinaseK (0.2 µg/ml final concentration) and incubating them at 37°C for one hour and at 55°C for one hour, respectively. DNA was purified with phenol/chloroform extraction and ethanol precipitation. DNA was pelleted and washed with 70% ethanol. Pellets were dried and resuspended in 20 uL of 10 mM Tris-HCl pH 8.0. A small aliquot of chromatin (2-5% of the volume used for immunoprecipitation) was saved as input chromatin. Input chromatin was not subjected to immunoprecipitation, but was de-crosslinked and purified together with ChIPed samples. Quantitative real-time PCR was carried out with a Rotor-Gene Q (Qiagen) thermal cycler to verify the enrichment of specific DNA sequences; each sample was analyzed in triplicate. ChIPed DNA was diluted 1:5, input DNA was diluted 1:250. For each sample, triplicate PCR reactions were run with 5 uL of diluted DNA, 1 uM primer mix and FastStart SYBR Green Master (Roche). Amplification was carried out as follows: 10s at 95°C, 15 seconds at 60°C, 20s at 72°C for 45 cycles. The amount of immunoprecipitated DNA in each sample was determined as fraction of input [amplification efficiency^(Ct INPUT-Ct ChIP)], and normalized to IgG control. Primers are listed in TABLE 4.

For ChIP-seq, ~200 µg of chromatin were incubated with 10 µg of antibody overnight at 4°C. Antibody/antigen complexes were recovered with ProteinA-Dynabeads (Invitrogen) for 2h at 4°C. Two large scale preparations of chromatin immunoprecipitated with various antibodies (and their Input chromatin) were prepared. Library preparation and sequencing were performed at the Istituto di Genomica Applicata (Udine). DNA concentration was determined with a fluorometric assay (Quant-iT™ DNA Assay Kit, high sensitivity, Life Technologies) and 2-3 ng served as template to generate the library with Ovation Ultra Low

Library Prep Kit (NuGEN) according to manufacturer's instructions. Sequencing was performed with Illumina HiSeq2500. About 60 mln sequences per sample were obtained.

Chromatin conformation capture (3C)
Adherent cells were incubated with a solution containing 1.5% formaldehyde for 10 min at room temperature, followed by 5 min treatment with 0.125 M glycine/PBS. Cells were incubated with 0.05% trypsin for 10 min at 37 °C, before completely detaching them with a cell scraper. Collected cells were pelletted, washed in PBS and incubated with lysis buffer for 15 min at 4 °C. Nuclei were digested with HindIII restriction enzyme (NEB), and highly diluted digested chromatin was ligated with T4 DNA ligase (NEB). De-crosslinked DNA fragments were purified by phenol–chloroform extraction and ethanol precipitation. A reference template was generated by digesting, mixing and ligating bacterial artificial chromosomes spanning the genomic regions of interest. 3C templates and the reference template were used to perform semiquantitative PCR with GO Taq G2 Flexi DNA Polymerase (Promega). Primers flanked the HindIII restriction sites located close to MYC and TOP2A promoters (anchors) and enhancers (primer sequences are provided in TABLE 5). Data are presented as the ratio of amplification obtained with 3C templates from MDA-MB-231 cells and with the reference template. PCR performed on control 3C template obtained from not-crosslinked cells never yielded any product. PCR products were verified by sequencing.

Bioinformatic analysis was carried out in the lab of Prof. Bicciato in Modena University by Mattia Forcato PhD.

Peak Calling and Data Analysis
Uniquely-mapping, non redundant reads were aligned using Bowtie (version 0.12.7) to build version hg19 of the human genome (GRCh37/hg19). Redundant reads were removed using SAMtools. The IDR (Irreproducible Discovery Rate) framework was used to assess the consistency of replicate experiments and to obtain a high confidence single set of peak calls for each Transcription Factor as described in the ChIP-seq guidelines of the ENCODE consortium. MACS2 version 2.0.10 was used to call peaks in individual replicates using IgG ChIP-seq as control sample and an IDR threshold of 0.01 was applied for all datasets to identify an optimal number of peaks.
Normalized read density (reads per million, rpm) was calculated from pooled replicates using MACS2 callpeak function and displayed using Integrative Genomics Viewer (IGV). Heatmaps were generated using a custom R script which considers a 2-kb window centered on peak summits and calculates the normalized reads density with a resolution of 50 bp. The genomic location of the peaks and their distance to TSS of annotated genes were calculated using annotatePeakInBatch function of ChIPpeakanno R package and GENCODE annotation version 16. Only genes classified as protein coding and with status equal to KNOWN were considered.
The findOverlappingPeaks function of the same package was used with default parameters to identify overlapping peaks and calculate the distance between their summits. TAZ peaks coordinates and summit positions were used to represent common peaks between YAP and TAZ peaks (YAP/TAZ peaks) and were used when comparing YAP/TAZ peaks with other ChIP-seq data.

Definition of MDA-MB-231 promoters and enhancers
Raw reads for ChIP-seq data of histone modifications (H3K4me1, H3K4me3 and H3K27ac) in MDA-MB-231 were downloaded from SRA (SRP028597) and aligned using Bowtie version 0.12.9 to build version hg19 of the human genome retaining only uniquely mapped

reads. Redundant reads were removed using SAMtools. Peak calls and read density tracks were generated using SPP version 1.11 with default parameters and using as control sample the IgG ChIP-seq data generated in our laboratory because of the low sequencing depth of the Input DNA contained in SRP028597. The distance between histone modifications peaks and the transcription start sites (TSS) of protein coding genes (GENCODE v. 16 and REFSEQ annotations), and the overlap between histone marks peaks were calculated as previously described for TF peaks. The presence of H3K4me1 and H3K4me3 peaks, their genomic locations and their overlap were the criteria used to define promoters and enhancers: i) H3K4me3 peaks not overlapping with H3K4me1 peaks and close to a TSS (± 5kb) were defined as promoters, as NA otherwise; ii) H3K4me1 peaks not overlapping with H3K4me3 peaks were defined as enhancers; iii) regions with the co-presence of H3K4me1 and H3K4me3 peaks were visually inspected on IGV and were defined as promoters, enhancers or NA after the evaluation of the proximity to a TSS and the comparison of the enrichment signals. Finally, promoters or enhancers were defined as active if overlapping with H3K27ac peaks.

YAP/TAZ peaks annotation

YAP/TAZ peaks were annotated as promoters or enhancers if their summit was overlapping with promoter or enhancer regions as defined above. Peaks with the summit falling in regions with no H3K4me1 or H3K4me3 peaks, or in NA regions were defined as "not assigned" and discarded from subsequent analyses.

YAP/TAZ peaks summits were compared with FAIRE peaks using the list downloaded from GSE49651.

YAP/TAZ peaks falling on promoters were assigned to the closest TSS. YAP/TAZ peaks falling on active enhancers were annotated using the chromatin interactions reported in Jin et al, derived from a high resolution Hi-C experiment; the data sheets report the genomic locations of all target peaks interacting with more than 10 thousands anchors located at gene promoters. YAP/TAZ peaks overlapping with these target peaks were assigned to the corresponding interacting promoter region. Finally, YAP/TAZ peaks falling on inactive enhancers were not assigned to targets.

Motif discovery in ChIP-seq peaks

De novo motifs discovery was performed with findMotifsGenome function of Homer software. Motifs were searched in 500 bp windows centered at the peak summits. Occurrences of de novo and known motifs inside the peaks were found using annotatePeaks function of the same software. Known motifs were retrieved from Homer motif database and from JASPAR database (http://jaspar.genereg.net).

Gene Ontology analysis

Gene Ontology (GO) analyses were performed using DAVID. GO terms with a Benjamini-Hochberg FDR ≤ 5% were considered significantly enriched. GO terms significantly enriched among YAP/TAZ direct positive target genes could be assigned to two broad categories: “cell proliferation” and “RNA metabolism and transport”.

Promoters of the genes involved in cell proliferation were defined as 1000 bp windows centered at the TSS. De novo motifs discovery and occurrence of known motifs were performed as described above. Used known motifs are E2F4(E2F) from Homer motif database and (MA0024.1) for E2F1 from JASPAR database.

Analysis of public ChIP-seq data

ChIP-seq datasets for histone modifications that were re-analyzed in this study are from Rhie et al.

For data of the ENCODE project, aligned reads and peak calls were downloaded from the ENCODE project repository. When available, TF peaks uniformly generated by the ENCODE Analysis Working Group (available at http://hgdownload.cse.ucsc.edu/goldenPath/hg19/encodeDCC/wgEncodeAwgTfbsUniform/) were used. Otherwise, aligned reads and peak calls of the first replicate were used. Genomic annotation of TEAD4 or TEAD1 peaks and overlap between peaks were calculated as described for ChIP-seq data of MDA-MB-231 cells.

REFERENCES

Aragona, M., Panciera, T., Manfrin, A., Giulitti, S., Michielin, F., Elvassore, N., … Piccolo, S. (2013). A Mechanical Checkpoint Controls Multicellular Growth through YAP/TAZ Regulation by Actin-Processing Factors. *Cell*, *154*(5), 1047–1059. http://doi.org/10.1016/j.cell.2013.07.042

Azzolin, L., Panciera, T., Soligo, S., Enzo, E., Bicciato, S., Dupont, S., … Piccolo, S. (2014). YAP/TAZ Incorporation in the β-Catenin Destruction Complex Orchestrates the Wnt Response. *Cell*, *158*(1), 157–170. http://doi.org/10.1016/j.cell.2014.06.013

Bartucci, M., Dattilo, R., Moriconi, C., Pagliuca, A., Mottolese, M., Federici, G., … De Maria, R. (2015). TAZ is required for metastatic activity and chemoresistance of breast cancer stem cells. *Oncogene*, *34*(6), 681–690. http://doi.org/10.1038/onc.2014.5

Bodega, B., Ramirez, G., Grasser, F., Cheli, S., Brunelli, S., Mora, M., … Aune, T. (2009). Remodeling of the chromatin structure of the facioscapulohumeral muscular dystrophy (FSHD) locus and upregulation of FSHD-related gene 1 (FRG1) expression during human myogenic differentiation. *BMC Biology*, *7*(1), 41. http://doi.org/10.1186/1741-7007-7-41

Cai, J., Zhang, N., Zheng, Y., de Wilde, R. F., Maitra, A., & Pan, D. (2010). The Hippo signaling pathway restricts the oncogenic potential of an intestinal regeneration program. *Genes & Development*, *24*(21), 2383–8. http://doi.org/10.1101/gad.1978810

Calo, E., & Wysocka, J. (2013). Modification of enhancer chromatin: what, how, and why? *Molecular Cell*, *49*(5), 825–37. http://doi.org/10.1016/j.molcel.2013.01.038

Camargo, F. D., Gokhale, S., Johnnidis, J. B., Fu, D., Bell, G. W., Jaenisch, R., & Brummelkamp, T. R. (2007). YAP1 increases organ size and expands undifferentiated progenitor cells. *Current Biology : CB*, *17*(23), 2054–60. http://doi.org/10.1016/j.cub.2007.10.039

Chen, Q., Zhang, N., Gray, R. S., Li, H., Ewald, A. J., Zahnow, C. A., & Pan, D. (2014). A temporal requirement for Hippo signaling in mammary gland differentiation, growth, and tumorigenesis. *Genes & Development*, *28*(5), 432–7. http://doi.org/10.1101/gad.233676.113

Chiang, C.-M. (2009). Brd4 engagement from chromatin targeting to transcriptional regulation: selective contact with acetylated histone H3 and H4. *F1000 Biology Reports*, *1*(98), 98. http://doi.org/10.3410/B1-98

Cordenonsi, M., Zanconato, F., Azzolin, L., Forcato, M., Rosato, A., Frasson, C., … Piccolo, S. (2011). The Hippo Transducer TAZ Confers Cancer Stem Cell-Related Traits on Breast Cancer Cells. *Cell*, *147*(4), 759–772. http://doi.org/10.1016/j.cell.2011.09.048

Devaiah, B. N., Case-Borden, C., Gegonne, A., Hsu, C. H., Chen, Q., Meerzaman, D., … Singer, D. S. (2016). BRD4 is a histone acetyltransferase that evicts nucleosomes from chromatin. *Nature Structural & Molecular Biology*, *23*(August 2015), 1–12. http://doi.org/10.1038/nsmb.3228

Dominguez-Sola, D., & Gautier, J. (2014). MYC and the control of DNA replication. *Cold Spring Harbor Perspectives in Medicine*, *4*(6), a014423.

http://doi.org/10.1101/cshperspect.a014423

Dupont, S., Morsut, L., Aragona, M., Enzo, E., Giulitti, S., Cordenonsi, M., … Piccolo, S. (2011). Role of YAP/TAZ in mechanotransduction. *Nature*, *474*(7350), 179–183. http://doi.org/10.1038/nature10137

Filippakopoulos, P., & Knapp, S. (2014). Targeting bromodomains: epigenetic readers of lysine acetylation. *Nature Reviews Drug Discovery*, *13*(5), 337–356. http://doi.org/10.1038/nrd4286

Galli, G. G., Carrara, M., Yuan, W.-C., Valdes-Quezada, C., Gurung, B., Pepe-Mooney, B., … Camargo, F. D. (2015). YAP Drives Growth by Controlling Transcriptional Pause Release from Dynamic Enhancers. *Molecular Cell*, 1–10. http://doi.org/10.1016/j.molcel.2015.09.001

Hansen, C. G., Moroishi, T., & Guan, K.-L. (2015). YAP and TAZ: a nexus for Hippo signaling and beyond. *Trends in Cell Biology*, *25*(9), 1–15. http://doi.org/10.1016/j.tcb.2015.05.002

Harvey, K. F., Zhang, X., & Thomas, D. M. (2013). The Hippo pathway and human cancer. *Nature Reviews Cancer*, *13*(4), 246–257. http://doi.org/10.1038/nrc3458

Hong, W., & Guan, K.-L. (2012). The YAP and TAZ transcription co-activators: key downstream effectors of the mammalian Hippo pathway. *Seminars in Cell & Developmental Biology*, *23*(7), 785–93. http://doi.org/10.1016/j.semcdb.2012.05.004

Houzelstein, D., Bullock, SL., Lynch, DE., Grigorieva, EF., Wilson, VA., Beddington, RS., (2002). Growth and early postimplantation defects in mice deficient for the bromodomain-containing protein Brd4. *Molecular Cell Biology*, *22(11)*, 3794–802. http://doi.org/10.1128/mcb.22.11.3794-3802.2002

Jin, F., Li, Y., Dixon, J. R., Selvaraj, S., Ye, Z., Lee, A. Y., … Ren, B. (2013). A high-resolution map of the three-dimensional chromatin interactome in human cells. *Nature*, *503*(7475), 290–4. http://doi.org/10.1038/nature12644

Kharchenko, P. V, Tolstorukov, M. Y., & Park, P. J. (2008). Design and analysis of ChIP-seq experiments for DNA-binding proteins. *Nature Biotechnology*, *26*(12), 1351–9. http://doi.org/10.1038/nbt.1508

Kim, M., Kim, T., Johnson, R. L., & Lim, D.-S. (2015). Transcriptional Co-repressor Function of the Hippo Pathway Transducers YAP and TAZ. *Cell Reports*, *11*(2), 270–282. http://doi.org/10.1016/j.celrep.2015.03.015

Koos, B., Andersson, L., Clausson, C.-M., Grannas, K., Klaesson, A., Cane, G., & Söderberg, O. (2014). Analysis of Protein Interactions in situ by Proximity Ligation Assays (pp. 111–126). http://doi.org/10.1007/82_2013_334

Korb, E., Herre, M., Zucker-Scharff, I., Darnell, R. B., & Allis, C. D. (2015). BET protein Brd4 activates transcription in neurons and BET inhibitor Jq1 blocks memory in mice. *Nature Neuroscience*, *18*(10), 1464–73. http://doi.org/10.1038/nn.4095

Liu-chittenden, Y., Huang, B., Shim, J. S., Chen, Q., Lee, S., Anders, R. A., … Pan, D. (2012). Genetic and pharmacological disruption of the TEAD – YAP complex suppresses the oncogenic activity of YAP, 1300–1305. http://doi.org/10.1101/gad.192856.112.1300

Lovén, J., Hoke, H. A., Lin, C. Y., Lau, A., Orlando, D. A., Vakoc, C. R., … Young, R. A. (2013). Selective inhibition of tumor oncogenes by disruption of super-enhancers.

Cell, *153*(2), 320–34. http://doi.org/10.1016/j.cell.2013.03.036

Makita, R., Uchijima, Y., Nishiyama, K., Amano, T., Chen, Q., Takeuchi, T., … Kurihara, H. (2008). Multiple renal cysts, urinary concentration defects, and pulmonary emphysematous changes in mice lacking TAZ. *American Journal of Physiology. Renal Physiology*, *294*(3), F542–F553. http://doi.org/10.1152/ajprenal.00201.2007

Mo, J.-S., Park, H. W., & Guan, K.-L. (2014). The Hippo signaling pathway in stem cell biology and cancer. *EMBO Reports*, *15*(6), 642–56. http://doi.org/10.15252/embr.201438638

Morin-kensicki, E. M., Boone, B. N., Stonebraker, J. R., Teed, J., Alb, J. G., Magnuson, T. R., … Milgram, S. L. (2006). Defects in Yolk Sac Vasculogenesis , Chorioallantoic Fusion , and Embryonic Axis Elongation in Mice with Targeted Disruption of Yap65 Defects in Yolk Sac Vasculogenesis , Chorioallantoic Fusion , and Embryonic Axis Elongation in Mice with Targeted Disrupt. *Molecular and Cellular Biology*, *26*(1), 77–87. http://doi.org/10.1128/MCB.26.1.77

Moroishi, T., Park, H. W., Qin, B., Chen, Q., Meng, Z., Plouffe, S. W., … Guan, K. (2015). A YAP / TAZ-induced feedback mechanism regulates Hippo pathway homeostasis. *Genes & Development*, 1271–1284. http://doi.org/10.1101/gad.262816.115.

Nguyen, L. T., Tretiakova, M. S., Silvis, M. R., Lucas, J., Klezovitch, O., Coleman, I., … Vasioukhin, V. (2015). ERG Activates the YAP1 Transcriptional Program and Induces the Development of Age-Related Prostate Tumors. *Cancer Cell*, *27*(6), 797–808. http://doi.org/10.1016/j.ccell.2015.05.005

Nishioka, N., Inoue, K., Adachi, K., Kiyonari, H., Ota, M., Ralston, A., … Sasaki, H. (2009). The Hippo signaling pathway components Lats and Yap pattern Tead4 activity to distinguish mouse trophectoderm from inner cell mass. *Developmental Cell*, *16*(3), 398–410. http://doi.org/10.1016/j.devcel.2009.02.003

Oh, H., Slattery, M., Ma, L., Crofts, A., White, K. P., Mann, R. S., & Irvine, K. D. (2013). Genome-wide Association of Yorkie with Chromatin and Chromatin-Remodeling Complexes. *Cell Reports*, *3*(2), 309–318. http://doi.org/10.1016/j.celrep.2013.01.008

Pan, D. (2010). The Hippo Signaling Pathway in Development and Cancer. *Developmental Cell*, *19*(4), 491–505. http://doi.org/10.1016/j.devcel.2010.09.011

Panciera, T., Azzolin, L., Fujimura, A., Di Biagio, D., Frasson, C., Bresolin, S., … Piccolo, S. (2016). Induction of Expandable Tissue-Specific Stem/Progenitor Cells through Transient Expression of YAP/TAZ. *Cell Stem Cell*, *0*(0), 157–170. http://doi.org/10.1016/J.STEM.2016.08.009

Piccolo, S., Dupont, S., & Cordenonsi, M. (2014). The biology of YAP/TAZ: hippo signaling and beyond. *Physiological Reviews*, *94*(4), 1287–312. http://doi.org/10.1152/physrev.00005.2014

Pott, S. & Lieb, J. (2015). What are super-enhancers?. *Nature Genetics*, *47*, 8–12. http://doi.org/10.1038/ng.3167

Qing, Y., Yin, F., Wang, W., Zheng, Y., Guo, P., Schozer, F., … Pan, D. (2014). The Hippo effector Yorkie activates transcription by interacting with a histone methyltransferase complex through Ncoa6. *eLife*, *3*. http://doi.org/10.7554/eLife.02564

Ramos, A., & Camargo, F. D. (2012). The Hippo signaling pathway and stem cell biology. *Trends in Cell Biology*, *22*(7), 339–346. http://doi.org/10.1016/j.tcb.2012.04.006

Rao, S. S. P., Huntley, M. H., Durand, N. C., Stamenova, E. K., Bochkov, I. D., Robinson, J. T., … Aiden, E. L. (2014). A 3D Map of the Human Genome at Kilobase Resolution Reveals Principles of Chromatin Looping. *Cell*, *159*(7), 1665–1680. http://doi.org/10.1016/j.cell.2014.11.021

Rhie, S. K., Hazelett, D. J., Coetzee, S. G., Yan, C., Noushmehr, H., & Coetzee, G. A. (2014). Nucleosome positioning and histone modifications define relationships between regulatory elements and nearby gene expression in breast epithelial cells. *BMC Genomics*, *15*(1), 331. http://doi.org/10.1186/1471-2164-15-331

Schmidt, D., Wilson, M. D., Spyrou, C., Brown, G. D., Hadfield, J., & Odom, D. T. (2009). ChIP-seq: using high-throughput sequencing to discover protein-DNA interactions. *Methods (San Diego, Calif.)*, *48*(3), 240–8. http://doi.org/10.1016/j.ymeth.2009.03.001

Shi, J., & Vakoc, C. R. (2014). The Mechanisms behind the Therapeutic Activity of BET Bromodomain Inhibition. *Molecular Cell*, *54*(5), 72–736. http://doi.org/10.1016/j.molcel.2014.05.016

Shu, D., Li, H., Shu, Y., Xiong, G., Carson, W. E., Haque, F., … Guo, P. (2015). Systemic Delivery of Anti-miRNA for Suppression of Triple Negative Breast Cancer Utilizing RNA Nanotechnology. *ACS Nano*, *9*(10), 9731–40. http://doi.org/10.1021/acsnano.5b02471

Shu, S., Lin, C. Y., He, H. H., Witwicki, R. M., Tabassum, D. P., Roberts, J. M., … Polyak, K. (2016). Response and resistance to BET bromodomain inhibitors in triple-negative breast cancer. *Nature*, 1–24. http://doi.org/10.1038/nature16508

Skibinski, A., Breindel, J. L., Prat, A., Galván, P., Smith, E., Rolfs, A., … Kuperwasser, C. (2014). The Hippo transducer TAZ interacts with the SWI/SNF complex to regulate breast epithelial lineage commitment. *Cell Reports*, *6*(6), 1059–72. http://doi.org/10.1016/j.celrep.2014.02.038

Stein, C., Bardet, A. F., Roma, G., Bergling, S., Clay, I., Ruchti, A., … Bauer, A. (2015). YAP1 Exerts Its Transcriptional Control via TEAD-Mediated Activation of Enhancers. *PLOS Genetics*, *11*(8), e1005465. http://doi.org/10.1371/journal.pgen.1005465

Tremblay, A. M., & Camargo, F. D. (2012). Hippo signaling in mammalian stem cells. *Seminars in Cell and Developmental Biology*, *23*(7), 818–826. http://doi.org/10.1016/j.semcdb.2012.08.001

Varelas, X. (2014). The Hippo pathway effectors TAZ and YAP in development, homeostasis and disease. *Development*, *141*(8), 1614–1626. http://doi.org/10.1242/dev.102376

Varelas, X., Samavarchi-Tehrani, P., Narimatsu, M., Weiss, A., Cockburn, K., Larsen, B. G., … Wrana, J. L. (2010). The Crumbs Complex Couples Cell Density Sensing to Hippo-Dependent Control of the TGF-β-SMAD Pathway. *Developmental Cell*, *19*(6), 831–844. http://doi.org/10.1016/j.devcel.2010.11.012

Wu, S.-Y., Lee, A.-Y., Lai, H.-T., Zhang, H., & Chiang, C.-M. (2013). Phospho switch triggers Brd4 chromatin binding and activator recruitment for gene-specific targeting. *Molecular Cell*, *49*(5), 843–57. http://doi.org/10.1016/j.molcel.2012.12.006

Wu, S., Liu, Y., Zheng, Y., Dong, J., & Pan, D. (2008). The TEAD/TEF family protein Scalloped mediates transcriptional output of the Hippo growth-regulatory pathway. *Developmental Cell*, *14*(March), 388–398. http://doi.org/10.1016/j.devcel.2008.01.007

Yu, F.-X., Zhang, K., & Guan, K.-L. (2014). YAP as oncotarget in uveal melanoma. *Oncoscience*, *1*(7), 480–1. http://doi.org/10.18632/oncoscience.57

Zanconato, F., Battilana, G., Cordenonsi, M., & Piccolo, S. (2016). YAP/TAZ as therapeutic targets in cancer. *Current Opinion in Pharmacology*, *29*, 26–33. http://doi.org/10.1016/j.coph.2016.05.002

Zanconato, F., Cordenonsi, M., Piccolo, S. (2016). YAP/TAZ at the Roots of Cancer. *Cancer Cell*, *29*(6), 783–803. http://doi.org/10.1016/J.CCELL.2016.05.005

Zanconato, F., Forcato, M., Battilana, G., Azzolin, L., Quaranta, E., Bodega, B., … Piccolo, S. (2015). Genome-wide association between YAP/TAZ/TEAD and AP-1 at enhancers drives oncogenic growth. *Nature Cell Biology*, *17*(9), 1218–27. http://doi.org/10.1038/ncb3216

Zhang, H., Liu, C. Y., Zha, Z. Y., Zhao, B., Yao, J., Zhao, S., … Guan, K. L. (2009). TEAD transcription factors mediate the function of TAZ in cell growth and epithelial-mesenchymal transition. *Journal of Biological Chemistry*, *284*(20), 13355–13362. http://doi.org/10.1074/jbc.M900843200

Zhang, H., Ramakrishnan, S. K., Triner, D., Centofanti, B., Maitra, D., Győrffy, B., … Shah, Y. M. (2015). Tumor-selective proteotoxicity of verteporfin inhibits colon cancer progression independently of YAP1. *Science Signaling*, *8*(397).

Zhang, W., Nandakumar, N., Shi, Y., Manzano, M., Smith, A., Graham, G., … Yi, C. (2014). Downstream of Mutant KRAS, the Transcription Regulator YAP Is Essential for Neoplastic Progression to Pancreatic Ductal Adenocarcinoma. *Science Signaling*, *7*(324).

Zhao, B., Li, L., Wang, L., Wang, C.-Y., Yu, J., & Guan, K.-L. (2012). Cell detachment activates the Hippo pathway via cytoskeleton reorganization to induce anoikis. *Genes & Development*, *26*(1), 54–68. http://doi.org/10.1101/gad.173435.111

Zhao, B., Ye, X., Yu, J., Li, L., Li, W., Li, S., … Guan, K. (2008). TEAD mediates YAP-dependent gene induction and growth control, *Genes & Development* 22, 1962-1971. http://doi.org/10.1101/gad.1664408.2007

Zhao, B., Zhao, B., Wei, X., Wei, X., Li, W., Li, W., … Guan, K. (2007). Inactivation of YAP oncoprotein by the Hippo pathway is involved in cell contact inhibition and tissue growth control. *Genes & Development*, 2747–2761. http://doi.org/10.1101/gad.1602907.Hpo/Sav

Zhao, R., Nakamura, T., Fu, Y., Lazar, Z., & Spector, D. L. (2011). Gene bookmarking accelerates the kinetics of post-mitotic transcriptional re-activation. *Nature Cell Biology*, *13*(11), 1295–304. http://doi.org/10.1038/ncb2341

FIGURES

Figure 1. ChIP-sequencing method

A. Schematic workflow of a chromatin-immunoprecipitation (ChIP) experiment.
B. Electrophoretic gel to control size of chromatin fragments after sonication that should be between 200-600bp.
C. Sequence of passages that illustrates the alignment of sequenced tags to the genome, resulting in two peaks that flank the binding region of the protein of interest.

Figure 1

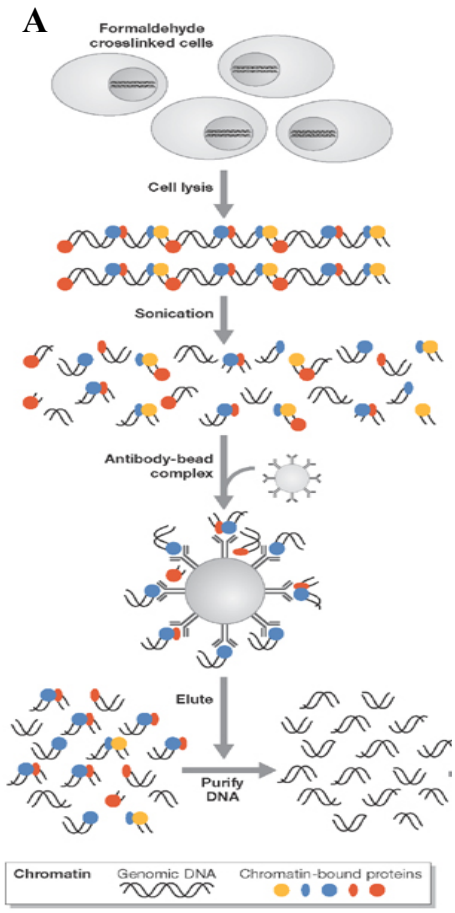
A
Formaldehyde crosslinked cells
Cell lysis
Sonication
Antibody-bead complex
Elute
Purify DNA
Chromatin
Genomic DNA
Chromatin-bound proteins

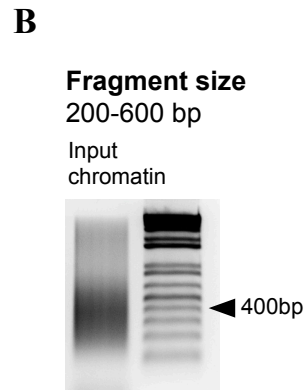
B
Fragment size
200-600 bp
Input chromatin
400bp

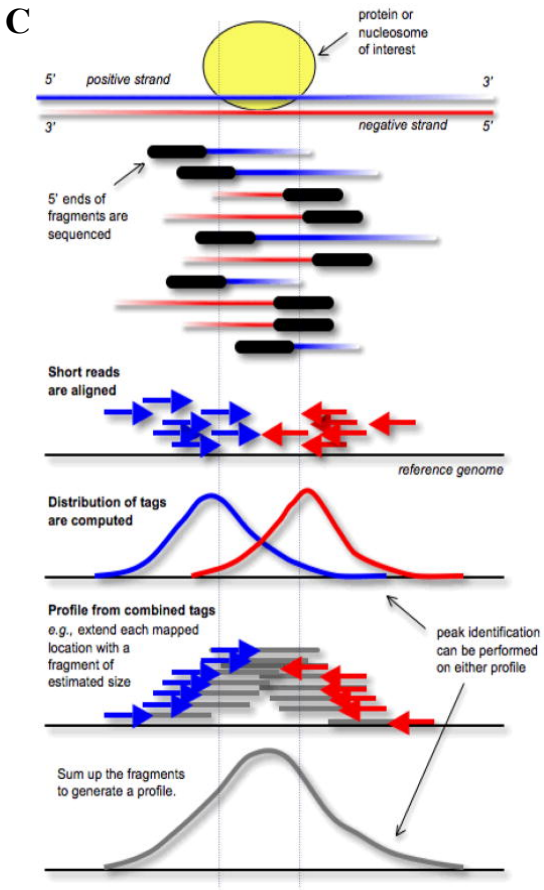
C
protein or nucleosome of interest
5'
positive strand
3'
3'
negative strand
5'
5' ends of fragments are sequenced
Short reads are aligned
reference genome
Distribution of tags are computed
Profile from combined tags
e.g., extend each mapped location with a fragment of estimated size
peak identification can be performed on either profile
Sum up the fragments to generate a profile.

Figure 2. Chromatin immunoprecipitation of endogenous YAP/TAZ

A. Immunoblot to control the result of the immunoprecipitation from MDA-MB-231 crosslinked cells. Chromatin immunoprecipitated with anti-YAP antibody is enriched with YAP protein, while chromatin immunoprecipitated with anti-TAZ antibody is enriched with TAZ and YAP proteins. Chromatin immunoprecipitated with pre-immune rabbit IgG, used as control, is not enriched with YAP and TAZ proteins.

B. qPCR of ChIPed DNA to verify the enrichment of known YAP/TAZ-bound sequences (CTGF and Cyr61 promoters), that are immunoprecipitated by YAP and TAZ from control cells, but not from YAP/TAZ-depleted cells or negative control ChIPs with pre-immune rabbit IgGs. A genomic fragment belonging to the β-globin locus is negative control locus. Relative DNA binding was calculated as fraction of input and normalized to IgG. Data are presented as mean + SD of two independent replicates.

Figure 2

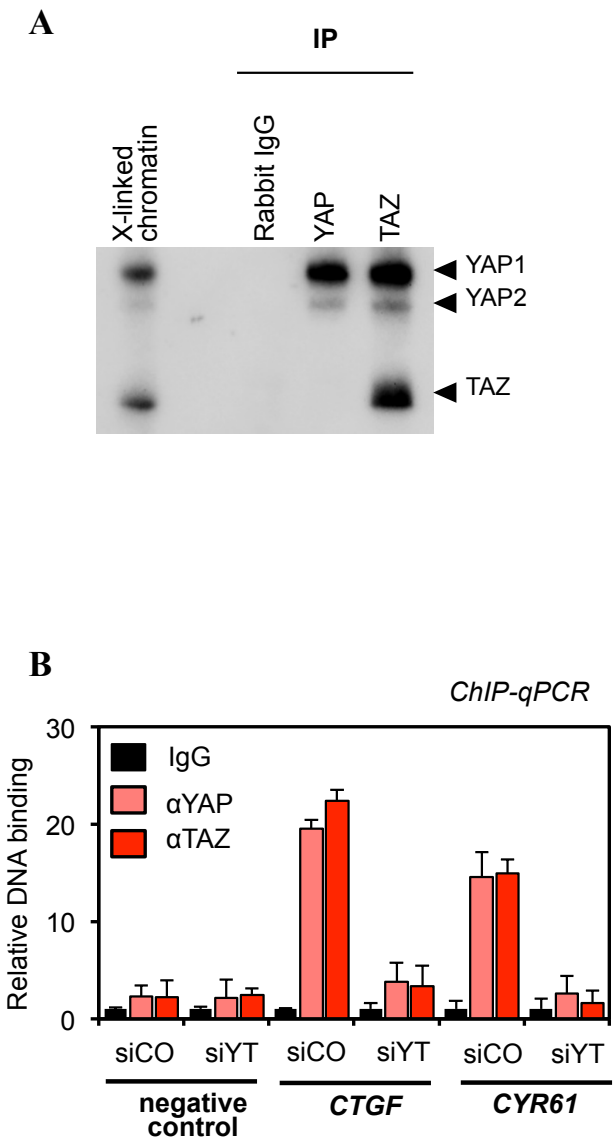
A
IP
X-linked chromatin
Rabbit IgG
YAP
TAZ
YAP1
YAP2
TAZ
B
ChIP-qPCR
Relative DNA binding
30
20
10
0
IgG
αYAP
αTAZ
siCO
siYT
siCO
siYT
siCO
siYT
negative control
CTGF
CYR61

Figure 3. YAP/TAZ ChIP-sequencing

A. Deep sequencing results of ChIPed DNA samples. Two independent experiments were performed (#1, #2). IP YAP/TAZ corresponds to IP with anti-TAZ antibody.
B. Venn diagrams showing the overlap of peaks identified in ChIP-seq experiments with YAP and TAZ antibodies. Overlapping peaks are defined YAP/TAZ peaks.
C. ChIP-seq profiles of YAP and TAZ peaks at positive control loci and other known YAP/TAZ-regulated genes. YAP and TAZ peaks were present on the investigated promoters, whereas negative control sample (IgG) displayed few tags aligned with the same regions, without any appreciable difference with background noise.
D. ChIP-qPCR to validate YAP/TAZ binding sites identified through ChIP-seq. ANKRD1, Axl, AMOTL2, AJUBA and WTIP sequences (but not a negative control locus, data not shown) were enriched in YAP- and TAZ-immunoprecipitated chromatin, but not in negative control IP (IgG) or in chromatin obtained from YAP/TAZ-depleted cells. Relative DNA binding was calculated as fraction of input and normalized to IgG. Data are presented as mean + SD of two independent replicates.

Figure 3

A

Sequencing results

	Mapped reads	Non redundant reads
Control IP (R-IgG) #1	67,123,535	47,255,567
Control IP (R-IgG) #2	45,982,569	36,628,806
IP YAP #1	52,833,034	40,417,609
IP YAP #2	54,356,265	44,014,326
IP YAP/TAZ #1	60,995,512	46,767,183
IP YAP/TAZ #2	65,426,065	46,986,868

B

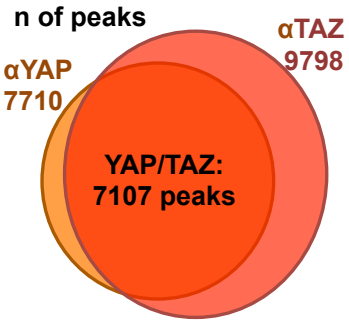

C

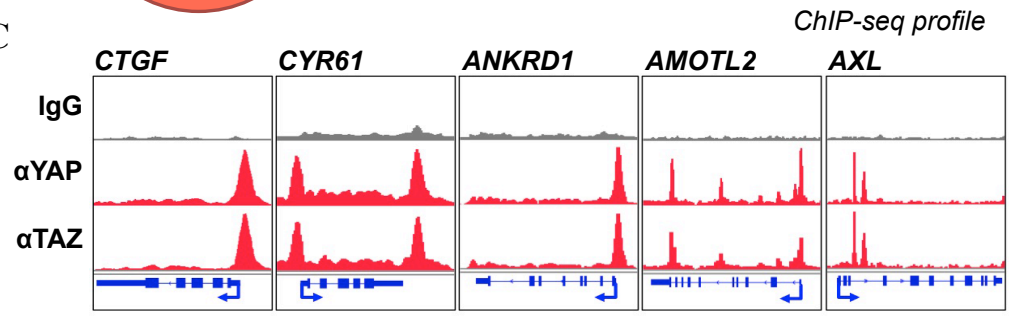

D

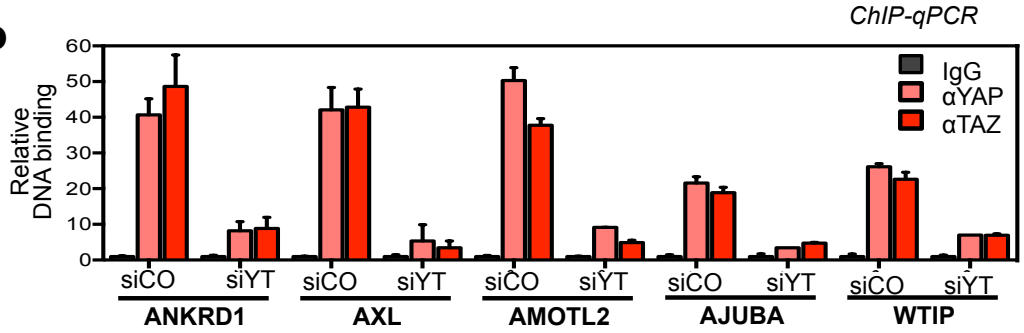

Figure 4. Distribution of YAP/TAZ binding sites in the genome

A. Graphical representation of YAP/TAZ peaks distribution in the genome, with respect to protein coding genes deposited in the Gencode database. Peaks were associated to a gene if they laid within 1 kb upstream or 1 kb downstream of the transcription start site (TSS).
B. Distribution of YAP/TAZ ChIP-seq peaks relative to the closest TSS; ~85% of peaks were located farther than 10kb from the closest TSS.
C. ChIP-seq profile showing examples of YAP/TAZ peaks categorized as "promoters", "active enhancers", "inactive enhancers" or not classified, based on published ChIP-seq data for histone modifications.
D. Graphical representation showing the fraction of YAP/TAZ peaks associated with each category: promoters, active enhancers, inactive enhancers or not classified.
E. Percentage of peaks within each category (promoters, active enhancers, inactive enhancers or not classified) localized in nucleosome-depleted regions, defined by Formaldehyde-assisted identification of regulatory elements followed by deep sequencing (FAIRE).

Figure 4

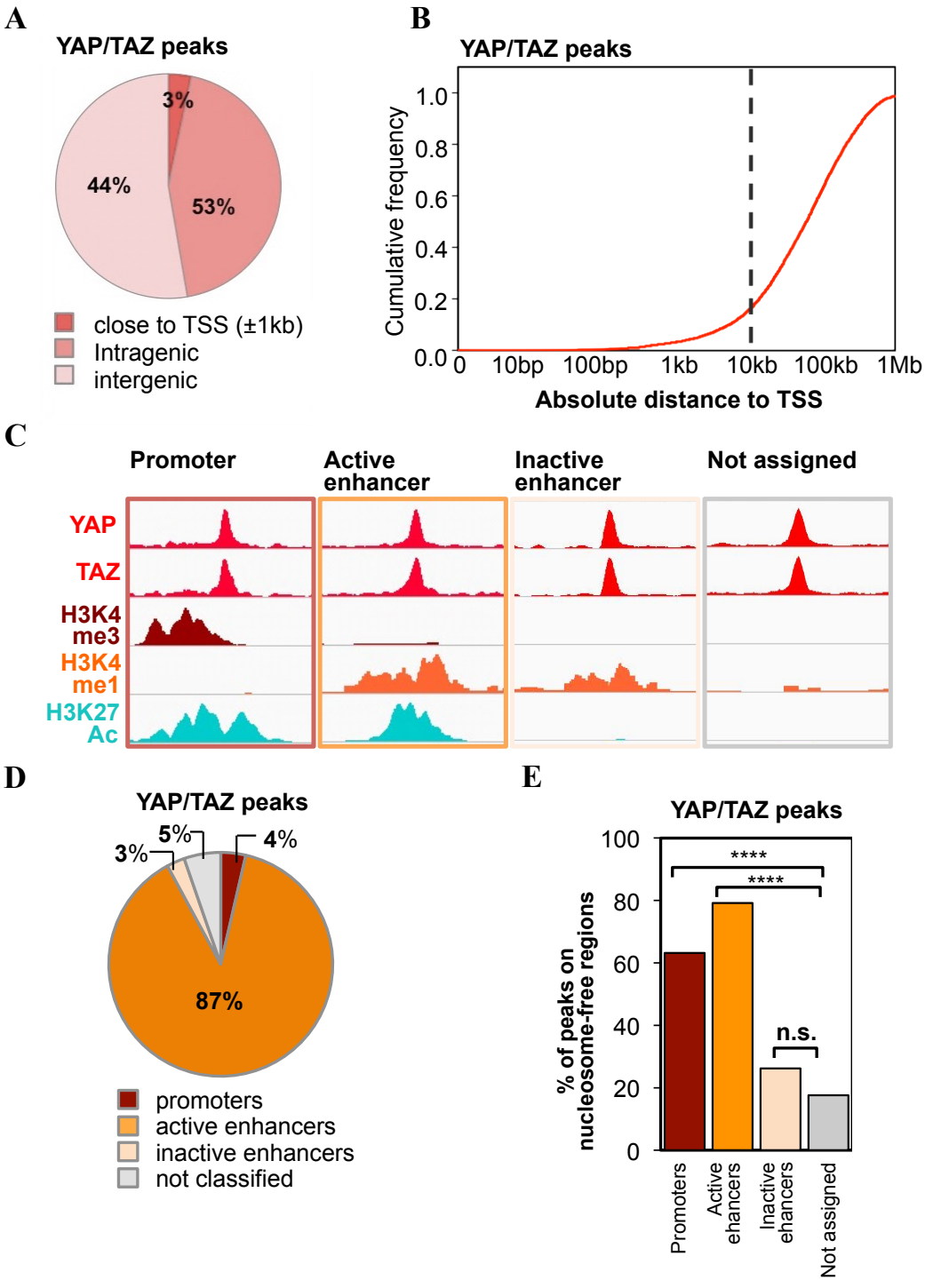
A
YAP/TAZ peaks
3%
44%
53%
close to TSS (±1kb)
Intragenic
intergenic
B
YAP/TAZ peaks
Cumulative frequency
1.0
0.8
0.6
0.4
0.2
0.0
0
10bp
100bp
1kb
10kb
100kb
1Mb
Absolute distance to TSS
C
Promoter
Active enhancer
Inactive enhancer
Not assigned
YAP
TAZ
H3K4 me3
H3K4 me1
H3K27 Ac
D
YAP/TAZ peaks
5%
4%
3%
87%
promoters
active enhancers
inactive enhancers
not classified
E
YAP/TAZ peaks
% of peaks on nucleosome-free regions
100
80
60
40
20
0
****
****
n.s.
Promoters
Active enhancers
Inactive enhancers
Not assigned

Figure 5. Association of YAP/TAZ peaks

Graphical representation of the procedure used to identify candidate YAP/TAZ direct target genes.

A. YAP/TAZ peaks located close to a TSS (± 5kb), and whose summit was overlapping with H3K4me3 peaks, were assigned to the nearest gene.

B. YAP/TAZ peaks located in enhancer regions, and whose summit was overlapping with H3K4me1 peaks, were assigned to promoters that can physically interact with them according to high resolution chromatin conformation capture data.

Figure 5

A

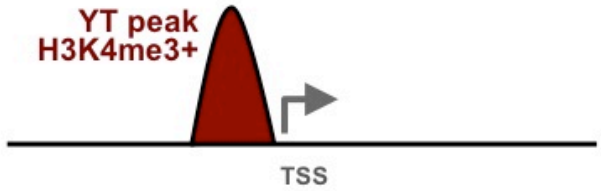

Peak assigned to the closest gene

B

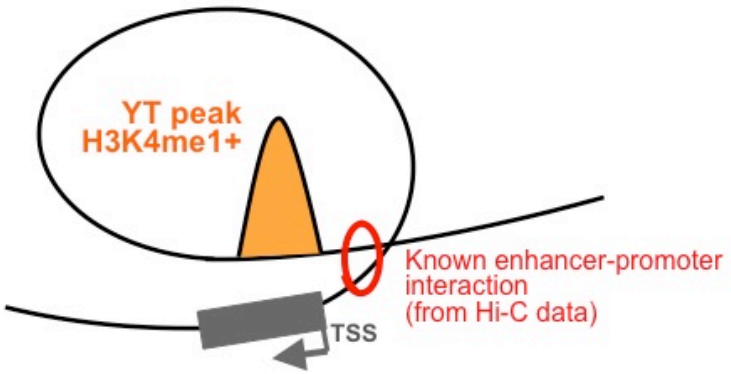

Peak assigned to the interacting gene

Figure 6. Identification of YAP/TAZ direct target genes

A. Overview of gene expression data obtained by Affymetrix Microarrays on MDA-MB-231 cells, transfected with two different mixes of YAP/TAZ siRNAs and compared to control siRNA.
B. Distance between YAP/TAZ binding sites and the TSS of the direct target genes they are associated to. 58% of YAP/TAZ-occupied enhancers are located farther than 100,000 bp from the corresponding TSS

Figure 6

A

	Affymetrix Mycroarray
YAP/TAZ siRNA 1	
modulated genes	3808/18875
downregulated	1985/18875
upregulated	1823/18875
YAP/TAZ siRNA 2	
modulated genes	6386/18875
downregulated	3320/18875
upregulated	3066/18875
POSITIVE YAP/TAZ TARGETS	**1534**
NEGATIVE YAP/TAZ TARGETS	**1457**

B

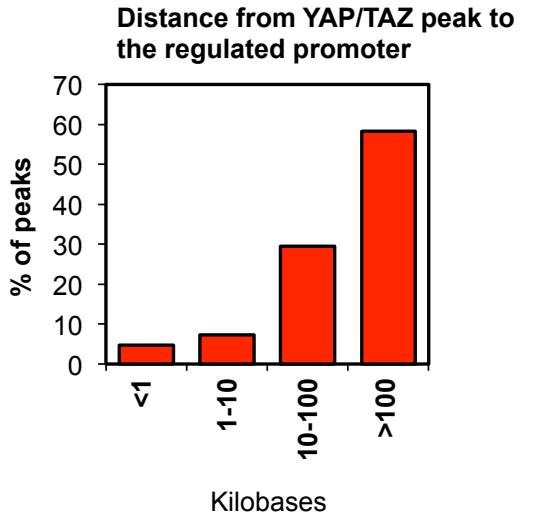

Figure 7. YAP/TAZ regulate a transcriptional program driving cell growth

A. Graphical representation of the biological functions associated to YAP/TAZ direct positive targets, identified by Gene Ontology (GO) analysis. By DAVID (Database for Annotation, Visualization and Integrated Discovery), 36% of YAP/TAZ targets resulted to be linked with cell cycle progression and 14% of the total are connected to RNA metabolism and RNA transport. No other biological processes were significantly regulated by YAP/TAZ.
B. mRNA levels of several candidate YAP/TAZ target genes involved in cell proliferation were evaluated by qRT-PCR using TaqMan Low Density Arrays, in cells transfected with control (siCO) or two pairs of YAP/TAZ siRNAs (siYT1, siYT2). mRNA levels were normalized to GAPDH.
C. Immunoblot on protein extract of MDA-MB-231 cells, to verify a subset of YAP/TAZ target genes, upon the depletion of YAP/TAZ by transfection with two different YAP/TAZ siRNAs, compared to a control siRNA (siCO). GAPDH is used as loading control.
D. ChIP-qPCR on MDA-MB-231 cells to verify YAP and TAZ binding to a subset of enhancers associated with a YAP/TAZ target genes. Relative DNA binding was calculated as fraction of input and normalized to IgG. Data from 2 biological replicates are shown. Negative control locus displayed background signal (data not shown).

Figure 7

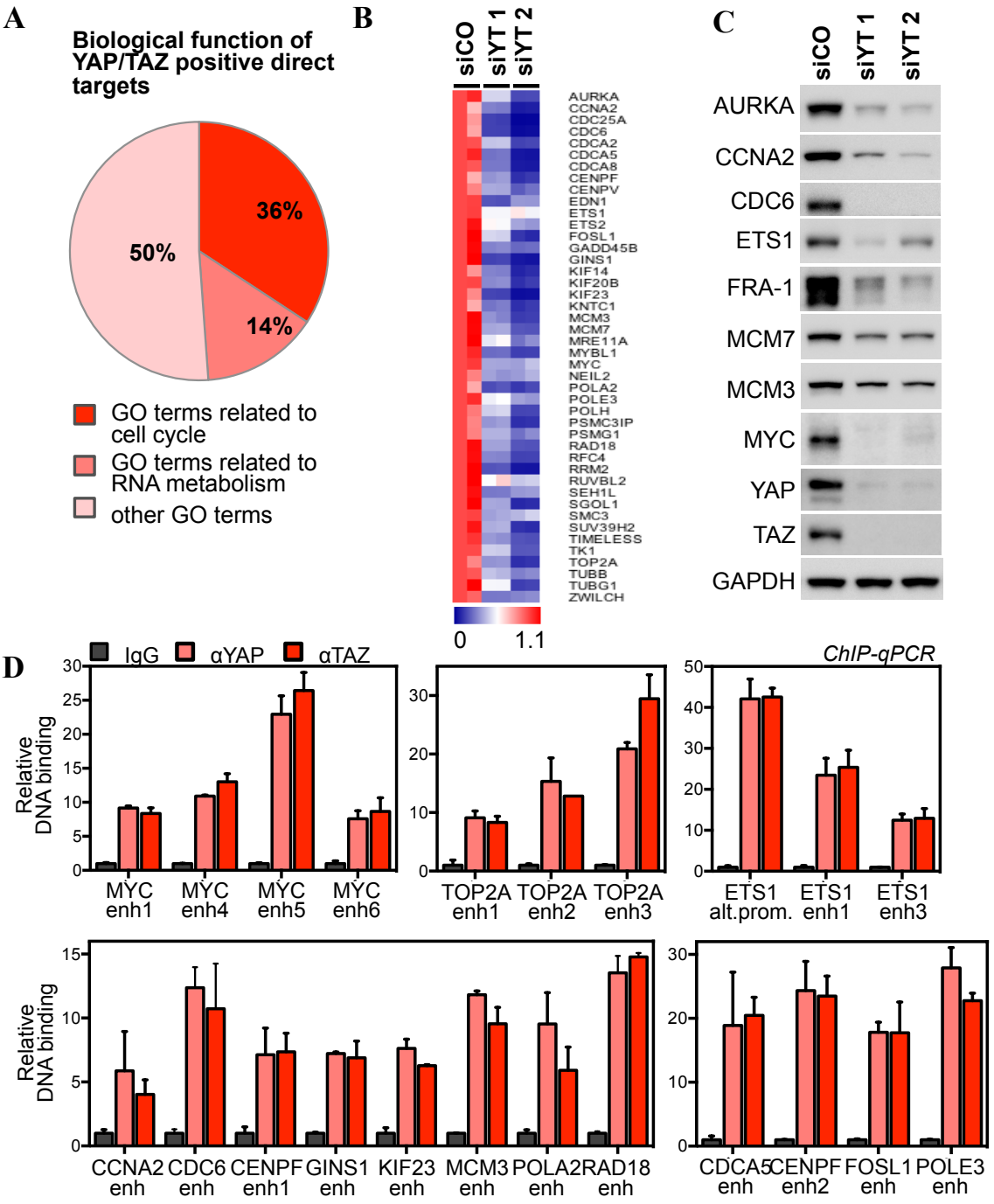
A
Biological function of YAP/TAZ positive direct targets
36%
14%
50%
GO terms related to cell cycle
GO terms related to RNA metabolism
other GO terms
B
siCO
siYT 1
siYT 2
AURKA
CCNA2
CDC25A
CDC6
CDCA2
CDCA5
CDCA8
CENPF
CENPV
EDN1
ETS1
ETS2
FOSL1
GADD45B
GINS1
KIF14
KIF20B
KIF23
KNTC1
MCM3
MCM7
MRE11A
MYBL1
MYC
NEIL2
POLA2
POLE3
POLH
PSMC3IP
PSMG1
RAD18
RFC4
RRM2
RUVBL2
SEH1L
SGOL1
SMC3
SUV39H2
TIMELESS
TK1
TOP2A
TUBB
TUBG1
ZWILCH
0
1.1
C
siCO
siYT 1
siYT 2
AURKA
CCNA2
CDC6
ETS1
FRA-1
MCM7
MCM3
MYC
YAP
TAZ
GAPDH
D
IgG
αYAP
αTAZ
ChIP-qPCR
Relative DNA binding
MYC enh1
MYC enh4
MYC enh5
MYC enh6
TOP2A enh1
TOP2A enh2
TOP2A enh3
ETS1 alt.prom.
ETS1 enh1
ETS1 enh3
CCNA2 enh
CDC6 enh
CENPF enh1
GINS1 enh
KIF23 enh
MCM3 enh
POLA2 enh
RAD18 enh
CDCA5 enh
CENPF enh2
FOSL1 enh
POLE3 enh

Figure 8. YAP/TAZ enhancers contact MYC and TOP2A promoters via chromatin looping

A. ChIP-seq profiles showing the position of YAP and TAZ binding sites (named "MYC enhancer 1", “MYC enhancer 4”) associated to *MYC* gene; no YAP/TAZ binding sites were detected close to its TSS.

B. C. Validation of the long-range interaction between YAP/TAZ-bound enhancers and the promoters of *MYC* (B) and *TOP2A* (C) by DNA looping, using 3C assay. The chart shows the frequency of interaction (measured as cross-linking frequency) between *MYC* or *TOP2A* promoter ("anchor") and the indicated sites surrounding YAP/TAZ peaks (green lines). Interaction frequency is higher close to YAP/TAZ peak. Data points are mean + SEM from 3 replicates.

D. ChIP-qPCR on MDA-MB-231 cells to compare H3K27ac levels (normalized to total H3 levels) in cells transfected with control (siCO) or YAP/TAZ siRNAs (siYT). Data are mean + SD of two replicate samples.

Figure 8

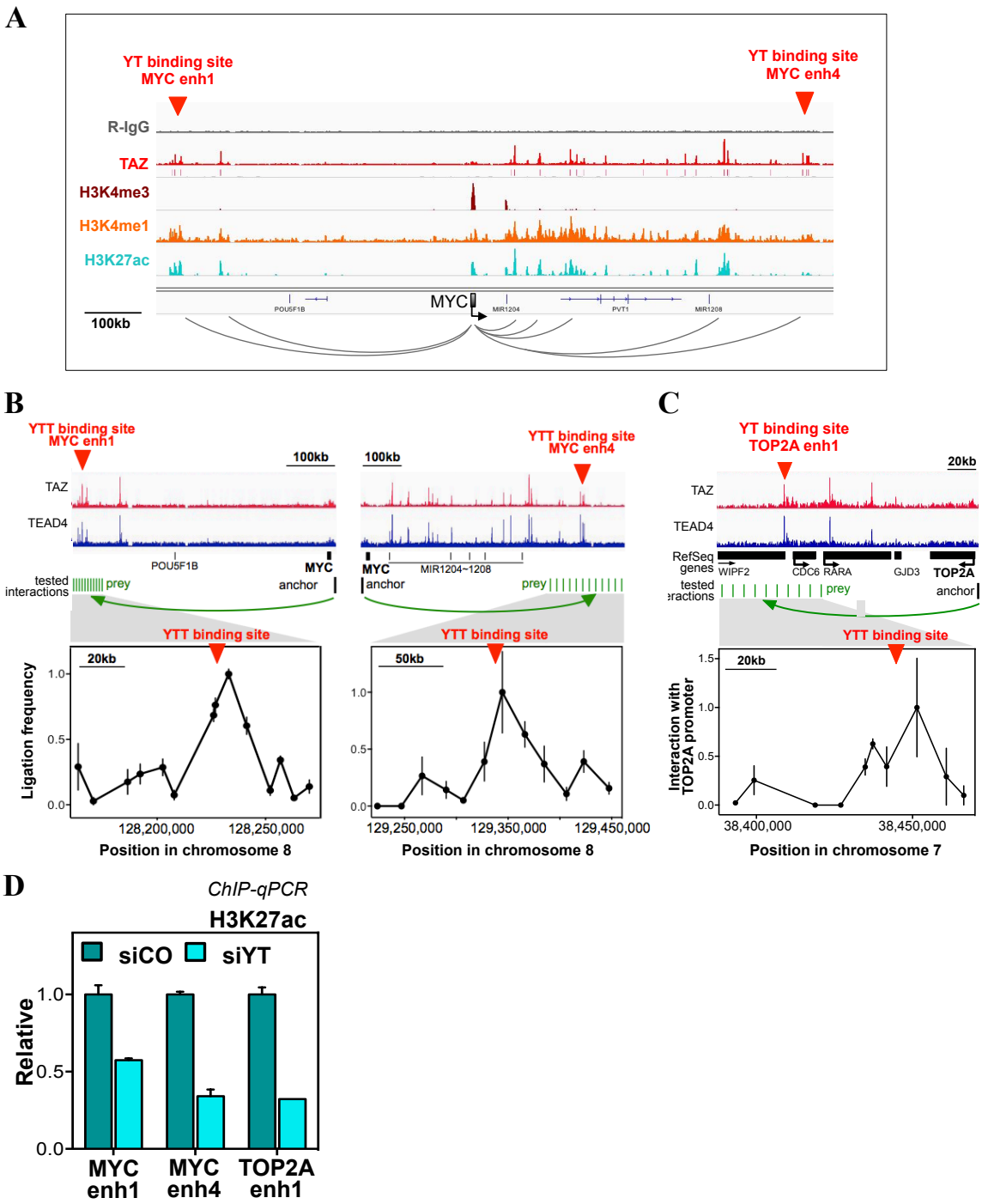
A
YT binding site
MYC enh1
YT binding site
MYC enh4
R-IgG
TAZ
H3K4me3
H3K4me1
H3K27ac
MYC
100kb
B
YTT binding site
MYC enh1
100kb
TAZ
TEAD4
POU5F1B
MYC
tested interactions
prey
anchor
YTT binding site
20kb
Ligation frequency
128,200,000
128,250,000
Position in chromosome 8
YTT binding site
MYC enh4
MYC
MIR1204~1208
50kb
129,250,000
129,350,000
129,450,000
Position in chromosome 8
C
YT binding site
TOP2A enh1
20kb
RefSeq genes
WIPF2
CDC6
RARA
GJD3
TOP2A
Interaction with TOP2A promoter
38,400,000
38,450,000
Position in chromosome 7
D
ChIP-qPCR
H3K27ac
siCO
siYT
Relative
MYC enh1
MYC enh4
TOP2A enh1

Figure 9. MYC is a mediator of YAP/TAZ-induced proliferation in breast cancer cells

A. Immunoblot on MDA-MB-231 protein extract to verify the downregulation of MYC after transfection with two different MYC siRNAs (siMYC1 and siMYC2), compared to a control siRNA (siCO). GAPDH is used as loading control.
B. Growth curve of MDA-MB-231 cells transfected with siCO or two different MYC siRNAs (siMYC1 and siMYC2). Cell growth is evaluated by crystal violet staining. At day 6 after transfection, we can see a decrease in proliferation of MYC depleted cells compared to control. Data are mean+SD of n= 8 biological replicates.
C. Percentage of MDA-MB-231 cells in G1, S and G2/M phases of the cell cycle, as determined by flow-cytometric analysis of DNA content. Cells were transfected with control siRNA (siCO) or MYC siRNAs (siMYC1 and siMYC2) 48h before fixation. Transfection of MYC siRNAs leads to G1 arrest. Data are mean + SD of three biological replicates.
D. Immunoblot on protein extract of MDA TetON EGFP (left), MDA TetON MYC-transduced cells (right) to verify the proper functioning of Tet-ON expression system. EGFP or MYC are expressed only in cells treated with Doxycycline ('+doxy'). GAPDH using as a loading control.
E. Growth curve and cell cycle phases analysis in MDA TetON EGFP and MDA TetON MYC transduced cells, after transfection of control siRNA (siCO) or a combination of YAP and TAZ siRNAs (siYT). Where indicated, EGFP or MYC expressions were induced with 0.1 μg/ml Doxycycline at the time of transfection. Cell growth (left panel) is evaluated by crystal violet staining. Data are mean+SD of n=8 biological replicates. Cell cycle phases are determined by flow-cytometric analysis of DNA content, in cells fixed 48h after transfection of siRNAs. Data are mean + SD of three biological replicates. MYC overexpression, but not EGFP, can rescue the growth and G1-block of YAP/TAZ depleted cells.

Figure 9

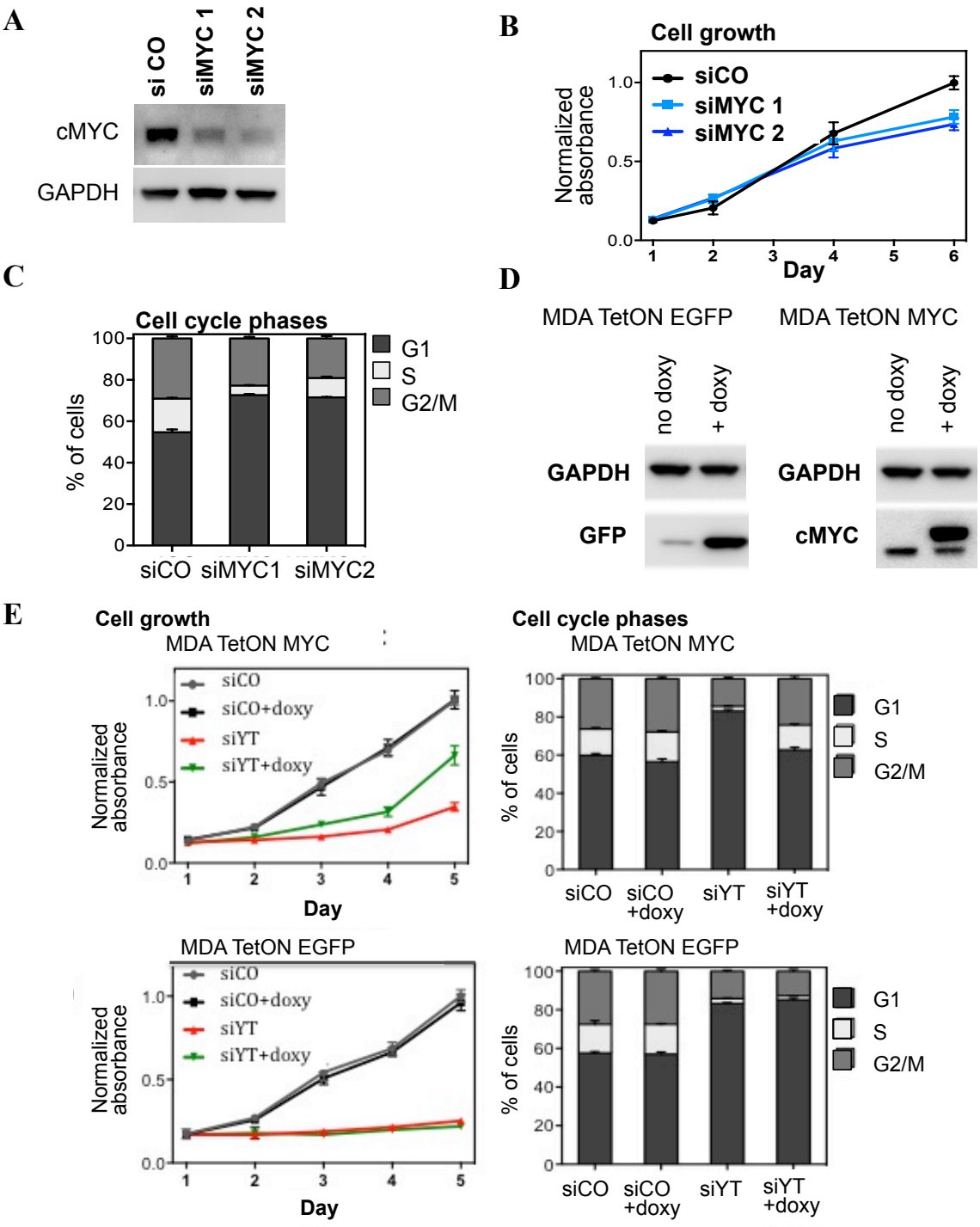
A
si CO
siMYC 1
siMYC 2
cMYC
GAPDH
B
Cell growth
siCO
siMYC 1
siMYC 2
Normalized absorbance
Day
C
Cell cycle phases
G1
S
G2/M
% of cells
siCO
siMYC1
siMYC2
D
MDA TetON EGFP
MDA TetON MYC
no doxy
+ doxy
GAPDH
GFP
cMYC
E
Cell growth
MDA TetON MYC
siCO
siCO+doxy
siYT
siYT+doxy
Normalized absorbance
Day
Cell cycle phases
MDA TetON MYC
% of cells
siCO
siCO +doxy
siYT
siYT +doxy
MDA TetON EGFP

Figure 10. Genome-wide recruitment of YAP/TAZ to chromatin through TEAD factors

A. Most recurrent motif in YAP/TAZ-bound sequences identified by de novo motif finding, corresponding to a TEAD binding site.
B. Graphical representation of YAP/TAZ peaks percentage containing at least one known TEAD-binding motif.
C. Position of TEAD motif relative to the summit of YAP/TAZ peaks. Graph shows the density of TEAD motifs at each position in a 500 bp window surrounding the summit of the corresponding YAP/TAZ peaks. TEAD motif frequently occupied the summit of YAP/TAZ peaks.
D. ChIP-qPCR to validate the specificity of TEAD4 antibody on control (siCO) and TEAD4-depleted MDA-MB-231 cells (siT4). Selected loci were enriched in TEAD4-immunoprecipitated chromatin, but not in negative control IP (IgG) or in chromatin obtained from TEAD4-depleted cells. Data are presented as mean + SD of two independent replicates.
E. Venn diagram showing the overlap of YAP/TAZ and TEAD4 peaks. 5522 YAP/TAZ binding sites (78%) overlapped with TEAD4 peaks.
F. Position of TEAD4 peaks relative to YAP/TAZ peaks. Graph shows the density of TEAD4 peak summit at each position in a 500 bp window surrounding the summit of the corresponding YAP/TAZ peaks. Summits of TEAD4 peaks are located at the summits of the corresponding YAP/TAZ peaks.
G. ChIP-seq profiles showing co-occupancy of *CTGF*, *ANKRD1* and *Axl* promoters by YAP, TAZ and TEAD4 in MDA-MB-231 cells.
H. Strong linear correlation resulting from measuring peak signals between the strengths of YAP (or TAZ) and TEAD4 peaks in the 5522 shared binding sites.
I. ChIP-qPCR showing YAP binding to ANKRD1 and Axl promoters in MDA-MB-231 cells transfected with control (siCO) or TEAD siRNAs (siTEAD). Relative DNA binding was calculated as fraction of input and normalized to IgG (IgG bars are omitted). Data are presented as mean + SD of two independent replicates.

Figure 10

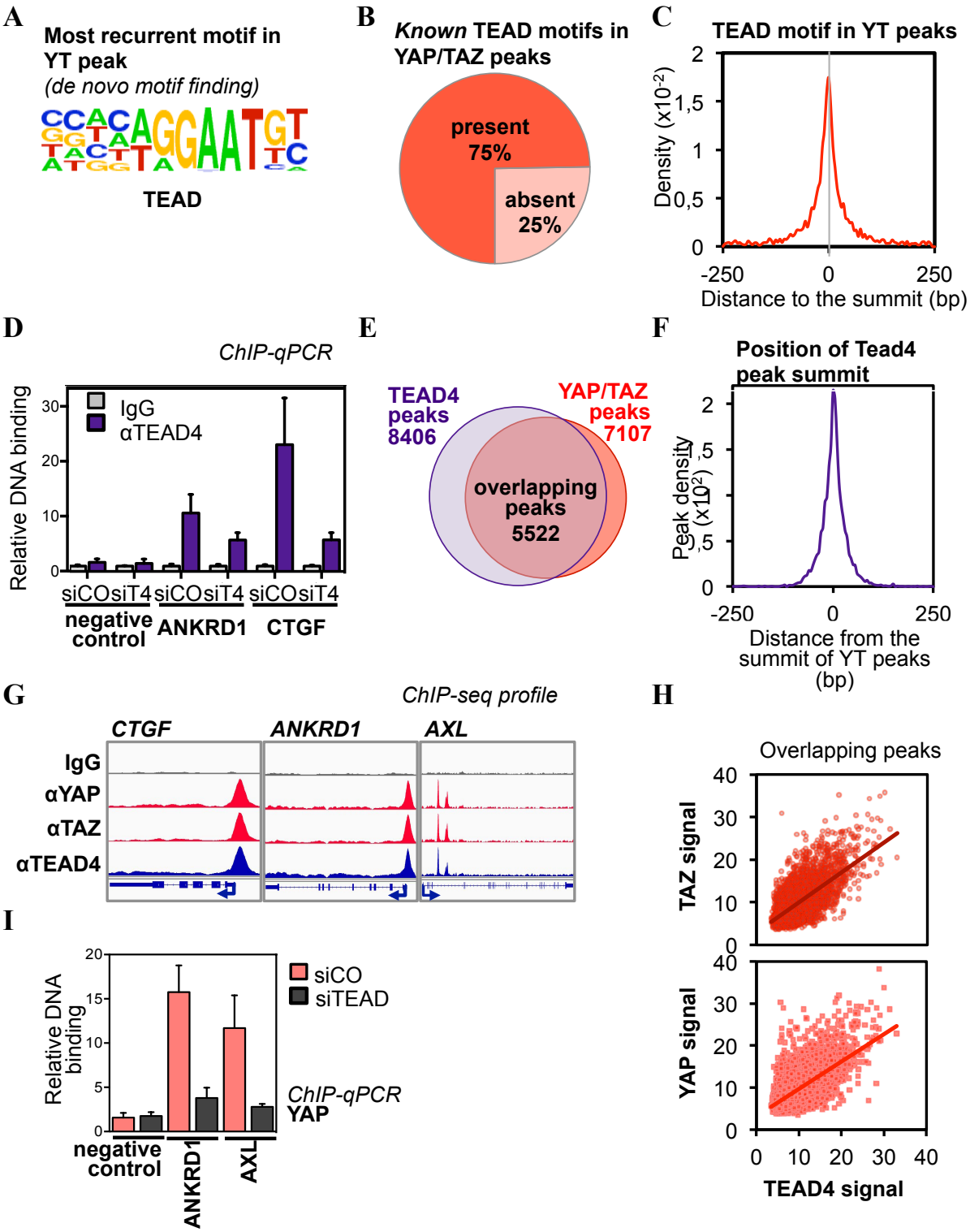
A
Most recurrent motif in YT peak
(de novo motif finding)
TEAD
B
Known TEAD motifs in YAP/TAZ peaks
present 75%
absent 25%
C
TEAD motif in YT peaks
Density (x10-2)
Distance to the summit (bp)
D
ChIP-qPCR
Relative DNA binding
IgG
αTEAD4
siCOsiT4 siCOsiT4 siCOsiT4
negative control
ANKRD1
CTGF
E
TEAD4 peaks 8406
YAP/TAZ peaks 7107
overlapping peaks 5522
F
Position of Tead4 peak summit
Peak density (x10-2)
Distance from the summit of YT peaks (bp)
G
ChIP-seq profile
CTGF
ANKRD1
AXL
IgG
αYAP
αTAZ
αTEAD4
H
Overlapping peaks
TAZ signal
YAP signal
TEAD4 signal
I
Relative DNA binding
siCO
siTEAD
ChIP-qPCR
YAP
negative control
ANKRD1
AXL

Figure 11. YAP/TAZ transcriptional and biological effects depended on TEAD factors

A. qRT-PCR to measure mRNA levels (normalized to *GAPDH*) for *TEAD1-4* in MDA-MB-231 cells transfected with two different mixes of TEAD1-4 siRNAs (siTEAD A or siTEAD B) or control siRNA (siCO). Data are presented as mean + SD of two biological replicates. The efficiency of TEAD depletion was also evaluated by qRT-PCR for the expression of the YAP/TAZ/TEAD targets *CTGF* and *ANKRD1*.

B. mRNA levels of several candidate YAP/TAZ target genes involved in cell proliferation were evaluated by qRT-PCR using TaqMan Low Density Arrays, in cells transfected with control (siCO) or TEAD siRNAs (siTEAD A and B). mRNA levels were normalized to GAPDH.

C. Growth curve of MDA-MB-231 cells transfected with control siRNA (siCO) or TEAD siRNAs (siTEAD A or siTEAD B). Cells were harvested at the indicated time points after siRNA transfection, and their amount was evaluated by crystal violet staining. Data are mean + SD of 8 technical replicates.

D. Cell cycle phases of MDA-MB-231 cells transfected with control siRNA (siCO) or TEAD siRNAs (siTEAD A or siTEAD B). Percentage MDA-MB-231 cells in G1, S and G2/M phases of cell cycle are determined by flow-cytometric analysis of DNA content, in cells fixed 48h after transfection of siRNAs. Data are mean + SD of three biological replicates.

E. Histogram shows growth rate of empty vector and YAP-transduced MDA-MB-231 cells, after transfection of control siRNA (siCO) or a combination of YAP and TAZ siRNAs (siYT 1). Sustained expression of YAP wild-type (wt), but not of TEAD-binding deficient YAPS94A, rescues cell proliferation in YAP/TAZ-depleted cells. Cells were harvested 24h or 6 days after siRNA transfection. Data are mean + SD of 8 technical replicates.

F. Histogram shows growth rate of empty vector and TAZ-transduced MDA-MB-231 cells, after transfection of control siRNA (siCO) or a combination of YAP and TAZ siRNAs (siYT 1). Sustained expression of TAZ wild-type (wt), but not of TEAD-binding deficient TAZS51A, rescues cell proliferation in YAP/TAZ-depleted cells. Cells were harvested 24h or 5 days after siRNA transfection. Data are mean + SD of 8 technical replicates.

Figure 11

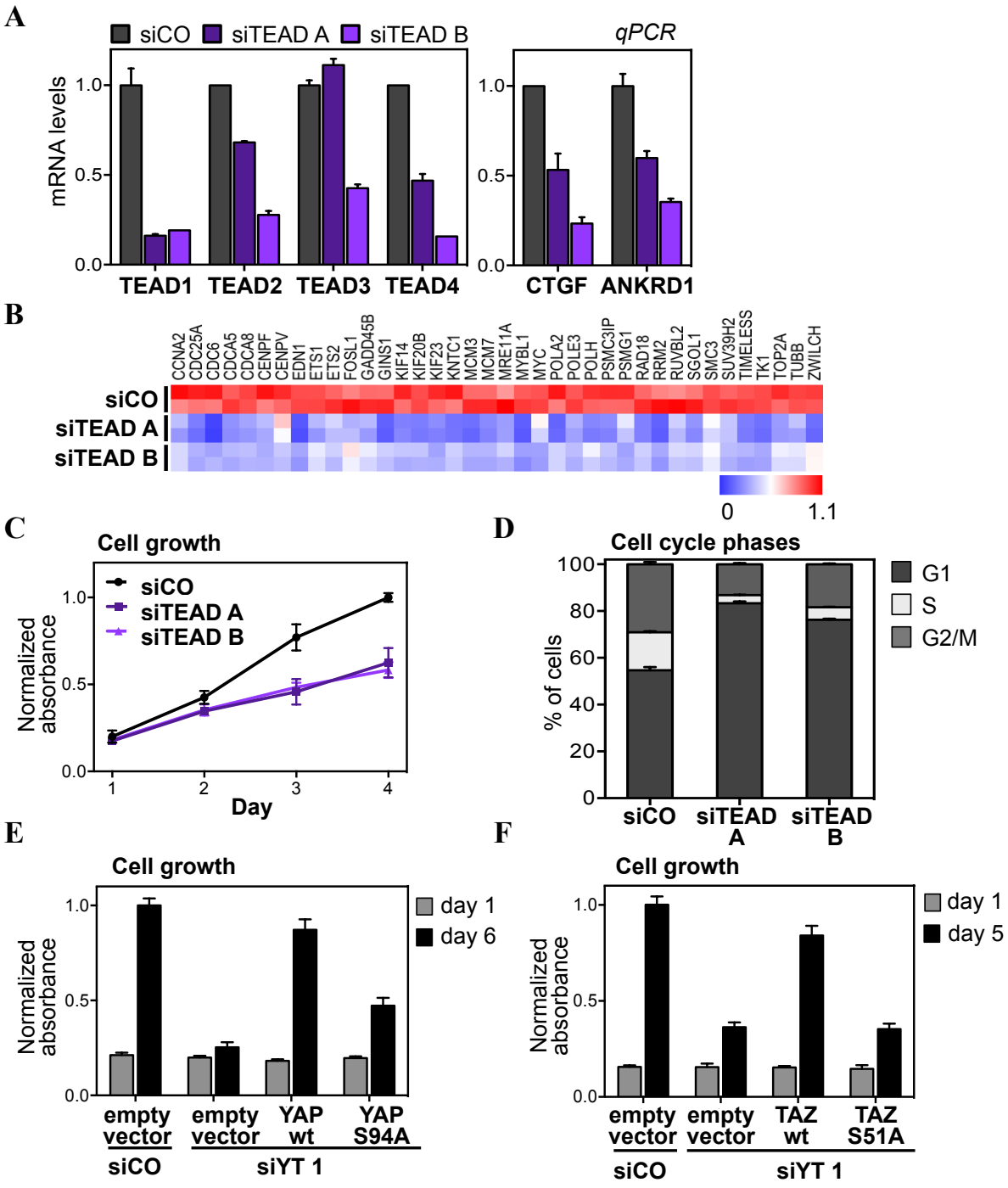
A
siCO
siTEAD A
siTEAD B
qPCR
mRNA levels
1.0
0.5
0.0
TEAD1
TEAD2
TEAD3
TEAD4
CTGF
ANKRD1
B
CCNA2
CDC25A
CDC6
CDCA5
CDCA8
CENPF
CENPV
EDN1
ETS1
ETS2
FOSL1
GADD45B
GINS1
KIF14
KIF20B
KIF23
KNTC1
MCM3
MCM7
MRE11A
MYBL1
MYC
POLA2
POLE3
POLH
PSMC3IP
PSMG1
RAD18
RRM2
RUVBL2
SGOL1
SMC3
SUV39H2
TIMELESS
TK1
TOP2A
TUBB
ZWILCH
siCO
siTEAD A
siTEAD B
0
1.1
C
Cell growth
siCO
siTEAD A
siTEAD B
Normalized absorbance
Day
D
Cell cycle phases
% of cells
G1
S
G2/M
E
Cell growth
day 1
day 6
Normalized absorbance
empty vector
empty vector
YAP wt
YAP S94A
siCO
siYT 1
F
Cell growth
day 1
day 5
Normalized absorbance
empty vector
empty vector
TAZ wt
TAZ S51A
siCO
siYT 1

Figure 12. YAP/TAZ/TEAD interact with BRD4

A. Immunoblot showing YAP, TEAD1 and BRD4 co-precipitation at endogenous protein level from MDA-MB-231 nuclear extracts. Aspecific IgGs are used as negative control.
B. Detection of endogenous BRD4/TEAD1 interactions in MDA-MB-231 cells by *in situ* PLA (proximity ligation assay). PLA was performed for the indicated protein dimers, and nuclei were counterstained with DAPI (blue). The detected dimers are represented by fluorescent dots (red). As control of the specificity of the interactions, no dots could be detected in the nuclei when we performed the PLA omitting either of the primary antibodies (data not shown).
C. Immunoblot showing isolated proteins captured by HA-BRD4 resin. HA-BRD4 protein was overexpressed in HEK293T cells and immobilized by anti-HA antibodies on protein A-agarose beads. HA-BRD4-loaded resin was incubated with FLAG-tagged YAP, TAZ, or TEAD1 isolated from HEK293T protein extracts. FLAG-YAP interacted with HA-BRD4 only in the presence of FLAG-TEAD1 (arrow), whereas FLAG-TAZ showed a tiny interaction with BRD4 and a stronger binding in the presence of FLAG-TEAD1.
D. Immunoblot showing isolated proteins captured by HA-YAP resin. HA-YAP resin was incubated with FLAG-tagged BRD4 and/or TEAD1. Bottom box: picture taken with a higher sensitivity detection reagent. FLAG-BRD4 interacted with HA-YAP only in the presence of FLAG-TEAD1.

Figure 12

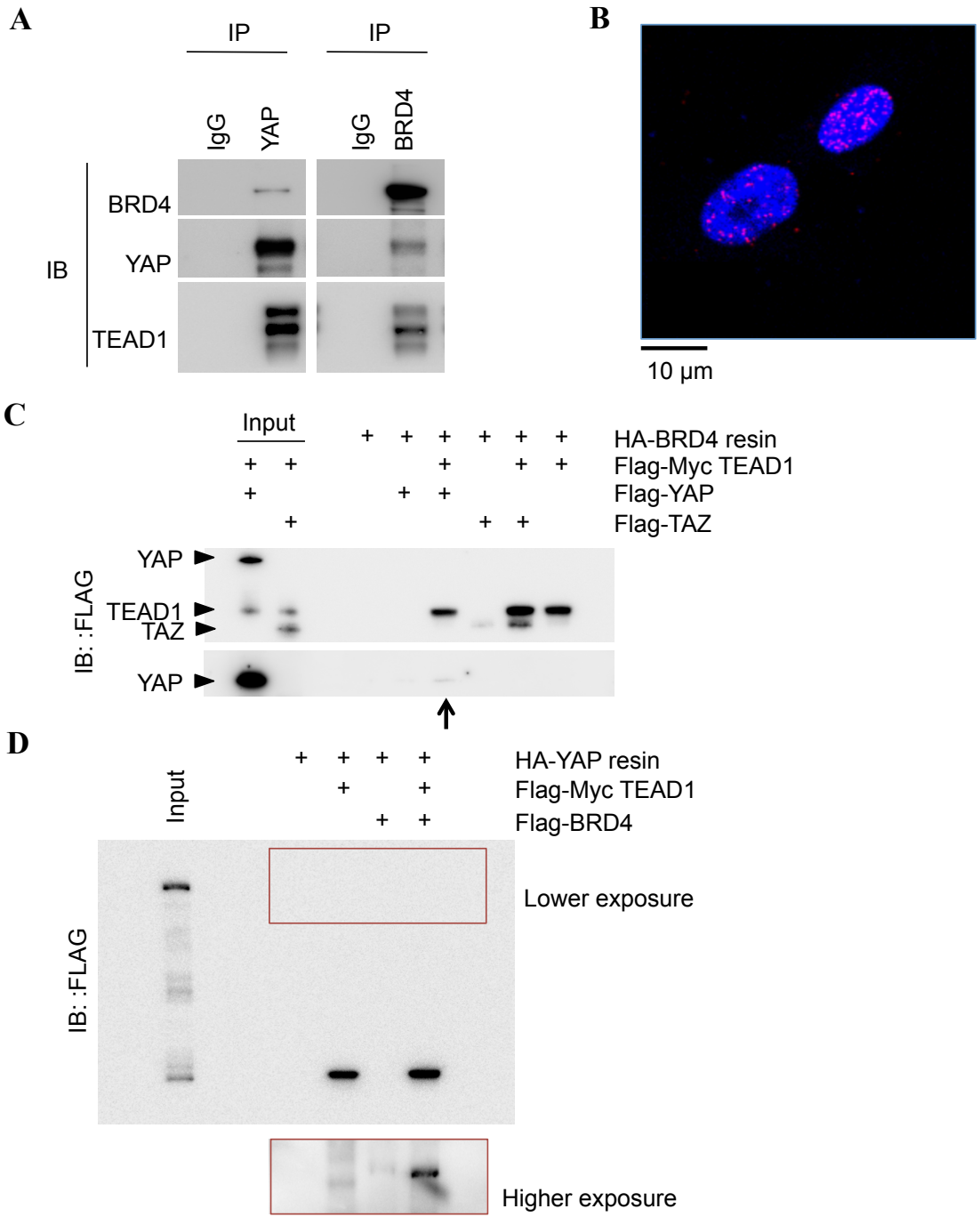
A
IP
IP
IgG
YAP
IgG
BRD4
IB
BRD4
YAP
TEAD1
B
10 μm
C
Input
HA-BRD4 resin
Flag-Myc TEAD1
Flag-YAP
Flag-TAZ
IB: :FLAG
YAP
TEAD1
TAZ
YAP
D
Input
HA-YAP resin
Flag-Myc TEAD1
Flag-BRD4
IB: :FLAG
Lower exposure
Higher exposure

Figure 13. BRD4 binds and regulated the cis-regulatory elements of YAP/TAZ/TEAD target genes

A. ChIP-qPCR to validate the specificity of BRD4 antibody on control (siCO) and BRD4-depleted MDA-MB-231 cells (siBRD4). Selected enhancer regions (CDC6 and TOP2A) were enriched in BRD4-immunoprecipitated chromatin, but not in negative control IP (IgG) or in chromatin obtained from BRD4-depleted cells. Relative DNA binding was calculated as fraction of input and normalized to IgG.
B. ChIP-qPCR to verify BRD4 binding on the promoters (TSS) and enhancers of established YAP/TAZ direct targets. BRD4 immunoprecipitated selected loci, but not negative control locus, from MDA-MB-231 cells cells. Relative DNA binding was calculated as fraction of input and normalized to IgG (negative control IP).
C. Unsupervised hierarchical clustering of MDA-MB-231 RNA-sequencing samples. Data from 2 biological replicates.
D. Venn diagrams showing the overlap between YAP/TAZ target genes and JQ1 sensitive genes identified by RNA-seq experiment. 68% of YAP/TAZ targets are also sensitive to JQ1.

Figure 13

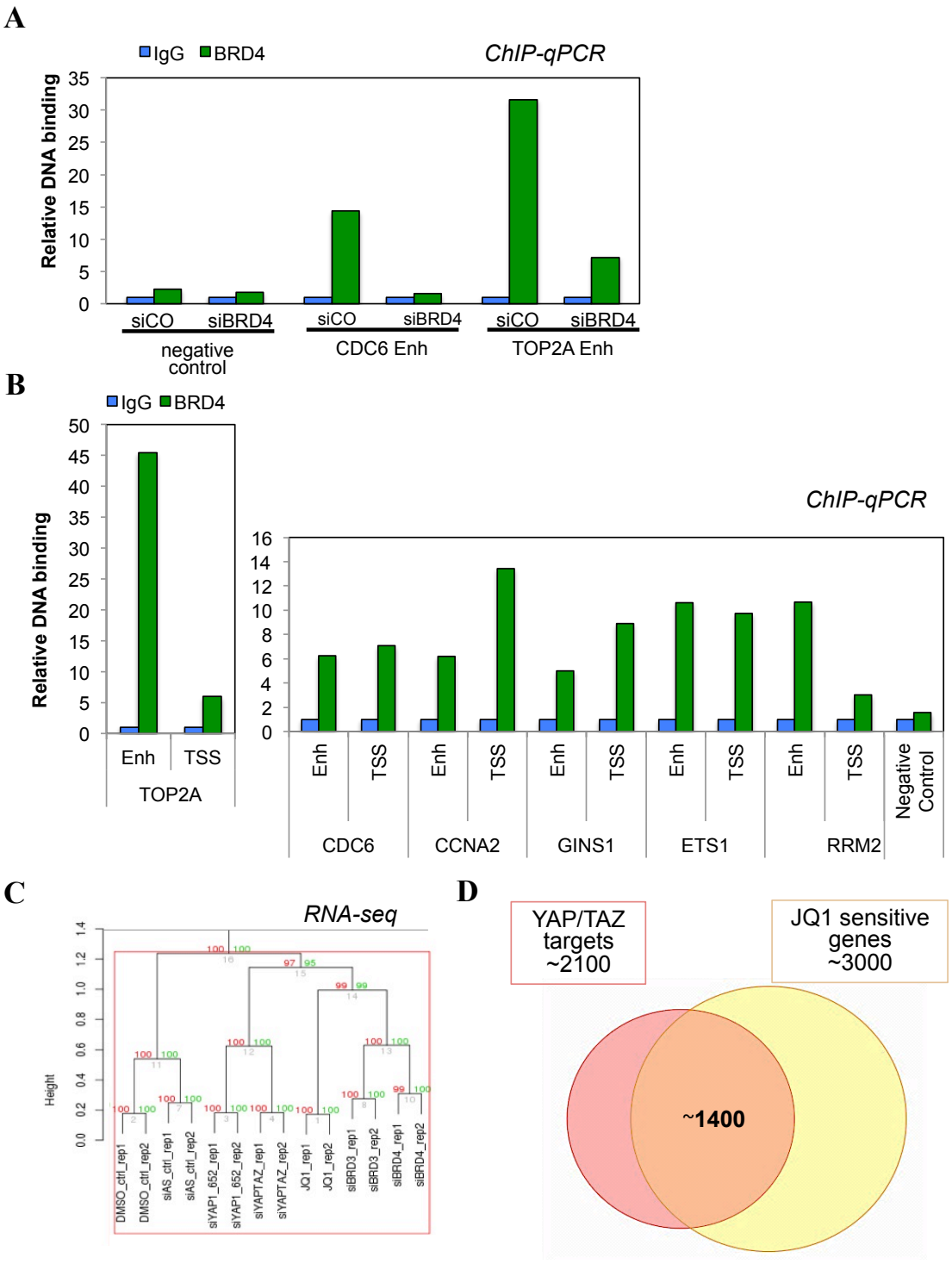
A
IgG
BRD4
ChIP-qPCR
Relative DNA binding
35
30
25
20
15
10
5
0
siCO
siBRD4
siCO
siBRD4
siCO
siBRD4
negative control
CDC6 Enh
TOP2A Enh
B
IgG
BRD4
ChIP-qPCR
Relative DNA binding
50
45
40
35
30
25
20
15
10
5
0
Enh
TSS
TOP2A
16
14
12
10
8
6
4
2
0
Enh
TSS
Enh
TSS
Enh
TSS
Enh
TSS
Enh
TSS
Negative Control
CDC6
CCNA2
GINS1
ETS1
RRM2
C
RNA-seq
Height
1.4
1.2
1.0
0.8
0.6
0.4
0.2
0.0
DMSO_ctrl_rep1
DMSO_ctrl_rep2
siAS_ctrl_rep1
siAS_ctrl_rep2
siYAP1_652_rep1
siYAP1_652_rep2
siYAPTAZ_rep1
siYAPTAZ_rep2
JQ1_rep1
JQ1_rep2
siBRD3_rep1
siBRD3_rep2
siBRD4_rep1
siBRD4_rep2
D
YAP/TAZ targets ~2100
JQ1 sensitive genes ~3000
~1400

Figure 14. BRD4 is instrumental for YAP/TAZ biological activity

A. Immunoblot showing the efficiency of BRD4 shRNAs in MDA-MB-231 cells by doxycycline treatment for 5 days. GAPDH serves as loading control.
B. MDA-MB-231 colonies formation in soft agar assay after BRD4 downregulation by doxycycline shRNA expression. $3*10^4$ cells/well were plated into soft agar in the absence or presence of doxycycline and allowed to grow for 3 weeks. BRD4 knockdown reduce the number of colonies formed by MDA-MB-231 cells. Three replicates were analyzed for each sample; data are presented as mean + SD.
C. Immunoblot showing esogenous constitutive YAP expression and the efficiency of inducible BRD4 shRNAs by doxycycline treatment for 5 days in MCF10A cells. GAPDH serves as loading control.
D. MCF10A colonies formation in soft agar assay dependent on YAP expression, in presence or absence of BRD4; BRD4 downregulation is induced by doxycycline-dependent expression of shRNAs. 10^4 cells/well were plated into soft agar in the absence or presence of doxycycline and allowed to grow for 3 weeks. YAP overexpression conferred MCF10A cells the capacity to seed colonies with high efficiency; BRD4 shRNAs reduced colony formation compared to cells expressing both YAP5SA and shCO. Three replicates were analyzed for each sample; data are presented as mean + SD.
E. MDA-MB-231 colonies formation in soft agar assay after treatments for three weeks with different doses of JQ1 inhibitor. Colonies did not grow at the lowest inhibitor concentration compare to vehicle (DMSO). Three replicates were analyzed for each sample; data are presented as mean + SD.
F. MCF10A colonies formation in soft agar assay dependent on YAP expression, after treatments with different doses of JQ1 inhibitor for three weeks. YAP5SA-overexpressing cells show a dose-dependent growth compare to vehicle (DMSO). Three replicates were analyzed for each sample; data are presented as mean + SD.
G. MCF10A colonies formation in soft agar assay dependent on YAP expression to verify if JQ1 affected colony progression, beyond colony initiation. JQ1 treatment started at different time points: at the moment of seeding, or 7 or 15 days later. Also after 15 days, fewer cells grew enough to form sizable colonies. Three replicates were analyzed for each sample; data are presented as mean + SD.

Figure 14

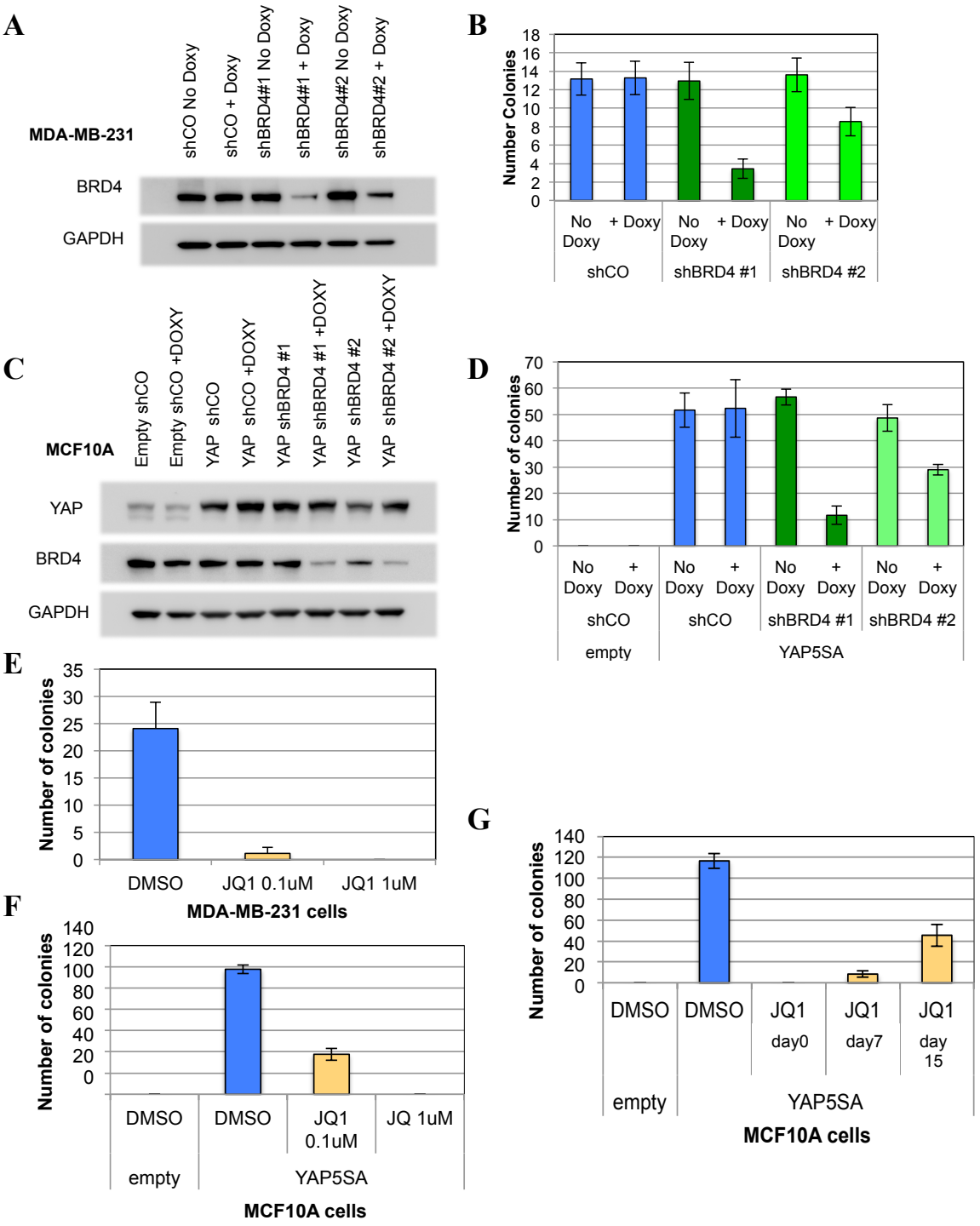
A
MDA-MB-231
shCO No Doxy
shCO + Doxy
shBRD4#1 No Doxy
shBRD4#1 + Doxy
shBRD4#2 No Doxy
shBRD4#2 + Doxy
BRD4
GAPDH
B
Number Colonies
No Doxy
+ Doxy
shCO
shBRD4 #1
shBRD4 #2
C
MCF10A
Empty shCO
Empty shCO +DOXY
YAP shCO
YAP shCO +DOXY
YAP shBRD4 #1
YAP shBRD4 #1 +DOXY
YAP shBRD4 #2
YAP shBRD4 #2 +DOXY
YAP
BRD4
GAPDH
D
Number of colonies
shCO
shBRD4 #1
shBRD4 #2
empty
YAP5SA
E
Number of colonies
DMSO
JQ1 0.1uM
JQ1 1uM
MDA-MB-231 cells
F
Number of colonies
DMSO
JQ1 0.1uM
JQ 1uM
empty
YAP5SA
MCF10A cells
G
Number of colonies
JQ1 day0
JQ1 day7
JQ1 day 15
empty
YAP5SA
MCF10A cells

Figure 15. JQ1 does not affect BRD4-TEAD interaction and YAP/TAZ recruitment on enhancers

A. Immunoblot showing isolated proteins captured by HA-BRD4 resin. HA-BRD4 resin was incubated with FLAG-tagged TEAD1 in presence or absence of JQ1 1μM inhibitor in the reaction buffer. HA-BRD4 was able to capture FLAG-TEAD1 also in the presence of JQ1.
B. Immunoblot showing YAP, TEAD1 and BRD4 co-precipitation at endogenous protein level from MDA-MB-231 cells, upon DMSO (control), JQ1 1μM or PFI-1 10μM treatment for 6hours. Aspecific IgGs are used as negative control. TEAD1 and YAP co-precipitated with BRD4 also in the presence of BET-inhibitors.
C. ChIP-qPCR to verify YAP/TAZ binding on enhancers of established YAP/TAZ direct targets in MDA-MB-231 cells treated with 1μM JQ1 for 6h (or DMSO as control). Anti-TAZ antibody immunoprecipitated selected loci from MDA-MB-231 cells cells also in the presence of JQ1. Negative control locus displayed background signal (data not shown). Relative DNA binding was calculated as fraction of input and normalized to DMSO.
D. ChIP-qPCR verifying release of BRD4 from promoters and enhancers of established YAP/TAZ direct targets, upon JQ1 1μM treatment for 3, 6 or 24 hours. BRD4 binding is reduced in the presence of JQ1 at 3 and 6 hours of treatment. Negative control locus displayed background signal (data not shown). Relative DNA binding was calculated as fraction of input and normalized to DMSO.

Figure 15

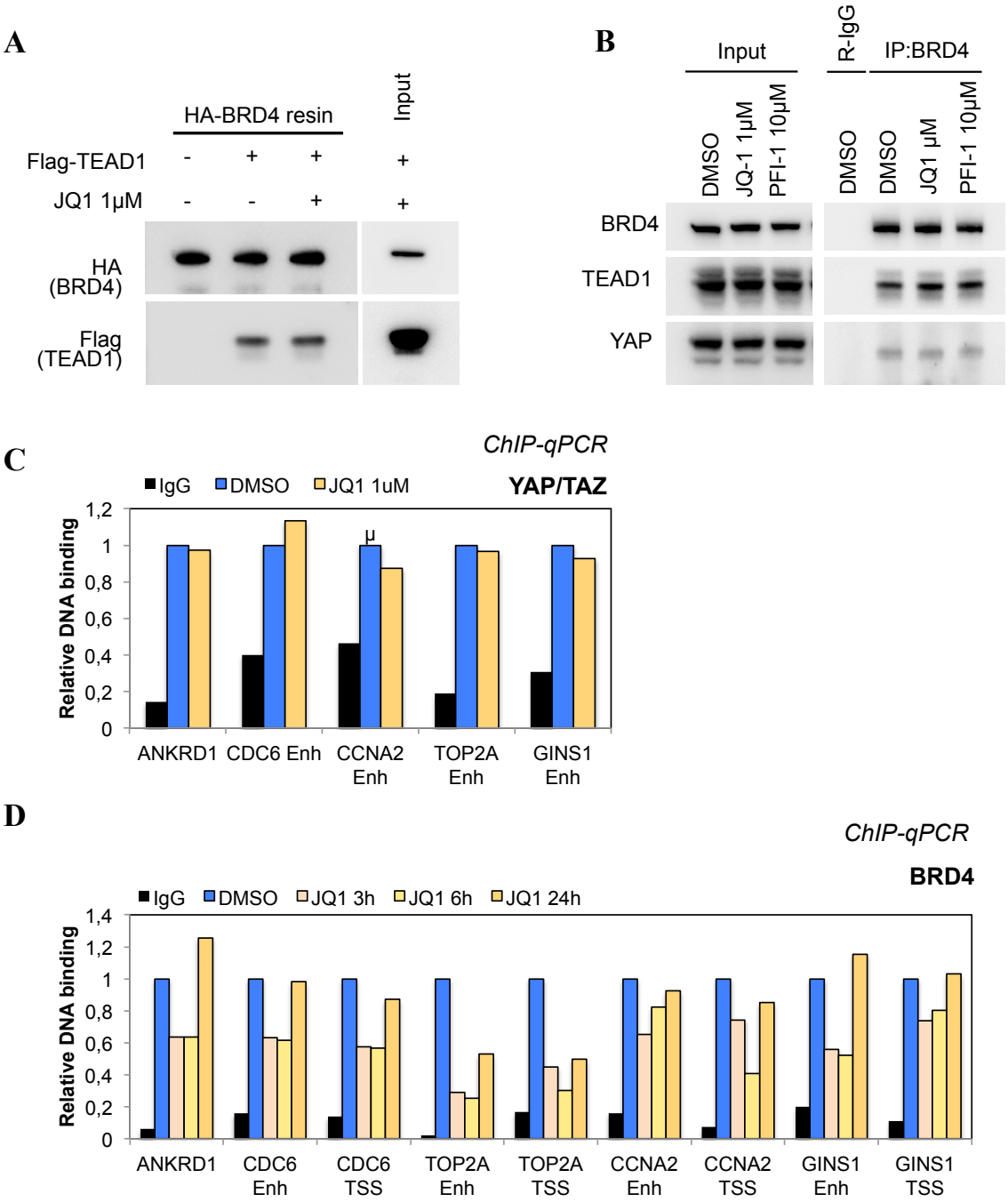
A
HA-BRD4 resin
Input
Flag-TEAD1
JQ1 1μM
HA (BRD4)
Flag (TEAD1)
B
Input
R-IgG
IP:BRD4
DMSO
JQ-1 1μM
PFI-1 10μM
DMSO
DMSO
JQ1 μM
PFI-1 10μM
BRD4
TEAD1
YAP
C
ChIP-qPCR
YAP/TAZ
IgG
DMSO
JQ1 1uM
Relative DNA binding
ANKRD1
CDC6 Enh
CCNA2 Enh
TOP2A Enh
GINS1 Enh
D
ChIP-qPCR
BRD4
IgG
DMSO
JQ1 3h
JQ1 6h
JQ1 24h
Relative DNA binding
ANKRD1
CDC6 Enh
CDC6 TSS
TOP2A Enh
TOP2A TSS
CCNA2 Enh
CCNA2 TSS
GINS1 Enh
GINS1 TSS

Figure 16. Loss of BRD4 impairs Pol II recruitment on YAP/TAZ/TEAD-regulated genes

A. Immunoblot on protein extract of MDA-MB-231 cells, to verify phosphorylation state of Pol II, upon the depletion of YAP/TAZ or BRDs by transfection with siRNAs, or JQ1 1μM treatment (24 hours) compared to a control siRNA (siCO). Phosphorylation of Pol II on Ser2 was reduced in all conditions compared to siCO. GAPDH is used as loading control.
B. ChIP-qPCR verifying Pol II binding to promoters of established YAP/TAZ direct targets upon downregulation of YAP/TAZ (siYAP/TAZ) or BRDs (siBRDs), or JQ1 1μM treatment for 24hours. GAPDH promoter represents a non-YAP/TAZ target. Negative control immunoprecipitation by IgG displayed background signal (data not shown). DNA enrichment was calculated as fraction of input.

Figure 16

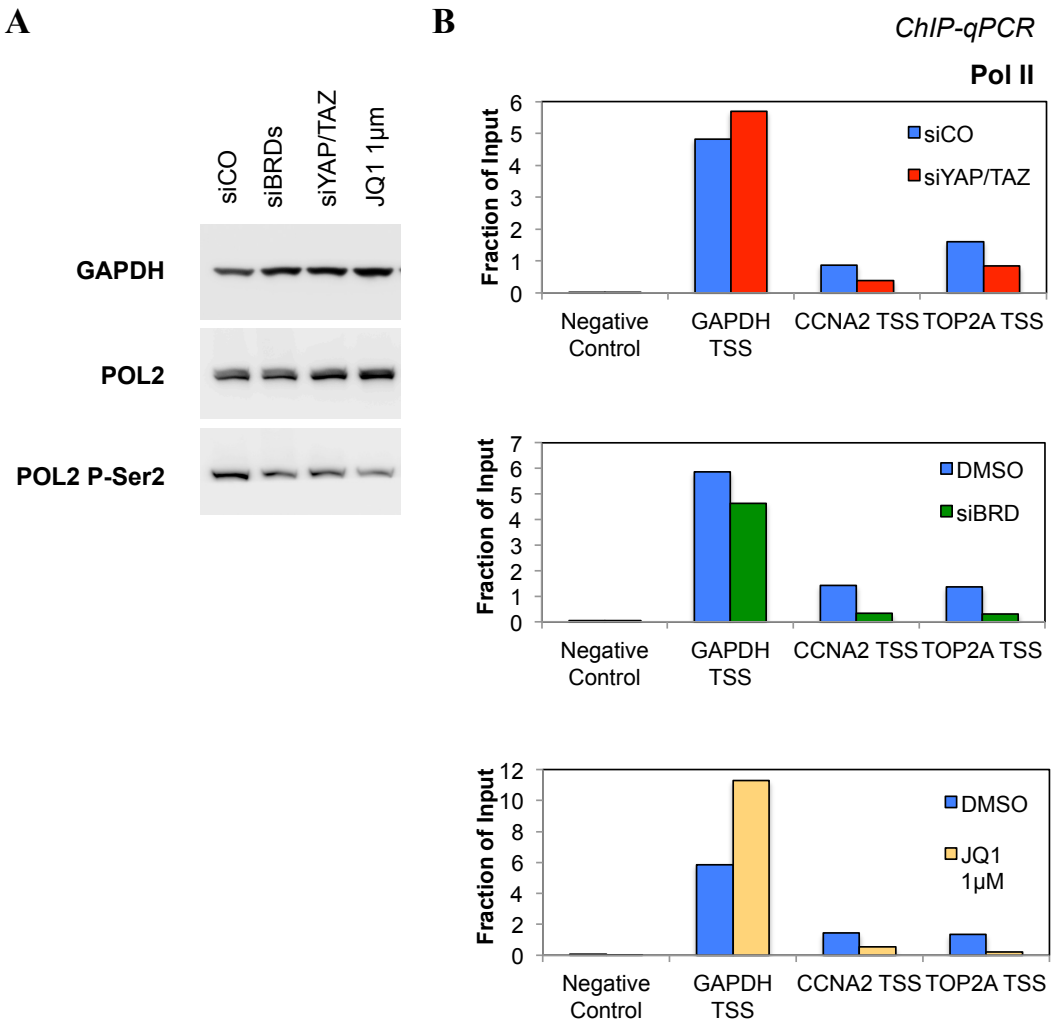
A
siCO
siBRDs
siYAP/TAZ
JQ1 1µm
GAPDH
POL2
POL2 P-Ser2
B
ChIP-qPCR
Pol II
Fraction of Input
siCO
siYAP/TAZ
Negative Control
GAPDH TSS
CCNA2 TSS
TOP2A TSS
DMSO
siBRD
DMSO
JQ1 1µM

TABLE 1

List of YAP/TAZ/TEAD direct target genes					
ABHD10	CKAP2L	GLTP	MRPL46	PSMC3IP	SSR3
ACAT2	CMIP	GNL2	MRPL52	PSMG1	SUV39H2
ADAMTS16	CNIH	GNL3	MRPL9	PSRC1	TAF5L
ADAMTS6	COL12A1	GPATCH4	MRRF	PSTPIP2	TBC1D2
ADRB2	CORO1C	GPN3	MTA2	PTGER2	TBC1D4
AFAP1L1	CRIM1	GRPEL1	MTFP1	PTPLA	TBCE
AIMP2	CRY1	GTPBP4	MTG1	PTPN2	TCOF1
AJUBA	CSE1L	HAT1	MTHFD1	PTRH2	TCP1
AKAP12	CSPP1	HAUS4	MTPAP	PTX3	TDP1
AMOTL2	CTGF	HBEGF	MUTYH	RAB11FIP1	TEAD4
ANKRD1	CTNNAL1	HIST1H3B	MYBL1	RABGEF1	THG1L
ANKRD32	CUTC	HNRNPM	MYC	RAD18	THOC1
ANKRD33B	CYC1	HSPA14	NAA15	RALGPS2	THOC6
ANXA3	CYP20A1	HSPA9	NAA25	RBL1	TIMELESS
APITD1	CYR61	HYI	NASP	RBM22	TIMM10
ARNTL2	DARS2	ICK	NAT10	RBM24	TIMM8A
ARSJ	DDAH1	IGFBP3	NCBP2	RCAN1	TK1
ASAP1	DDX21	IL12A	NCL	RCC1	TMEM106C
ASB1	DDX46	ILF3	NEDD4L	RHEB	TMEM194A
ATAD2	DDX47	IQGAP3	NEIL2	RND3	TMEM200B
ATG3	DDX56	IRAK1	NEURL1B	RNMTL1	TMEM201
AXL	DEK	ISG20L2	NFKB1	RPF2	TMEM209
B3GALNT2	DIAPH3	ITGB2	NMT2	RPL27A	TNFRSF12A
BANF1	DIS3L	KATNB1	NOB1	RPL3	TOE1
BASP1	DKC1	KIAA0391	NOC3L	RPP40	TOP2A
BCAT1	DKK1	KIAA1524	NOL10	RPUSD2	TRA2B
BCS1L	DNAJA3	KIF14	NOP14	RQCD1	TRDMT1
BOD1	DNTTIP2	KIF18B	NPM3	RRM2	TRIM14
BTBD10	DPH5	KIF20B	NUDCD1	RRP1B	TRIP6
BUB1B	DTYMK	KIF23	NUF2	RRS1	TRMT1
C11orf48	DUSP14	KIF2C	NUP188	RTN4IP1	TRMT5
C11orf83	E2F3	KLHDC4	NUP50	RUVBL2	TROAP
C12orf45	EDN1	KNTC1	NUP85	SAMD4A	TSEN2
C12orf65	EFTUD2	LARP4	NUP88	SART3	TTI1
C17orf89	EID2	LARP4B	NUP93	SEH1L	TUBB
C1orf109	EIF3D	LAYN	NXT1	SEPT11	TUBB6
C1QBP	EIF3J	LEPREL1	ODC1	SERPINE1	TUBG1
C4BPB	EIF4EBP1	LIMA1	OXNAD1	SERTAD2	U2AF1
C5orf28	EIF5A2	LMNB2	PABPC4	SERTAD4	UBE2E2
C9orf142	ENC1	LRIG3	PAK1IP1	SET	UBE2G2
C9orf40	ERCC6L	LRRC8C	PANK2	SF3A3	UBR4
CASC5	ERLIN1	LSG1	PAWR	SF3B3	UCK2
CCDC137	ETS1	LSM3	PCID2	SFXN4	URB2
CCDC15	ETS2	LZIC	PDCD5	SGOL1	USP36
CCDC85C	EXOSC2	MAD2L1BP	PHACTR1	SHMT2	USP44
CCNA2	F3	MAGOHB	PHF17	SLC1A5	UTP15
CDC25A	FAM46B	MALSU1	PHTF2	SLC25A32	UTP20
CDC42EP3	FAM57A	MAP3K1	PKN3	SLC35F3	WDR67
CDC6	FAM89A	MATN2	PKP4	SLC41A1	WDR74
CDCA4	FARSA	MCM3	PLAU	SLMO1	WDR85
CDCA5	FGF5	MCM7	PNPT1	SMC3	WSB2
CDCA8	FJX1	MED27	POC1A	SMTN	WTIP
CDH4	FLG	MED30	POLA2	SNAI2	WWC1
CDKN2AIPN	FOSL1	MEST	POLE3	SNAPC1	WWC2
CENPF	FOXF2	METAP2	POLH	SNRPD2	XPO5
CENPL	FST	METTL12	POLR1A	SNRPF	XPO6
CENPV	FTSJ2	METTL13	POLR1C	SOAT1	YOD1
CEP152	GADD45A	METTL8	PPIF	SOCS2	ZCCHC8
CEP290	GADD45B	MIIP	PPME1	SPATA5L1	ZMYND19
CEP55	GADD45GIP	MRE11A	PPRC1	SRBD1	ZNF259
CEP57	GEMIN4	MRPL18	PRMT1	SRRD	ZNF804A
CEP57L1	GINS1	MRPL21	PRMT5	SRSF2	ZNHIT6
CHUK	GJA1	MRPL24	PRPF4	SRSF3	ZWILCH

TABLE 2

List of Antibodies				
Antibody	**Company**	**Catalog Number**	**Description**	**Use**
normal rabbit IgG	sigma aldrich	I5006 - IgG from rabbit serum		ChIP, IP
normal mouse IgG	santa cruz	sc-2025		ChIP, IP
anti-YAP1	abcam	ab52771	Rabbit monoclonal	ChIP
anti-TAZ (WWTR1)	sigma aldrich	HPA007415	Rabbit polyclonal	ChIP
anti-YAP1	Proteintech	13584-1-AP	Rabbit polyclonal	IP,PLA
anti YAP/TAZ (63.7)	santa cruz	sc-101199	Mouse monoclonal	IB
anti-TEAD4 (TEF-3 antibody N-G2	santa cruz	sc-101184	Mouse monoclonal	ChIP
anti-TEF1	BD Biosciences	610923	Mouse monoclonal	IB, PLA
anti-Histone H3	abcam	ab1791	Rabbit polyclonal	ChIP
anti-Histone H3 (acetyl K27)	abcam	ab4729	Rabbit polyclonal	ChIP
anti-BRD4	Bethyl-LAB	A301-985A	Rabbit polyclonal	ChIP
anti-BRD4	Sigma	HPA015055	Rabbit polyclonal	IB
anti-BRD4	CST	E2A7X	Rabbit polyclonal	IP
anti-Pol II	abcam	ab817	Mouse monoclonal	ChIP, IB
anti-Pol II P-Ser2	abcam	ab5095	Rabbit polyclonal	IB
anti-GAPDH	millipore	MAB374	Mouse monoclonal	IB
anti-FOSL1 (Fra-1 R20)	santa cruz	sc-605	Rabbit polyclonal	IB
anti-ARK-1 (H-130)	santa cruz	sc-25425	Rabbit polyclonal	IB
anti-CyclinA (C-19)	santa cruz	sc-596	Rabbit polyclonal	IB
anti-Cdc6 (180.2)	santa cruz	sc-9964	Mouse monoclonal	IB
anti-Ets1 (C-20)	santa cruz	sc-350	Rabbit polyclonal	IB
anti-MCM7 (141.2)	santa cruz	sc-9966	Mouse monoclonal	IB
anti-MCM3 (N-19)	santa cruz	sc-9850	Goat polyclonal	IB
anti-cMyc	Cell Signaling Technology	9402S	Rabbit polyclonal	IB
anti-GFP	santa cruz	sc-8334	Rabbit polyclonal	IB
anti-FLAG M2	sigma aldrich	F1804	Mouse monoclonal	IB, IP
anti-HA	santa cruz	sc-7395	Mouse monoclonal	IB, IP

ChIP: chromatin immunoprecipitation
IP: immunoprecipitation
IB: immuno blot
PLA : proximity ligation assay

TABLE 3

siRNA sequences	
Name	Sequence (5' to 3')
siCO	AllStars Negative Control siRNA 1027280 (Qiagen)
siYT 1	GACAUCUUCUGGUCAGAGA dTdT (YAP) ACGUUGACUUAGGAACUUU dTdT (TAZ)
siYT 2	CUGGUCAGAGAUACUUCUU dTdT (YAP) AGGUACUUCCUCAAUCACA dTdT (TAZ)
siTEAD A	UGAAUGUGCAAUGAAGCGGCG dTdT
siTEAD B	GGCCGAUUUGUAUACCGAA dTdT (TEAD1) CCUGGUGAAUUUCUUGCACAA dTdT (TEAD2) UACCUUGCUCUCAAUCUGGAG dTdT (TEAD3) UUUCCUGCACACACGUCUCUU dTdT (TEAD4)
siMYC1	ACAUCAUCAUCCAGGACUG dTdT
siMYC2	GGUCAGAGUCUGGAUCACC dTdT
siBRD #3	GUAGCAGUGUCACGCCUUA dTdT (BRD2)
	CCUGCCGGAUUAUCAUAAA dTdT (BRD3)
	GAGGACAAGUGCAAGCCUA dTdT (BRD4)
siBRD #4	GUAGCAGUGUCACGCCUUA dTdT (BRD2)
	GCCCGUGGACGCAAUCAAA dTdT (BRD3)
	GCGUUUCCACGGUACCAAA dTdT (BRD4)

When the number is not specified, mix #1 was used.

When the number is not specified, mix #4 was used. For BRD4, a mix of anti-BRD4 siRNAs was used.

shRNA sequences	
shBRD4 #1	GCCTGGAGATGACATAGTCTTA
shBRD4 #2	ACAGTGACAGTTCGACTGATGA

TABLE 4

List of primers used for ChIP-qPCR		
Target gene	**Forward primer**	**Reverse primer**
HBB	GCTTCTGACACAACTGTGTTCACTAGC	CACCAACTTCATCCACGTTCACC
FAT3	GGCTTCCACTTCACACATTCC	TGCCCATTCTACTCTGGCTGTT
ANKRD1	AAAAAGGGCAGTGATGTGGTG	GAAGAGGGAGGGGAGGACAA
Axl	TGAGTAGGGACCAGGGTTGG	CCACCACACAGACATGCACA
AMOTL2	TGCCAGGAATGTGAGAGTTTC	AGGAGGGAGCGGGAGAAG
AJUBA	AGGAAAGAGTGTGGGGGTAGG	ACGCTGGGAACAAAGTCACG
WTIP	GCAGCGCCGTCTCCTTCCT	GCGGCGGAGGAATGTAAGCTC
CTGF	TGTGCCAGCTTTTTCAGACG	TGAGCTGAATGGAGTCCTACACA
CYR61	CACACACAAAGGTGCAATGGAG	CCGGAGCCCGCCTTTTATAC
ETS1 alternative promoter	CGTCTGATTCTCCACGCATTC	CGCTCGCCTTCATCCACAT
Myc enh1	TGCTCCTAAACCTCCTCACCA	TGCCCTTGATTTGCTGCTTT
Myc enh4	GGGGAACTCTCACTCTCCTTTGA	CCAGGGGGTCTTTACACAGC
Myc enh5	TTCCTGCCTTCTGAGTGGTG	TTTCCTGTGACTGCGGGTCT
Myc enh6	AGGGTCCTGGGCTTTTTCAG	GGGCCATTCGTCACCTTTTC
TOP2A enh1	GTGGAGTGTGGGCATCTGAG	CAATGGGGAAAGAAAGACTGTAGC
TOP2A enh2	CCCCACCCAGACAGGAAA	TGAGGCAGGGCAGTTTAGAA
TOP2A enh3	CCGAGGGTTGTTTTCCCATC	GACTGTGTGCGTGAGCGTGT
GINS1 enh	CCCCAAAAGTGTCCATGACC	CAGGATCACCCCCATCTCAA
CCNA2 enh	ACAGAAGGGGAGCGACTGG	CCCACCGTTTTCACTTTTTC
FOSL1 enh	CTCAGCCACTTCCACCCAGT	TCCAGCAGTCTCACCGAATC
CDC6 enh	GCTGGGCATCACAGTCTTGG	GGCATGGCTGGGTGACTC
KIF23 enh	CCCTCACACCCAGAAAGCTG	AATCACGCTGGCATTTTGCT
CENPF enh1	CCCCCTCTGCTATTGTTCTCAA	TGCCATTTTTCATTCCCACA
CENPF enh2	CCCCACCACCACTGCTTC	GGGAATCTCAGCCTTCTTGG
MCM3 enh	AGTTGGGATAGGCGGAGACC	GCAGGTGGGGCTTGTTTAGG
POLE3 enh	TGGTTTTTCCGTTCCTGGTG	CAGAGGGGAGGGGGTCTATG
RAD18 enh	GGCATTTGTGGCATTCCTG	CCTGATCCACTCCACCTTCG
POLA2 enh	ATGACGCTGGACAACAGGAGTC	CGACAGAAGAAATCCCTAAGAACC
ETS1 enh1	CCCTTGTCCCAACACACACA	AAAACTGTCTCCACCTCCTAATGC
ETS1 enh3	GACACCATCCCCTACAAATGC	CACAACTCTCTTTATCAGCAGCACA
CDCA5 enh	AGTGCTGCTCCCCCACACTA	CCTGCAAGGAAAGAGCTGGA
CDC6 TSS	CAAGGCGAAAGGCTCTGTGA	CAAGCCCCTGAACAAACTGC
CCNA2 TSS	CCCCTGCTCAGTTTCCTTTGGT	TGCAGTTCAAGTATCCCGCGA
TOP2A TSS	TTCCTTTAGCCCGCCCGAAG	TCCCGCCTCCCTAACCTGAT
GINS1 TSS	GCCGAGAGCCCAGATACCAT	CGTTGAAGGCAGGCAGTAG
ETS1 TSS	CCGCTCCTGAAGAAATGCAC	CGTCGATCTCAAGCCGACTC
RRM2 enh	AGGGCTGTTGCTCACCTCTTG	GCATTCTTCCTGGCTCTTTGTG
RRM2 TSS	TTAAAGGCTGCTGGAGTGAGG	CGGAGGGAGAGCATAGTGGA
GAPDH TSS	TCGCTCTCTGCTCCTCCTGT	GTTTCTCTCCGCCCGTCTTC

List of primers used for qPCR		
Target gene	**Forward primer**	**Reverse primer**
GAPDH	CTCCTGCACCACCAACTGCT	GGGCCATCCACAGTCTTCTG
CTGF	AGGAGTGGGTGTGTGACGA	CCAGGCAGTTGGCTCTAATC
ANKRD1	AGTAGAGGAACTGGTCACTGG	TGGGCTAGAAGTGTCTTCAGAT
TEAD1	GCCTCCCAACATCCATAGCA	TCTGTCCACCAGCCGAGATT
TEAD2	TGCCTTCTTCCTGGTCAAGTTC	GGCTCTCATACTGGCTGCTCA
TEAD3	GCCGTCTTCTCCACTTCCTC	CCAGGGGCTCATAACTGCTG
TEAD4	GGGCAGACCTCAACACCAAC	TGTCCATTCTCATAGCGAGCA

TABLE 5

Primers used for 3C assay	
MYC (gene)	
Anchor	CGGTAATGGCAAACGTGAA
MYC enhancer 1	
Bait 1	AGGTGGCCTTGTGTTAAATGAG
Bait 2	CAATCTAATGAAGAAAACAAGCAAAG
Bait 3	TGCACCTGGGGATCTTGT
Bait 4	TCAAGGCAAACTATTCCAAGA
Bait 5	CAAATCTTGTCGAGGAACTAATG
Bait 6	AGGAGAAGAAGGGAACAGGAAG
Bait 7	TCCAATAATCTAGTGTGACAGCAAA
Bait 8	AATTGGGAAAGGACTTGGAAAT
Bait 9	GGGGAGTACATTAGAGGAACAAA
Bait 10	GCTAATCTTCTATGAGCTTCGTCA
Bait 11	TAAATACCCCGGCTCCCTTA
Bait 12	GGCCTCACACCGAATAACTC
Bait 13	AGGCTGGCTGTTCCTGGT
Bait 14	GTGTGAAGTGGTTGATGAGAGG
MYC enhancer4	
Bait 1	CAATGGAGGAACCAAAGGTG
Bait 2	CAGCGACTGCCACAGATAAC
Bait 3	GCTGTGGTGGGAAAGAAAGATA
Bait 4	CCACCACCTGAGATACCTGAAT
Bait 5	TCATAGGGGGAGACAGAAGC
Bait 6	CCTCCTGGGGAACTCTCA
Bait 7	GGTGAGTGGGCTTTAGAATGAG
Bait 8	GTCCTATCAGCCAGAACTTAGCC
Bait 9	CCTTTATGCCCTCATTTATCCTT
Bait 10	TTTCCAGAGTTAGGACATGGACA
Bait 11	CCTCATTTGATCTACAAAGGCTCT
Bait 12	CTGAAGCAGGAACAGGAGAGAT

TOP2A (promoter)	
anchor	CCTGGAGAATAAACATCCTTTGC
TOP2A enhancer 1	
Bait 1	GTTGTGCCTTGGTGTGGA
Bait 2	AGGTCATTCCCTGACTTCTGTT
Bait 4	CTATGGCTCTGGAGGAGCTG
Bait 5	TCTGCTGGGAGTTACAAGATTTC
Bait 6	GGTGCCTTGTTGTGATGAATTA
Bait 7	TTGAAGATGGGAATGTGATCTG
Bait 8	AGGCACAGAAGCAAGAAACAAT
Bait 9	TTTGCTAATTTCAGTTCTGATTGC
Bait 10	GATGCTGACCTACATTCTTCCTTT
Bait 11	CTGAGCTTCTTGGCTTTCAGA

TABLE 6

TaqMan assays
ANKRD1-Hs00923599_m1
CCNA2-Hs00996788_m1
CDC25A-Hs00947994_m1
CDC6-Hs00154374_m1
CDCA5-Hs00293564_m1
CDCA8-Hs00983655_m1
CENPF-Hs00193201_m1
CENPV-Hs00396457_m1
CTGF-Hs01026927_g1
EDN1-Hs00174961_m1
ETS1-Hs00428293_m1
ETS2-Hs01036305_m1
FOSL1-Hs04187685_m1
GADD45B-Hs04188837_g1
GAPDH-Hs99999905_m1
GINS1-Hs00221421_m1
KIF14-Hs00208408_m1
KIF20B-Hs01027505_m1
KIF23-Hs00370852_m1
KNTC1-Hs00206854_m1
MCM3-Hs00172459_m1
MCM7-Hs00428518_m1
MRE11A-Hs00967443_m1
MYBL1-Hs00277143_m1
MYC-Hs00153408_m1
POLA2-Hs00160242_m1
POLE3-Hs00794385_m1
POLH-Hs00982625_m1
PSMC3IP-Hs00247433_m1
PSMG1-Hs00186605_m1
RAD18-Hs00892551_m1
RRM2-Hs00357247_g1
RUVBL2-Hs01090542_m1
SGOL1-Hs00386282_m1
SMC3-Hs00271322_m1
SUV39H2-Hs00226596_m1
TIMELESS-Hs01086966_m1
TK1-Hs01062123_m1
TOP2A-Hs01032137_m1
TUBB-Hs00962420_g1
ZWILCH-Hs01555249_m1